Hydrogen Bond-directed Self-assembly of Perylene Bisimide Organogelators

Dissertation zur Erlangung des
naturwissenschaftlichen Doktorgrades
der Julius-Maximilians-Universität Würzburg

vorgelegt von
Xueqing Li
aus Dezhou, China

Würzburg 2009

Eingereicht am: _____

bei der Fakultät für Chemie und Pharmazie

1. Gutachter: Prof. Dr. Frank Würthner

2. Gutachter: _____

der Dissertation

1. Prüfer: Prof. Dr. Frank Würthner

2. Prüfer: _____

3. Prüfer: _____

des öffentlichen Promotionscolloquiums

Tag des öffentlichen Promotionscolloquiums: _____

Doktorurkunde ausgehändigt am: _____

für meine Familie

List of Abbreviations

AFM	atomic force microscope
ACW	anti-clockwise
CD	circular dichroism
CGC	critical gelation concentration
CW	clockwise
DMF	*N*,*N*-dimethylformamide
DSC	differential scanning calorimetry
ESI	electrospray ionization
HOPG	highly ordered pyrolytic graphite
LD	linear dichroism
LC	liquid crystal / liquid crystalline
LMOG	low molecular-mass organogelator
MCH	methylcyclohexane
MALDI-TOF	matrix-assisted laser desorption injection time-of-flight
NMR	nuclear magnetic resonance
NRs	nanorods
PBI	perylene-3,4:9,10-tetracarboxylic acid bisimide
PR-TRMC	pulse-radiolysis time-resolved microwave conductivity
OPM	optical polarized microscopy
OPV	oligo-*p*-phenylene-vinylene
SEM	scanning electron microscope
STM	scanning tunneling microscope
THF	tetrahydrofuran
TMS	tetramethylsilane
TEM	transmission electron microscope
UV-vis	ultraviolet-visible

Table of Contents

Chapter 1

Introduction and Aim of this Thesis

Supramolecular self-organization is one of the key techniques for the "bottom-up" approach in nanotechnology, by which small molecules form well-defined larger nanostructures via multiple non-covalent intermolecular forces, such as hydrogen-bonding interactions, dipole-dipole interactions and van der Waals interactions including $\pi-\pi$ interactions.[1] Organogels are of particular interest for scientists in this area. The hierarchical formation from fibrous nanostructures to 3D network superstructures is reversible and controllable, which may feed various applications in devices design and processing.[2] To achieve photofunctional organogels, "designed" dye molecules have been incorporated in recent years, and applications as sensors, optoelectronic devices, and light harvesting modules have been demonstrated[3]

Towards these applications, robust organogelators are needed that are able to gelate a broad variety of media (e.g., solvents, liquid crystals, etc.) and exhibit favourable functional properties. Organogelators based on numerous electron-rich (*p*-type) aromatic building blocks such as porphyrins, phthalocyanines, oligo (phenylenevinylenes), oligothiophenes and tetrathiafulvalenes have been investigated in the recent past. However, organogels embedding their electron-poor (*n*-type) counterparts are still rare. Perylene bisimides (PBIs) are considered to be one of the best candidates, which have been extensively studied as *n*-type semiconductors in various applications such as optical recording media, organic photo- and semiconductors, and solar cells.[4]

The precise control of the dye-dye interaction and long-range ordering is essential to device performance. To realize a desired supramolecular structure, the

respective building blocks may be optimized towards an ideal packing and self-assembly behavior. However, a more simple approach may be given by variation of the environments, such as altering concentrations, temperature, or solvents used.[5] Recently, significant interests have been devoted to aggregation of dye molecules on the nanoscale and macroscopic-scale orientation of the supramolecular nanostructures by external perturbation such as stirring, shaking, etc..[6] The precise control of the self-assembly of dye molecules from nano- to macro- scales thus paves a way to fill in the requirements of many different technologies.

In 2004, Shinkai and coworkers reported for the first time PBI organogelator **1a** that contains cholesterol accessories (Figure 1).[7] Independently, a urea-based PBI gelator **2** which can form fluorescent gel was reported by Würthner and co-workers (Figure 2).[8] However, both gelators can only gelate a limited range of solvents at relative high concentrations. Notably, among the series of **1a - 1d** in Figure 1, only

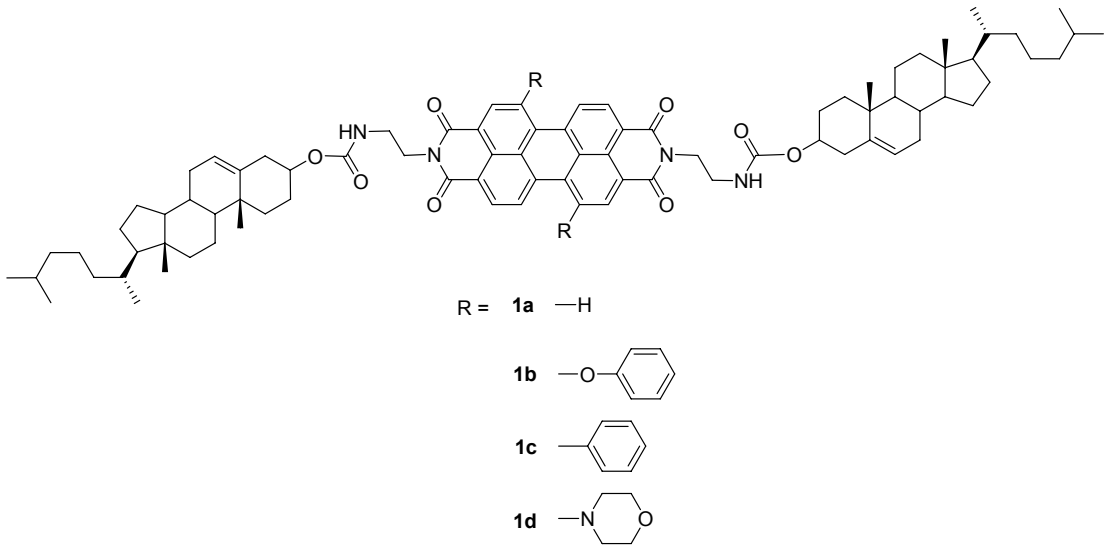

Figure 1. Molecular structures of cholesterol-based PBI derivatives

PBI **1a** showed gelator properties for some aromatic solvents such as benzene, xylene, and mixtures of *p*-xylene with alcoholic solvents. To achieve stable gels,

high concentrations are demanded (up to 0.5 wt/vol%, 3.8 mM). For the case of urea-based PBI gelator, only in tetrachloromethane the gelation can be observed.

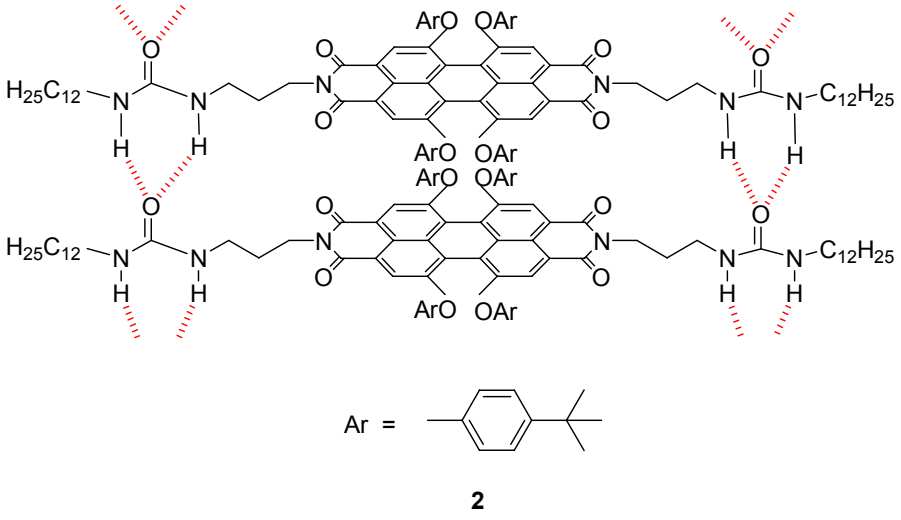

2

Figure 2. Packing of urea-based PBI gelators

The aim of this thesis is to develop new PBI gelators and to elucidate the relationship between molecular structure and aggregation/gel formation of PBIs. Furthermore, by choosing different solvents, temperature, or using external perturbation the morphology and orientation of nanofibers should be controlled.

Chapter 2 gives an overview on dye-based organogelator in the literature. This chapter will introduce some basic knowledge of organogels firstly, and then some examples on the gel formation from various dye molecules are given. Chiral aggregates based on achiral building blocks are introduced as well, including aspects of characterization, amplification and symmetry breaking of chirality.

Chapter 3 describes synthesis of a new *n*-type semiconducting perylene bisimide dye (Figure 3) that gelates a broad variety of organic solvents owning to its self-assembly into well-defined nano- and mesoscopic helical fibers and bundles. Such well-organized fibers and bundles that are composed of extended π-stacks of the electron poor dye provide efficient pathways for mobile *n*-type charge carriers.

Following the results from **Chapter 3**, **Chapter 4** investigates breaking of the

symmetry for these helical fibers generated from achiral PBI molecules. Both micro- and macroscopic effects are recognized in equilibrium or non-equilibrium environments, such as chiral solvents and mechanical stirring respectively.

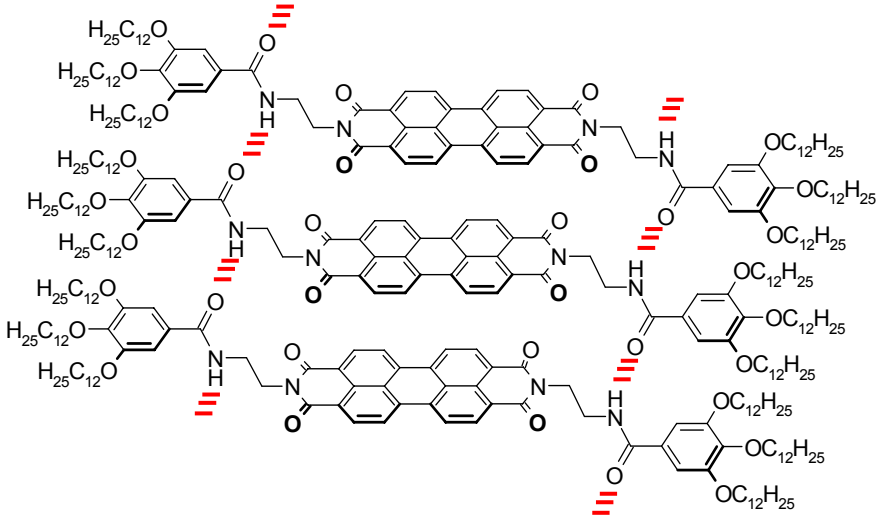

Figure 3. Concept for hydrogen bond-directed aggregation of PBI molecules as investigated in Chapter 3.

Chapter 5 studies the self-assembly behavior of core twisted perylene bisimide dye, which forms highly fluorescent J- aggregates in various organic solvents. Its gelation in polar solvents like acetone and dioxane is observed, whilst anisotropic highly viscous lyotropic mesophases are created in apolar solvents such as *n*-hexane or methylcyclohexane.

In **Chapter 6**, the research is focused on the synthesis of gold nanorods and thioacetyl functionalized perylene bisimides. By properly mixing the two components, the gold nanorods are connected end to end to form linear gold nanochains, which are characterized by UV/Vis/NIR spectroscopy and transmission electron microscopy.

Chapter 7 is a summary of this thesis.

References

1 J. M. Lehn, J. L. Atwood, J. E. D. Davies, D. D. MacNicol, F. Vögtle, *Comprehensive Supramolecular Chemistry,* Pergamon, New York, **1996**.

2 (a) P. Terech, R. G. Weiss, *Chem. Rev*. **1997**, *97*, 3133-3160; (b) N. M. Sangeetha, U. Maitra, *Chem. Soc. Rev.* **2005**, *34*, 821-836; (c) L. A. Estroff, A. D. Hamilton, *Chem. Rev*. **2004**, *104*, 1201-1217; (d) T. Ishi-I, S. Shinkai, *Top Curr Chem* 2005, **258**, 119-160; (e) D. J. Abdallah, R. G. Weiss, *Adv. Mater.* **2000**, *12*, 1237-1247; (f) H. Maeda, *Chem. Eur. J.,* **2008**, *14*, 11274-11282; (g) C. C. Lee, Christophe. Grenier, E. W. Meijer, A. P. H. J. Schenning, *Chem. Soc. Rev.* **2009**, *38*, 671-683

3 *Supramolecular Dye Chemistry,* F. Würthner, Ed., *Top Curr Chem* **2005**, *258*.

4 F. Würthner, *Chem. Commun.* **2004**, 1564-1579, and the literatures cited therein.

5 (a) K. R. MacKenzie, *Chem. Rev.* **2006**, *106*, 1931-1977; (b) M. Albrecht, *Chem. Rev.* **2001**, *101*, 3457-3497.

6 (a) J. M. Ribó, J. Crusats, F. Sagues, J. M. Claret, R. Ruvires, *Science* **2001**, *292*, 2063-2066; (b) A. Tsuda, Md. A. Alam, T. Harada, T. Yamaguchi, N. Ishii, T. Aida, *Angew. Chem. Int. Ed.* **2007**, *46*, 8198-8202; (c) M. Wolffs, S. J. George, Ž. Tomović, S. C. J. Meskers, A. P. H. J. Schenning, E. W. Meijer, *Angew. Chem. Int. Ed.* **2007**, *46*, 8203-8205; (d) G. P. Spada, *Angew. Chem. Int. Ed.* **2008**, *47*, 636-638.

7 K. Sugiyasu, N. Fujita, S. Shinkai, *Angew. Chem. Int. Ed.* **2004**, *43,* 1229-1233.

8 F. Würthner, B. Hanke, M. Lysetska, G. Lambright, G. S. Harms, *Org. Lett.* **2005**, *7*, 967-970.

Chapter 2

State of Knowledge

2.1 Structural and Functional Features of Organogel Systems

2.1.1 Definition and Principles

Gels are found in our life in various applications such as shampoo, toothpaste, cachou, jelly, and other wares. Most of these can be classified as polymer hydrogel, for they are derived from polymeric compounds in water, which have been know for centuries and applied in fields as diverse as food, medicine, cosmetics, pharmacology etc.[1] Only in recent years there has been a rapidly growing interest in low molecular-mass organogelators (LMOGs) which exhibit striking properties and the potential for different kind of applications. In general, the concept of "organogel" indicates that the gels are composed of small organic molecules rather than polymeric analogs, and they are often named as supramolecular or physical gel because this class of gels is motivated mainly by supramolecular forces such as hydrogen bonding, metal coordination, and dipole interactions.

Although gels are widely used and studied, the definition of a gel is somehow illegible so far from scientific point of view. About 80 years ago Dr. Dorothy Jordon Lloyd noted, "…the colloid condition, the gel, is easier to recognize than to define.[2] It is generally accepted that an organogel must comprise low concentration (in most cases, $c < 2$ wt %) of small molecular gelators in organic liquid and meet at least two stipulates[3]:

(a) The gel formed should appear solid-like macroscopically, while the materials are composed predominately of a liquid at the microscopic scale.

(b) The material should transform reversibly between sol-gel by applying or relieving a certain stress, such as temperature, concentration, additive, etc..

One can explore the structural character of a gel by macroscopic and microscopic methods. Macroscopically, a gel is solid-like but exhibits viscoelastic rheological behavior. The dictum of Jordon Lloyd is still true to date that: if it looks like a "Jello", it must be a gel. From the microscopic point of view a gel possesses continuous structures with one dimensional growth, such as fibers, strands or tapes.

In the case of the supramolecular gel, the colloid aggregates originate from small molecules that are connected by intermolecular interactions to give fibers with the dimension from the nanoscale to several microns. Those fibred structures are interconnected to form three dimensional networks, which immobilize the liquid components (solvent molecules) to a variable extent by surface tension.

Since we know what an organogel is, the question arises on how to find or to design a substance which can gelate one or more specified organic solvents. Although a wide range of organogelators have been reported, unfortunately, the invention of a new gelator is more a serendipity rather than prognosis so far.[4] As noted by Weiss and coworkers:

(1) What are the structural requirements for a molecule to gel an organic liquid?
(2) What is the relationship (if any) between the packing arrangements of gelator molecules in their bulk crystalline states and in their various aggregates in the gels?
(3) How does the molecular packing of gelators in their aggregates influence the mechanical, thermodynamic, optical, and other properties of the gels?

To find answers for these questions, many groups tried to elucidate the correlations among structures and electronic properties of the gelator, solvent, and the physical properties of their gels. Some guidelines for designing an organogelator based on our own experiences and results reported before are:

(a) The monomeric molecules are able to aggregate/self-assemble one-dimensionally through multiple self-complementary intermolecular

interactions;

(b) The aggregated structures such as rods, fibers, ribbons, tapes are expected to develop continuously into long scale fibers (from nano- to micrometers);

(c) The fibers should be able to further interconnect /entangle to 3D networks, which are essential for organogels in order to immobilize the solvent molecules.

Figure 1 shows a proposed scheme for the formation of organogels which indicates a hierarchical process from dissolved individual molecules to 3D entangled superstructures. Therefore, by rational design of molecular structures and precise control of their aggregation by altering the factors such as solvent, temperature, concentration, etc., it is possible to direct the self-assembly pathway towards formation of organogels.[5]

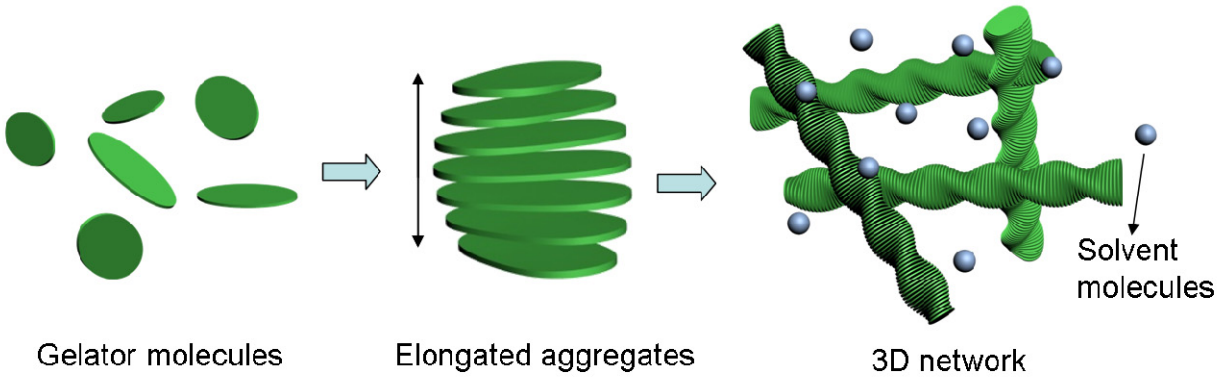

Figure 1. Proposed scheme of supramolecular gel formation.

2.1.2 Reversibility of Organogels

An organogel is usually prepared by heating the gelator molecule in an appropriate solvent until a clear isotropic solution is obtained. Subsequently, the mixture is cooled to room temperature, during which the molecules start to self-assemble into fibrous aggregates, networks, eventually yielding a gel.[6] The

gelation ability of a gelator in a specified solvent can be evaluated by critical gelation concentration (CGC) which indicates the lowest concentration of gelator molecules capable of gelling a liquid at room temperature. At a certain concentration an organogel is thermo-reversible thus the phase transition temperature (T_{sg}) from solution to gel (sol-gel) can be determined. The methods used for this purpose include differential scanning calorimetry (DSC), temperature sweep rheological experiments, and different spectroscopies (fluorescence, IR, NMR, etc.).[7] A diagram of T_{sg} versus concentration depicts clearly the condition required for sol-gel transition behaviors. An example from Shinkai's group is given in Figure 2, which clearly shows the sol-gel transition temperature of a cholesterol based PBI gelator at different concentrations.[8]

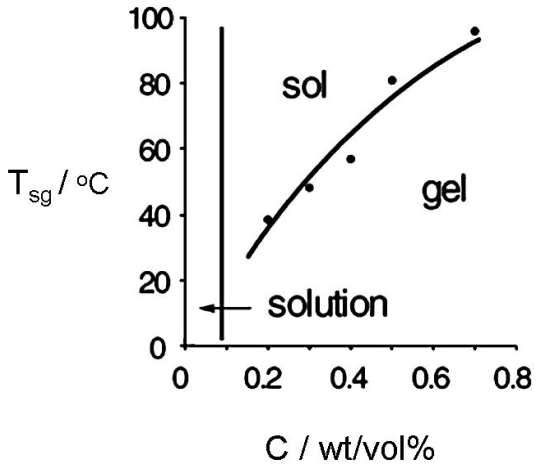

Figure 2. Plot of T_{sg} versus concentrations of a perylene gelator. Reprinted with permission from ref. 8. Copyright 2004 WILEY-VCH Verlag GmbH & Co. KGaA, Weinheim.

For the majority of organogelators, organogels are formed only in specific organic media. The 3D superstructures are maintained by a subtle balance between gelator-gelator interaction and gelator-solvent interaction.[9] Beside of self-driven factors which influence the formation of organogels, such as temperature and concentration, external driving forces are found to affect the reversibility of the gels significantly. One example is given by pyrene-based derivatives, which indicates

the chemo-responsive behavior of the organogel.[10] As shown in Figure 3, the formation of organogels is mediated by a two components donor-acceptor interaction, i.e., electron-rich pyrene derivatives and electron poor

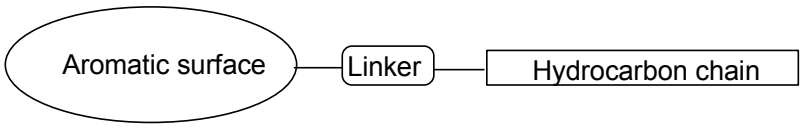

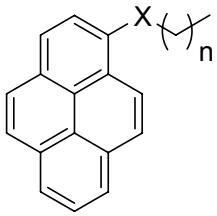

X	n	
COO	15	**1**
COO	7	**2**
CONH	15	**3**
CH_2	14	**4**
CH_2	10	**5**
CH_2	0	**6**
O	13	**7**
OCO	14	**8**
NHCO	16	**9**
NHCO	10	**10**
NHCO	6	**11**
NHCOO	15	**12**
NHCOO	11	**13**
NHCOO	9	**14**
NHCONH	15	**15**

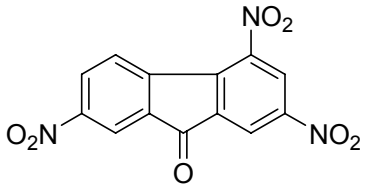

TNF 16

Figure 3. Pyrene-based gelators. Organogel formation is induced by trinitrofluorenone additive.

2,4,7-trinitrofluorenone (TNF, **16**). The pyrene based compounds with amide, urethane, and urea linkers formed gels on their own in various solvents by cooperation of π-π-stacking and hydrogen bonding interactions. However, for those derivatives with ester, ether, or alkyl linkages, which lack the capability for hydrogen bonding, the organogels can not be observed in a single component system but, are formed in a number of hydroxylic and hydrocarbon solvents by means of charge transfer interaction with the addition of TNF molecules. Interestingly, the compound with hydrogen bonding functionality did not gelate the solvents in the presence of TNT because of incompatible hydrogen-bonding and donor-acceptor interaction geometries.

In another example, Shinkai's group reported a series of cholesterol derivatives

containing a benzocrown ether moiety, which show metal-responsive functions (Figure 4).[11] Li^+, Na^+, K^+ are able to coordinate with 18-crown-6 ether in gelator **17** leading to an increase of the sol-gel phase transition temperature in the presence of these metals, stabilized with increasing metal concentration. Accordingly the gel is stabilized by metal ions.

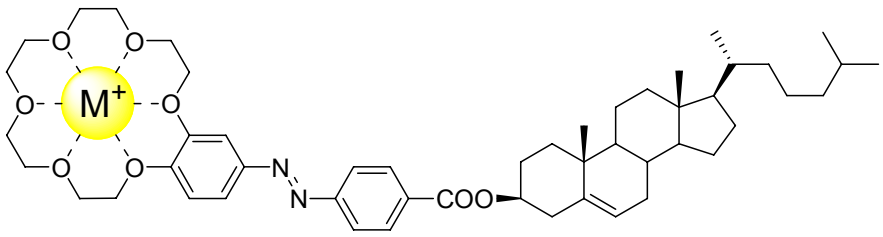

17

Figure 4. Metal responsive organogelator.

Beside of metal coordination, the counter anions can control the state of a gel as well without the need of specific interactions with gelator molecule, which was recently reviewed by Maeda comprehensively.[5] For example, Lee et at. reported sol-gel interconversion of coordination polymers formed by complexation of Ag^+ and dendrimer like oxyethylene-substituted bispyridine derivative **18** (Figure 5).[12] The assembled structures depend on the counter anions such as BF_4^-, F^- and $C_2F_5CO_2^-$. The ionic radii of the anions are crucial to determine the morphology of the aggregates. The addition of F^- to the BF_4^- salt of **18**·Ag^+, which is in the gel state, result in the transformation into the solution state by formation of free monomeric **18** and AgF salt. Further, the addition of $C_2F_5CO_2^-$ also transforms the gel into solution composed of the fairly dispersed assemblies of linear polymers. In all the cases, the transition between the solution and gel states was found to be fully reversible.

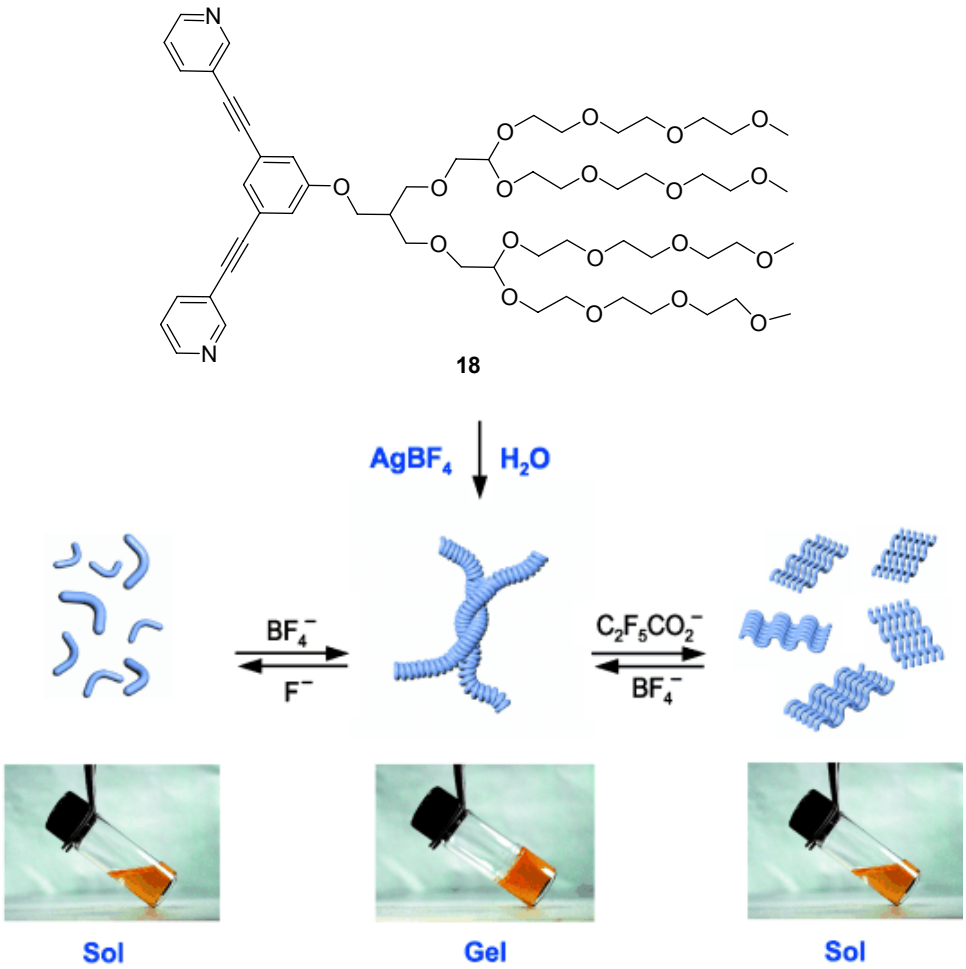

Figure 5. Schematic representation of reversible polymerization and reversible conversion between folded and unfolded conformations of a coordination chain upon counter-anion exchange. Reprinted with permission from ref. 12. Copyright 2005 WILEY-VCH Verlag GmbH & Co. KGaA, Weinheim.

Organogels that are based on hydrogen-bonding interactions, e.g., between amide or urea groups, are usually responsive to the addition of H-bonding so-solvents or chemicals. Either hydrogen bond donor solvents such as acid and alcohol, or acceptor solvents such as acetone and acetonitrile, are capable to break the intermolecular hydrogen bonds between gelator molecules, consequently resulting in the transition from gel to solution.[13] Only in some rare cases, the participation of the solvent molecules leads to the formation of organogels,[14] or varies the pattern intermolecular interactions.[15]

It is well known that some heterocyclic compounds such as pyridine, quinoline, furan, thiophene, et al., can be protonated, thus organogels comprising these functional groups are proton-responsive accompanying with spectral or morphologic changes. For example, a 1,10-phenanthrolinene-appended cholesterol compound (**19,** Figure 6) was found to act as a proton-sensitive fluorescent gelator.[16] Gels of **19** show violet emission for most organic media, whereas, only the acetic acid gel shows a yellow emission. Fluorescence spectra were recorded for gels upon addition of TFA. As shown in Figure 6, the intensity of the violet emission at 396 nm decreased, whereas a yellow emission around 530 nm was newly generated, which is attributed to the **19**·H^+ species. An energy transfer process from **19** to **19**·H^+ in the gel phase was also proposed, based on the fact that, already in the presence of 0.2 equiv. of TFA the violet emission was quenched completely, whereas the intensity of the newly generated yellow emission subsequently increases up to 2.0 equiv. with increasing TFA concentration.

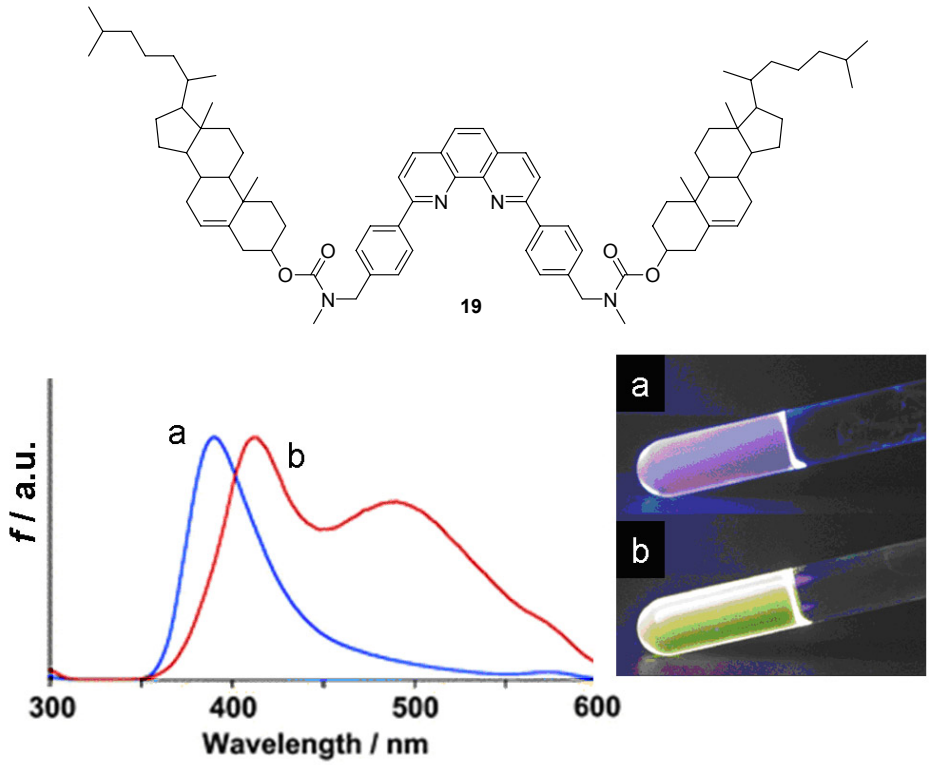

Figure 6. Proton-responsive gels based on 1,10-phenanthrolinene-appended cholesterol gelator **19**.

The spectra indicate fluorescent changes of **19** in the gel phase without (a) and with (b) TFA. The right side shows the gels under UV light. Reprinted with permission from ref. 16. Copyright Royal Society of Chemistry 2003.

Photo responsive organogel are mostly observed in azobenzene derivatives by *trans-cis* isomer transition upon photo irradiation,[17] or in photo induced ring-closing-opening derivatives such as spiropyran-containing [18] and dithienylethene[19] derivatives. Figure 7 gives some examples of photo responsive building blocks which are popular components of this class of organogelators. The substituents could be cholesterol derivatives, sugars, aliphatic alkyl chains, urea/imide units, or other function groups which are facile for the gel formation. Upon UV irradiation, the conformation of the molecules changes and consequently the aggregation of the molecules differs significantly, resulting in the sol-gel transition. The phase transition of sol-gel is governed by exposing the sample under UV/visible light irradiation or by heating/cooling process.[9, 34]

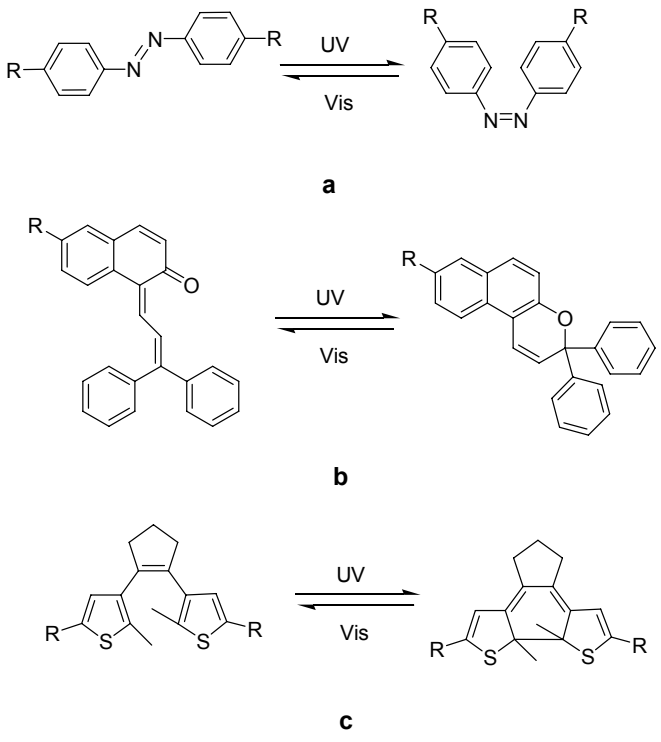

Figure 7. Some examples of photo responsive motif in organogelators: (a) azobenzene derivatives; (b) pyran derivatives and (c) dithienylethene derivatives.

With their remarkable thermo-reversibility, chemical /physical sensitivity, and diversity of nanostructures, organogels are potentially applicable in various fields, such as xerographic photoreceptors, [20] photorefractive materials, [21] bulk *p*-*n*-heterojunction solar cells,[22] light-responsive sensory systems,[23] as well as scaffolds for biomedicine.[24] The fibrous network of supramolecular gels and the sol-gel transformation properties have been used as templates to create inorganic nanotubes[25] and to assemble nanoparticles.[26] Most recently, the mixture of carbon nanotubes with an OPV based organogel was found to be superhydrophobic which appears promising for the application as water-resistant coatings.[27] To approach more exploitation of organogels new molecular structures with specific functionality are desired, and the self-organization behaviour of these molecules, and the chemical/physical properties of gels need to be understood in depth.

2.2 Dye Based Organogelators

There are many types of organogelators.[7, 28] One of the most simple structures in this family comes from fatty acid derivatives, such as 12-hydroxyoctadecanoic acid and its related salts, which are know for decades to create hardened materials from organic liquids by the formation of 3D networks like a "sponge".[29] Steroid /cholesterol based derivatives are also know to thicken aqueous salt solution resulting in thermotropic mesophases,[30] and the gelation of them can be extended to various organic liquid by proper structural functionalization.[31] Therefore, the Attachment of cholesterol moiety to functional molecules such as dyes, crow ethers, et al. is regarded as a straightforward strategy in the gelator design.[32] Other organogels from saccharide[33] and urea/amide derivatives [13] are also reported widely.

We emphasize here on dye-based organogels, because the fibers in these soft materials comprise specific π-electron interactions which offer interesting optical

and electronic properties.[34] In addition, the extended π-conjugated system of aromatic dyes provides self-assembly capabilities, by which various nanostructures can be created and be precisely controlled. There are many functionalized dyes which are reported to form organogels, such as porphyrins, phthalocyanines, phenylenevinylenes, perylenes, etc. The formation of the gels is typically related to a combination of π-π-stacking of aromatic moieties, plus at least one or more other interactions such as hydrogen bonding or metal coordination.

Porphyrin based gelators

Porphyrin based gelators have been extensively studied. For example, Shinkai's group reported a series of porphyrin derivatives that form organogels either in aqueous media or in organic solvents. Some of these gelators are designed by appending cholesterol moieties to the porphyrin, because the face to face π-π aggregation of the aromatic groups stabilizes the one-dimensional columnar packing of cholesterols.[35] Another important strategy is to introduce hydrogen bonding functionalities, such as amide and urea, onto the periphery of porphyrin molecules, by which the central dye aggregates are further reinforced by the hydrogen bonding interactions among amide or urea groups.[36] Recently, a new porphyrin based gelator was reported (**20**, Figure 8), in which polymerizable diacetylene units are covalently connected to the porphyrin core. The pre-aggregated fibrous supramolecular structures driven by π-π-stacking and H-bonding can act as photo-polymerization template. Upon photo-irradiation, highly elongated nanowires are formed by in-situ polymerization of diacetylene groups. As seen in Figure 8b and c, the polymerized fibers do not show any defect and resemble the pre-aggregated precursor.[37]

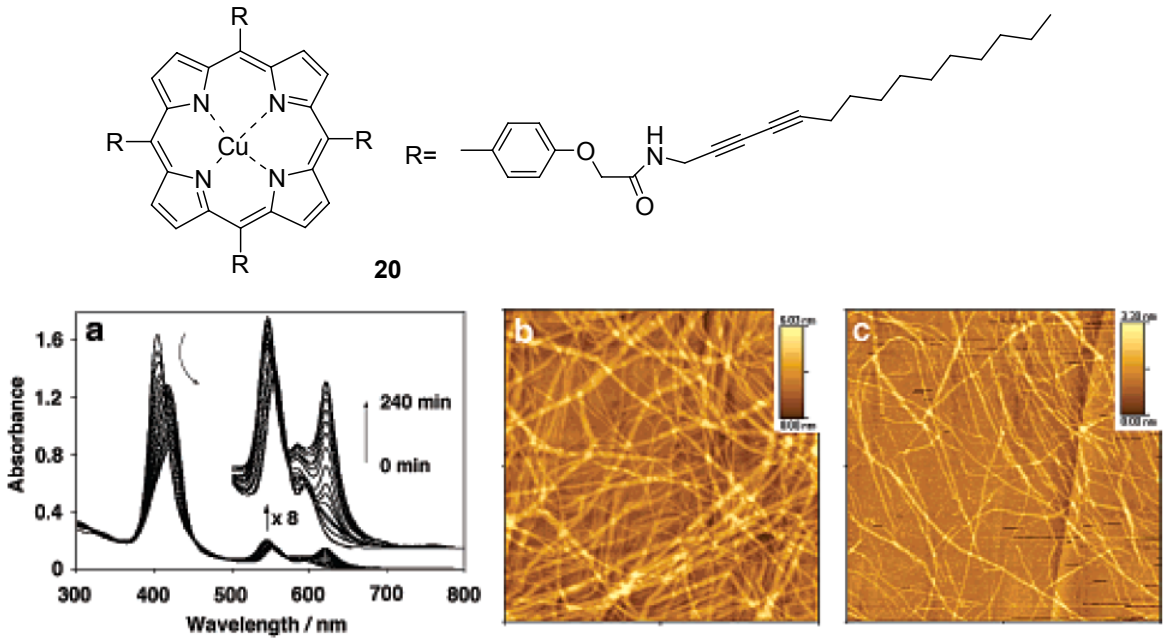

Figure 8. Molecular structure of porphyrin based gelator **20**. (a) Time dependence of the UV−vis spectral change of the decalin gel of **20** upon UV irradiation. AFM images of (b) the decalin gel of **20** and (c) the decalin gel of **20** after UV irradiation. Reprinted with permission from ref. 37. Copyright 2005 American Chemical Society.

OPV based gelators

Oligo(*p*-phenylenevinylene)s are a preferred class of π-conjugated dye molecules which show structure-dependent optical and electronic properties.[38] The first example of an OPV gelator was reported by Ajayaghosh's group, who found accidentally that OPV derivatives **21** having two hydroxymethyl groups and six dodecyloxy side chains can gelate hexane, cyclohexane, decane, toluene, et al.. The hydroxymethyl groups facilitate linear hydrogen-bonded polymeric structures, cooperating with π-stacking and van der Waals interactions, which result in lamellar ribbons and further entangled gel networks (Figure 9).[39] By tailoring the OPVs with different non-covalently interacting functional groups, a series of new photonically and electronically active supramolecular architectures were designed

and extensively studied in Ajayaghosh's lab, where very interesting scientific phenomena were explored on OPV based gelators, such as light emitting properties, donor-acceptor interactions, and chirality transfer.[40]

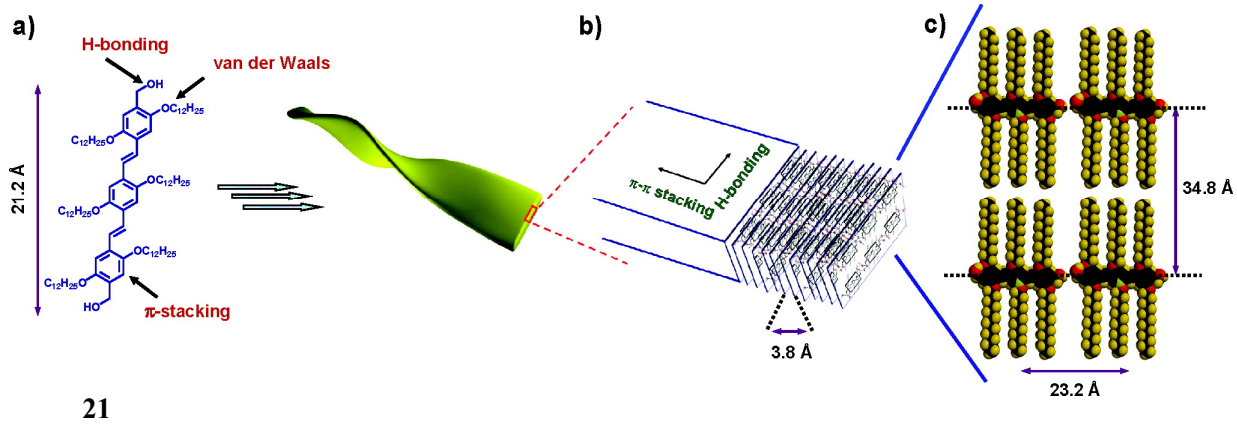

21

Figure 9. Schematic view of the lamellar packing of **21** in the gel state: (a) structure of **21**; (b) side view of the lamellar packing of the OPVs in a self-assembled tape; (c) top view of the molecular model of OPVs on a layer. Reprinted with permission from ref. 40. Copyright 2007 American Chemical Society.

Phthalocyanine based gelators

Nolte reported an organogel from a phthalocyanines dye (**22**) with four crown ether rings and periphery alkyl chains in chloroform upon aggregation.[41] TEM observation showed that the gel contains a network of fibers, which are built up of parallel fine strands from unitary molecular packing. When chiral chains are introduced, phthalocyanines **23** can also form gels in chloroform, and the chiral information transfers from the periphery tails to the aromatic center, which results in a right-handed helical molecular stacking. These structures, in turn, self-assemble to form coiled-coil aggregates with an overall left-handed helicity (A and B in Figure 10). Interestingly, addition of potassium ions to these fibers leaves the structures intact, but blocks the chiral transfer from the tails to the cores,

leading to loss of the helicity of the fibers (C and D). These tunable chiral materials have potential in optoelectronic applications and in sensor devices.

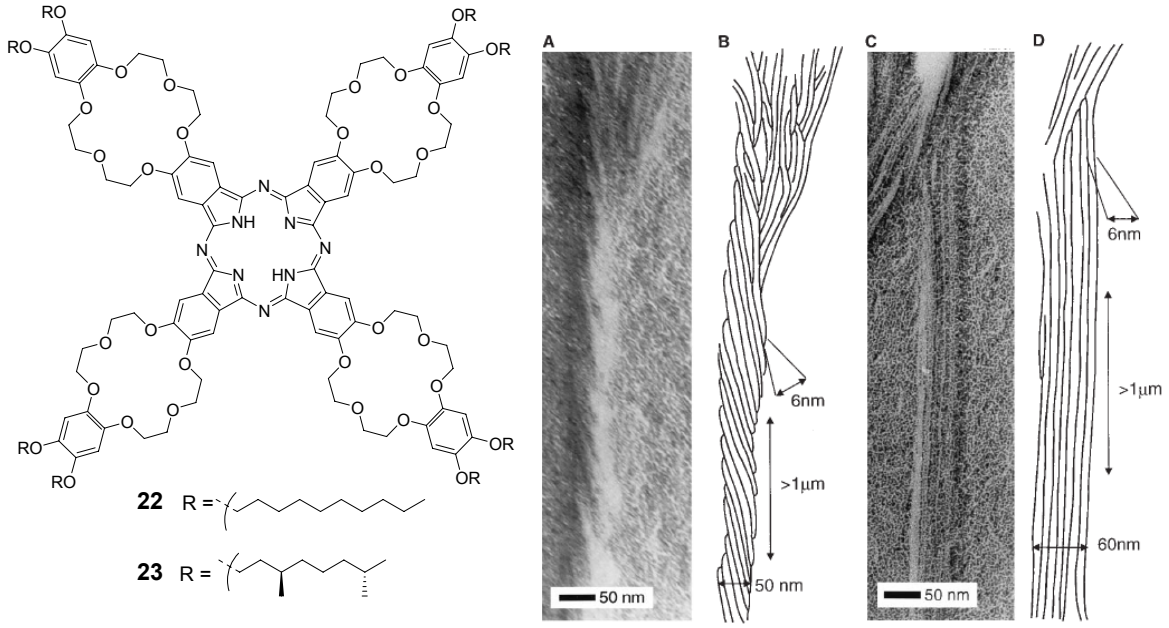

Figure 10. Phthalocyanine based gelators **22** and **23**. (A) TEM image of left-handed coiled-coil aggregates of **23** in chloroform. (B) Schematic representation of the helices in (A); (C) **23** formed non-helical rods in chloroform in the presence of KCl. (D) Schematic representation of the rods in (C). Reprinted with permission from ref. 41b. Copyright 1999 American Association for the Advancement of Science.

Perylene bisimide based gelators

Perylene bisimides are important and widely investigated dyes which serve as functional colorants and *n*-type semiconducting materials in various applications such as optical recording media, organic photo- and semiconductors, and solar cells.[42] However, with respect to their incorporation in organogels, only in 2004, Shinkai reported the first perylene bisimide based organogelator (**24**, Figure 11) which can partially gelate aromatic solvents such as benzene, toluene and *p*-xylene.

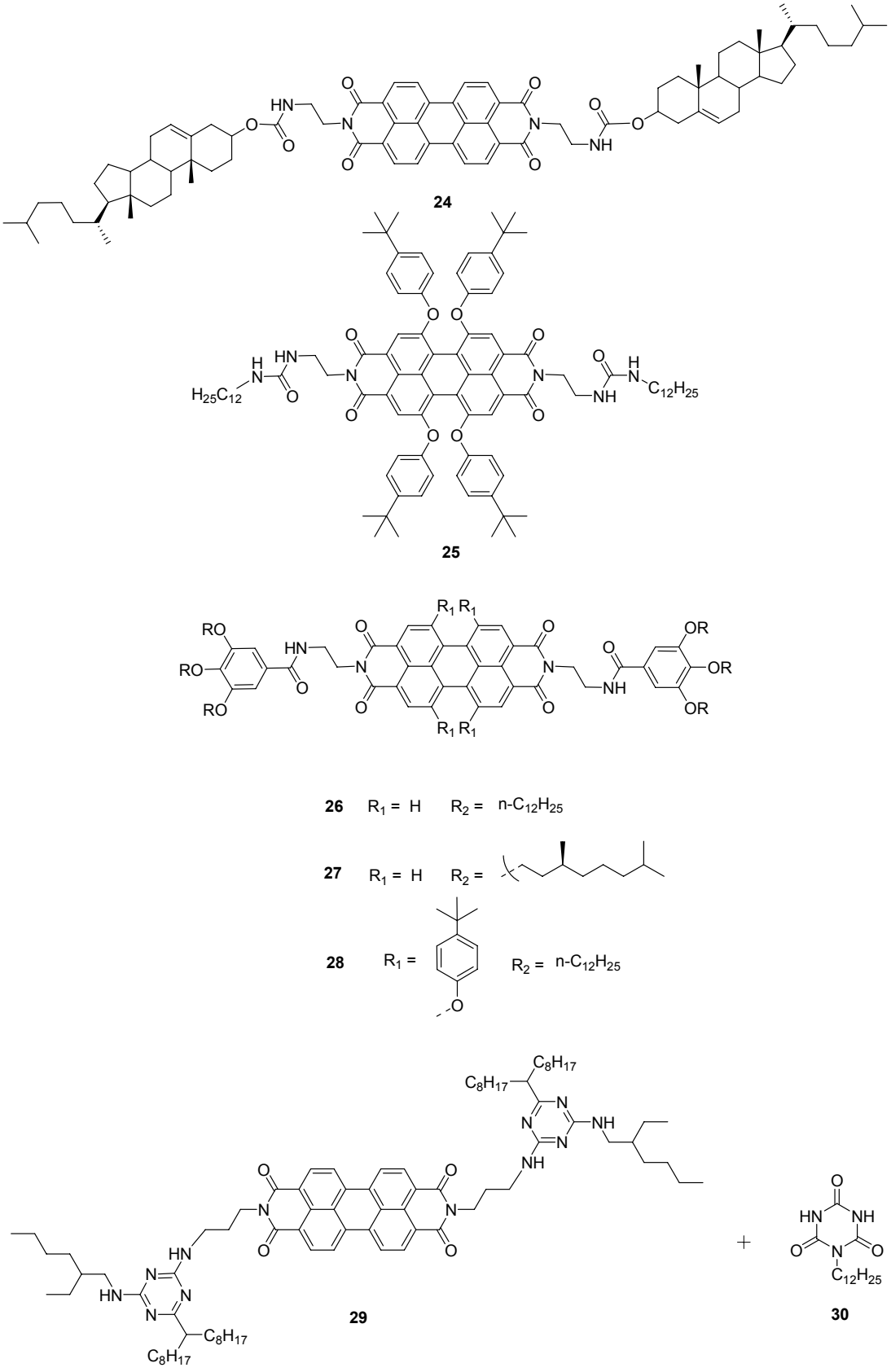

Figure 11. Perylene bisimides based organogelators

By adding alcoholic solvents, the solubility of **24** was increased and stable organogels can be created in various mixed solvents.[8] Shortly afterwards, Würthner's group reported on a urea-containing tetraphenoxy substituted perylene bisimides **25** which forms fluorescent organogels in toluene and tetrachloromethane through hydrogen-bonding and π-π-stacking interactions.[43] However, both of these two gelators can only gelate a limited range of solvents at high concentrations or low temperatures.

Subsequently Würthner and coworkers reported a more versatile PBI based gelator **26** in which amide groups were introduced to strengthen the dye packing by hydrogen bonds. The synergic interactions of π–π-interaction, hydrogen-bonding, and the van der Waals forces between the peripheral alkyl chains enforce the PBI self-assembly to form well-defined helical and red-colored H-type aggregates.[44] Based on the fact that gelator **26** is intrinsically achiral, the aggregated helical fibers adopt both right-handed and left-handed helicities. By virtue of exterior non-equilibrium forces such as chiral solvents, a single helicity can be generated. Furthermore, macroscopic alignment of the nanofibers is realized in the vortex flow upon magnetic stirring.[45]

Very interestingly, when the peripheral achiral alkyl chains of **26** were replaced by chiral ones, PBI **27** showed J-type aggregation behavior and black gels in various organic solvents. The significant changes in the optical properties originate from the subtle alteration of peripheral alkyl chains, in which the branches of the chain influence the packing behavior of the aromatic cores. This gelator could be applied in organogel/polymer system to generate donor-acceptor bulk heterojunction nanostructures suitable for light-induced charge generation and charge transport.[46]

The introduction of bulky phenoxy groups to the bay-area of PBIs results in the twist of PBI core, as a result the molecules, e.g. PBI **28**, become more crowded, and forms columnar J-aggregates in various apolar solvents such as toluene and methylcyclohexane by π-π interaction and hydrogen-bonding. Those aggregated

structures lack the capability to form a gel but form lyotropic mesophases at higher concentrations.[47] However, in some hydrogen-bond acceptor solvents such as acetone and dioxane, the participation of the solvent molecules in hydrogen bonding significantly reduced the aggregation propensity but enforced the gel formation at higher concentrations.

Most recently, Yagai's group developed melamine-linked PBIs which self-aggregate and co-aggregate with *N*-dodecylcyanurates through complementary triple hydrogen bonds (**29** and **30**, Figure 11). PBI **29** forms H-type aggregates by π–π interactions. These aggregates are disrupted by the addition of **30** to form new hydrogen-bonded aggregates (**29·30**). The resulting supramolecular polymers afford ribbon-like morphology in cyclic alkanes and rope-like morphology in acyclic alkanes to form gels.[48]

Other dye based gelator

There are many other dye based organogelators reported such as thiophene dyes,[49] azobenzene-based derivatives, [50] merocyanine dyes, triphenylenes [51] and hexabenzocoronenes.[52] It has been suggested that expected that these dye-based organogels should be applicable in various new fields such as molecular recognition, catalysis, nano-materials, etc.[34]

2.3 Supramolecular Chirality

Nature utilizes chiral species to realize specified function in complex systems. Precise recognition of small molecules by macromolecular building blocks triggers important functions such as chemical reactions, transport through membrane, vision, etc.. Therefore, molecular recognition has attracted considerable attention in supramolecular science with the goal to mimic biological functions.[53] Many

bio-macromolecules as well as synthetic small molecules are found to self-assemble spontaneously to form fibrous aggregates with helical structures. It appears that the helical morphology is a general motif for supramolecular aggregates.[54]

Many inherent chiral building blocks form helical fibrous superstructures with homo-chirality. Interestingly, supramolecular helicity has been developed from achiral molecules as well. Although the left-handed and right-handed helicities appear in equal amounts, by addition of non-racemic guests or application of external chiral forces, the chirality can be transferred to the aggregates, generating a preferential formation of one enantiomeric helical conformer.[55]

We will introduce briefly in this part some aspects of chiral nanofibers generated from achiral building blocks, such as the methodology on characterization, sign amplification, and chiral separation, based on some recent investigations in this field.

2.3.1 Characterization of Supramolecular Chirality

Chiral aggregates are commonly prepared from solutions by increasing the concentrations of the solutions of small molecule based supramolecular building blocks, the free molecules start to interact with each other form aggregate structures. When the solvents are evaporated, the morphology of the aggregates remain (or at least mostly remain) in the solid state, although the dimension might be enlarged because the fine fibers are often bundled together. To characterize chiral aggregate, skillsets have been developed both in solution and in solid state.

In solution

The interaction of two adjacent chromophores results in an exciton-coupled UV/Vis absorption spectrum, which typically differs from the one of non-interacting chromophores. In case where the two chromophores are oriented in

chiral fashion, an exciton-coupled CD spectrum is observed which is characterized by a bisignate Cotton effect. Based on exciton theory, extended helical aggregates of chromophores also give bisignate CD signal. Thus CD spectroscopy is by far the most powerful technique used to identify a helical arrangement of chromophores in solution.

Unfortunately, although CD spectroscopy is very convenient to assign the helical packing of chromophores for small aggregates in solution, CD spectra may be contaminated for larger aggregates by various artifacts. For example, macroscopic anisotropic orientation of chromophores can lead to CD signals that are not arising from chiral arrangements.[56] It was found that flow can induce macroscopic orientation of the supramolecular aggregates, and the orientation is dependent on the flow direction. Flow in a cuvette can arise during stirring, convection, or shaking. This is especially the case for extended nanofibers that consist of regularly arranged chromophores, which have high aspect ratios and are thus easily aligned by flow to give artifact CD signals.[54]

Now the question is how we can distinguish if a measured CD spectrum is real or not? Further, if the CD signal is contaminated partially by artifact, how can we extract the real CD from the observed data? Recently, Meijer and Schenning answered these questions by combining the CD and LD (linear dichroism) studies systemically to rule out the common artifacts:[54, 57]

(a) The LD spectrum should be recorded under the same conditions as the CD measurement. If the signal is non-zero in the chromophores' absorption region, this indicates the macroscopic alignment of the transition dipole moments of chromophores, which can result in CD artifacts; if no LD signal can be observed, one can rule out the macroscopic orientation of the aggregates and the observed CD spectrum should be real.

(b) Flow can be intentionally created in the cuvette while the CD spectra are measured to make a quick test if the CD spectrum is influenced. For example, the solution can be shacked, stirred with a magnetic bar (in both clockwise and anticlockwise directions), or the temperature of the solution can be altered to

create a slight convection. If these actions result in any changes in the intensity or shape of the CD signal, the possibility of CD artifact should be considered.

(c) Once a single-handed helical aggregate has been investigated, one can pursue with its opposite enantiomer: if a mirror-imaged CD spectrum is observed when the sample is measured under the same conditions, we can conclude that the CD signal is real, because CD artifacts arising from LD due to macroscopic alignment will not change sign for the enantiomeric sample.

Some of the supramolecular aggregates consist of helical fibers but do not show a Cotton effect. The reason is due to the presence of equal amounts of left- and right-handed helical aggregates. This situation is especially common for aggregates from achiral small molecular building blocks. In this case, it is possible to generate an observable CD sign by using the method of chiral induction (samples are given in following parts).[58] Chiral additives or a chiral environment (e. g., chiral solvents) may interact with the helical fiber or influence the self-assembly of the building blocks to afford helical assemblies that show CD signal.

Recently, cryo-TEM technique has been developed for studies of samples at cryogenic temperature to elucidate the helicity of the aggregates in solution state. Unlike other microscopic technology such as AFM, STM, and normal TEM, which can generate surface-induced artifact during drying or staining, cryo-TEM ensures fixation of the morphology of the structures in solution. Thus it would appear to be the microscopic method of choice for the characterization of helical nanofibers, although limitations are present by the difficult samples preparation and less common protocols for non-aqueous media.[59]

In solid state

Compared to spectroscopy, microscopic analysis of aggregates is more straightforward to determine the helical structures. Parameters such as length, width, helical pitch, and handedness of the helices can be easily visualized. In

particular, a racemic sample which forms helical fibers but is not CD active can still be identified by microscopy. Individual fiber which is either in left-handed or in right-handed helicity can be investigated. The most common used microscopic analyses are AFM, TEM, and SEM.

AFM measures samples by deposition of aggregates from the solution onto a smooth substrate by spin-coating or drop-casting. In order to rule out the possibility that the helical aggregates are formed by the template effect of the substrate during drying on the surface, the same sample can be applied on different substrates such as HOPG (highly ordered pyrolytic graphite), silicon wafer and gold. If similar morphology can be observed from different substrates, it is a good indication that the structures obtained on the surface are closely related to those in solution.

However, sometimes aggregates that give strong CD signals in solution and are presumably helical fail to display helical features by AFM. The reasons might be (a) the helical structure is lost upon deposition from solution onto a surface as mentioned above; (b) many soluble nanofibers are jacketed by long, possibly disordered solubilizing chains that effectively shield the helical backbone of the helix from view by the AFM tip; (c) the helical aggregates are insufficiently distinct which is bellower than the instrumental resolution.[54, 60]

TEM allows visualization of helicity by deposition of aggregate solutions or suspensions onto a supporting film or grid (such as copper grid) to give two-dimensional images. In contrast, SEM is more convenient to measure dry gels directly and give three-dimensional images.[61]

Other technology such as X-ray diffraction can also be applied on some more crystal-like helical aggregate to give precise data, such as distance of the individual chromophores, which are not easily observed by microscopy. However, X-ray diffraction data are often less sufficient in quality to deduce a helical architecture since it requires that the nanofibers have high intramolecular order and uniaxial orientation in the bulk. Thus X-ray is often used as a supplementary method to spectroscopy and microscopy on helical nanofibers.[54]

2.3.2 Amplification and Formation of Homochiral Aggregates.

Chirality Amplification

A racemic mixture of opposite handed helical nanofibers can be obtained when achiral building blocks are utilized in the self-assembly process. Although helical fibers can be observed by microscopy, the system is overall CD silent because the two handedness of helicity are equal in amount. Interestingly, when a substoichiometric amount of chiral monomers are co-assembled with achiral counterparts, nanofibers of a single handedness can form owing to a chiral amplification phenomenon called "sergeants and soldiers principle", wherein the assembly of a large amount of achiral molecules (soldiers) is controlled by a few chiral molecules (sergeants).[62]

An example for this concept was given by Ishi-I and coworkers (Figure 12).[63] Disk-shaped triazine triamides self-assemble to from columnar helical aggregates through π–π stacking and hydrogen-bonding interactions. When the achiral triazine triamide (soldier component **31**) is mixed with a tiny amount of the chiral triazine triamide (sergeant component **32**), control of the intrinsic supramolecular helicity of the self-assembled soldier component by the sergeant component leads to chiral amplification and formation of a pseudo-enantiomeric aggregate with only one handedness of the helix. The chiral amplification of the aggregate system was monitored by CD spectroscopy. In octane solution, the Cotton effects of the mixture of **31** and **32** are observable in the presence of a tiny amount of chiral component **32** (0.01 mol %). With only 1 mol % of **32** the magnitude of CD intensity is as strong as that of the diastereomeric aggregate system composed only of **32**, which indicates the chiral amplification does occur with preferential formation of one of the two helical aggregates.

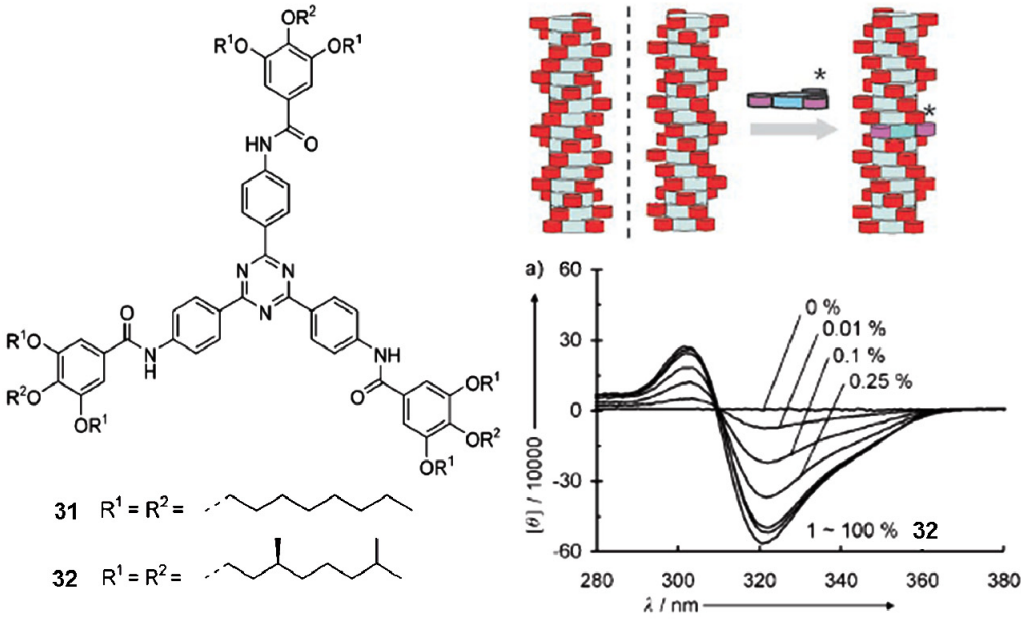

Figure 12. Schematic explanation of chiral amplification for achiral molecule **31** in the presence of tiny amount of chiral **32**, and the corresponding CD spectra of **31** upon addition of various amount of **32**. Reprinted with permission from ref. 63. Copyright 2006 WILEY-VCH Verlag GmbH & Co. KGaA, Weinheim.

In another approach, chiral additives of different molecular structures were found to affect the aggregate morphology and to direct preferential helicity[57, 64] Berlepsch and coworkers reported that carbocyanine dye based J-aggregates were enantiomerically enriched by the addition of chiral alcohols, i.e., (*R*)-2-octanol and (*S*)-2-octanol. As shown in Figure 13, the CD signal increases by a factor of about 100 when the chiral (*R*)-2-octanol is added to an aggregated solution in water. The signature of the CD spectra reverse if the enantiomeric (*S*)-2-octanol is used instead. This reversal of signature reveals a correlation between the chirality of the added alcohol and the aggregates' CD spectra, which supports the concept of controlling the chirality of the dye aggregates by coordination of chiral additives.[65]

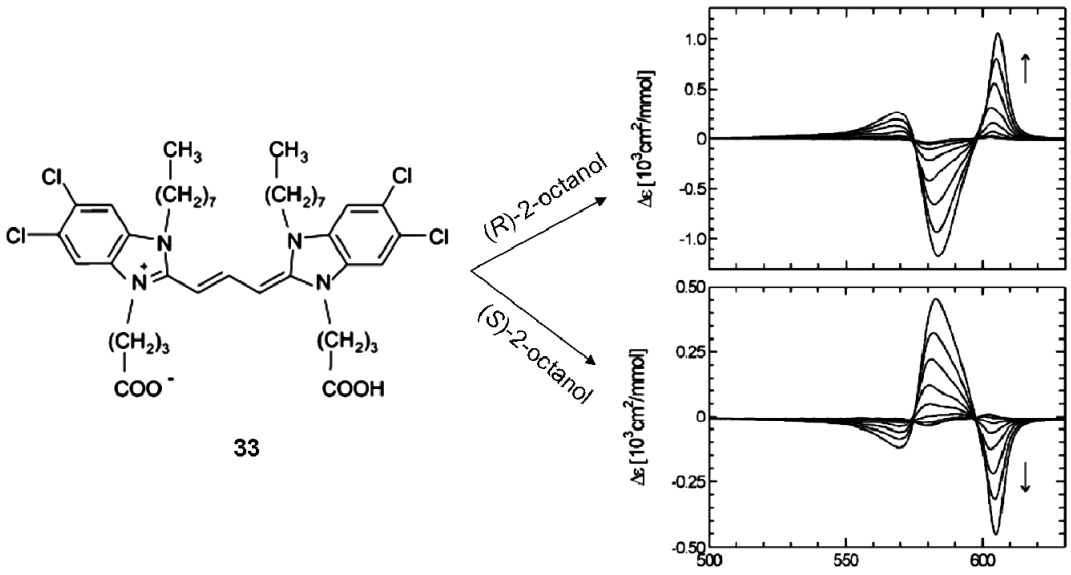

Figure 13. Chirality selection of carbocyanine dye **33** by addition of chiral alcohols in aqueous solution. Reprinted with permission from ref. 65. Copyright 2003 American Chemical Society.

Dähne's and kirstein's group reported on formation of chiral J-aggregates from achiral cyanine dyes, in which the enantiomeric symmetry is spontaneously broken at a primary state of nucleation. The mechanism was suggested that, during the dissolve process of the materials into solution, a certain excess of one enantiomer of the dye is found at the surface of the crystallites, small nuclei are formed from the surface molecules which are dissolved first, and the enantiomeric excess at the crystal surface might be transferred to the aggregate morphology. Once generated, the preferred handedness is templated to the J-aggregates during the period of growth to micrometer-long bundles of the aggregates. In contrast to other chiral supramolecular system we discussed above, this observation of asymmetric aggregates generation is not initiated by any chiral auxiliaries.[66]

Formation of Homochiral Aggregates by Symmetry Breaking

It is an interesting phenomenon that homochiral structures can be obtained by self-assembly from achiral molecular building units. Because self-aggregation typically affords both left-handed and right-handed helicities in equal amount, the

origin of symmetry-breaking into one-handed helicity is still a matter of controversial debate.

Ribó et al. reported on the self-assembly of achiral porphyrin dye **34** into homochiral J-aggregates. The chirality sign of these aggregates can be controlled by vortex motion, caused by either stirring or rotary evaporation. This phenomenon has been explained as spontaneous chiral symmetry breaking. The possibility that the weak stirring forces cause energy differences between enantiomers were ruled out. It was found that the chiral vortex can only act at the meso-scale level, that is, after the kinetically controlled growth of the nucleating supramolecular structure. The results suggest an enhancing effect of stirring upon spontaneous symmetry-breaking processes in the diffusion-limited generation of the high-molecular-weight homoassociates (Figure 14).[67]

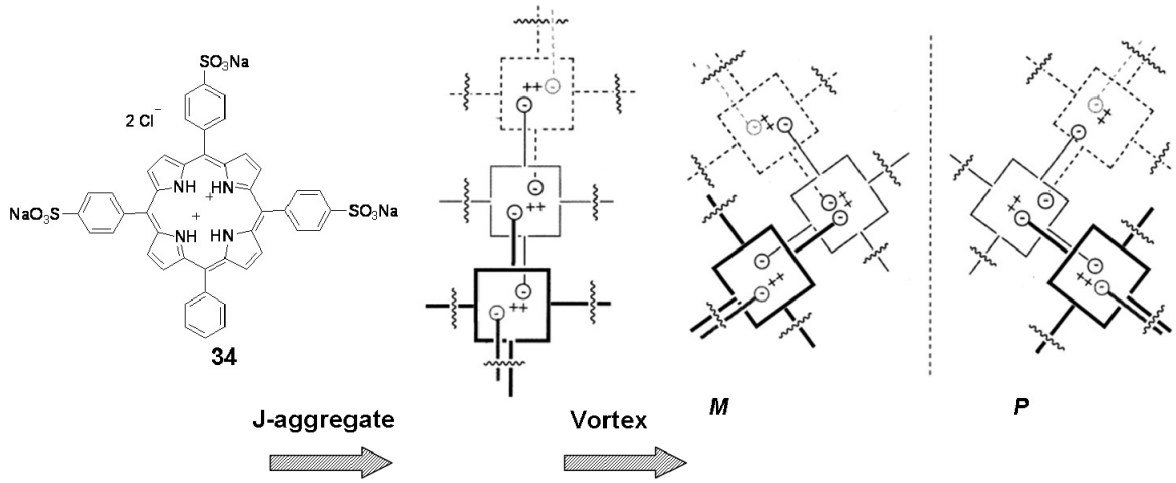

Figure 14. Molecular structure of **34** and schematic illustration of the J-aggregate state, as well as the *M* and *P* conformational equilibrium that is influenced by vortex motions. Reprinted with permission from ref. 67b. Copyright 2001 WILEY-VCH Verlag GmbH & Co. KGaA, Weinheim.

More recently, Aida and co-workers reported their findings that spin-coated films of dendritic zinc porphyrin J-aggregates can chiroptically memorize the spinning direction.[68] When a solution of **35** in chloroform was spin-coated in a clockwise

direction, the resulting film displayed an intense bisignate CD spectrum. On the other hand, spin-coating of the same solution in an anticlockwise direction resulted in the appearance of a mirror image CD spectrum (Figure 15). Although the pressure of a CD artifact by LD has been excluded in the original paper (intensities of the CD band did not change upon rotation the samples along an axis perpendicular to the substrate surface), more recent result of the same group point at a macroscopic alignment effect (see next paragraph).[69]

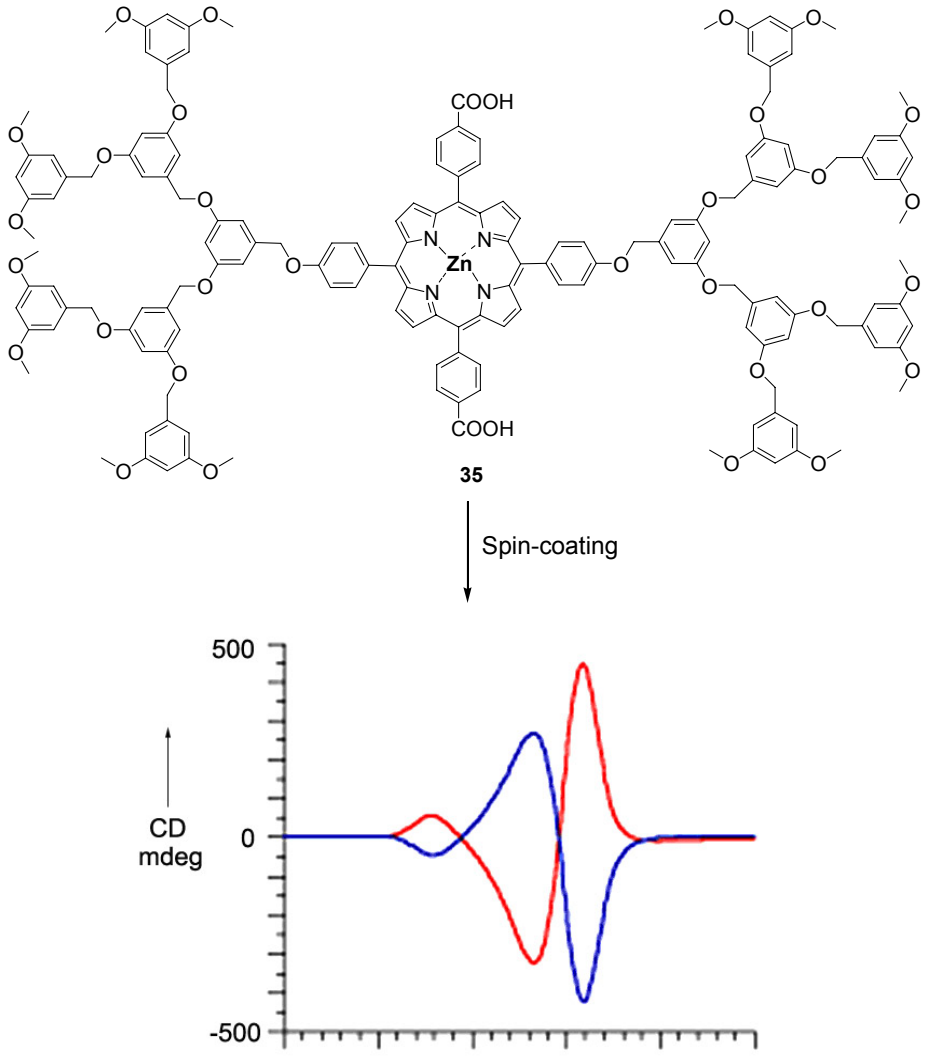

Figure 15. Molecular structure of **35** and the CD spectra of thin films prepared by spin-coating a solution of **35** in chloroform in the clockwise (red curves) and counterclockwise (blue curves) directions. Reprinted with permission from ref. 68. Copyright 2004 WILEY-VCH Verlag GmbH & Co. KGaA, Weinheim.

Macroscopic Alignment

The occurrence of strong bisignate CD signals up macroscopic alignment of nanofibers in solution was recently reported by the groups of Aida and Meijer (Figure 16). [69] Achiral zinc porphyrin dendrimer **36** forms J-aggregates through π–π interactions and hydrogen-bonding to give a supramolecular polymer. A hydrocarbon solution of **36** without stirring was CD-silent, while an intense bisignate CD signal appeared under the influence of vortex stirring. When the solution was stirred, it provided intense CD signals at the Soret absorption band arising from J-aggregated zinc porphyrin. Reversal of the stirring direction resulted in an inversion of the CD sign. The sample lost all the CD activity when the rotary stirring was stopped.

Similar phenomena were also observed for the achiral OPV derivatives **37** by Meijer and coworkers. They pointed out that the appearance of CD signals in solutions of achiral assemblies can be observed even in unstirred solution when the assemblies reach a certain length. The CD responses are a consequence of partial alignment of the fibers owing to the convective flow which is enhanced by altering the temperature or simply shaking the solution.[70]

In both studies, the observed bisignate CD effect cab be explained by the vortex-flow induced macroscopic alignment of the nanofibers These studies showed that various fibrous supramolecular assemblies can be partially oriented in fluid, nonviscous media by convective flow, shaking, or stirring. Macroscopic alignment of the fibers is able to afford or to modify a circular dichroism signal. These results are therefore significant for anyone working on self-assembled systems in which (partial) alignment arising from boundary conditions and flows may be common.[71]

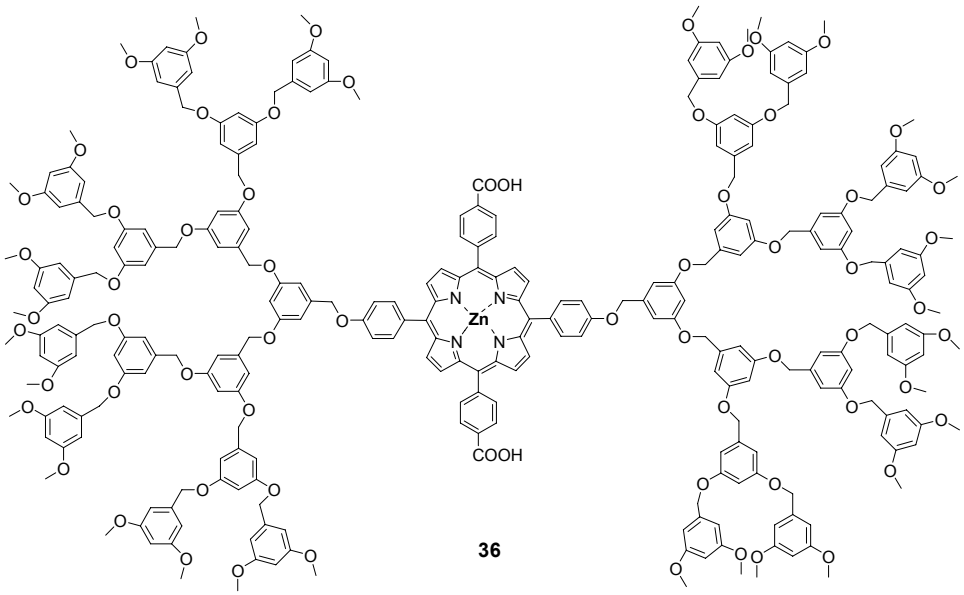

36

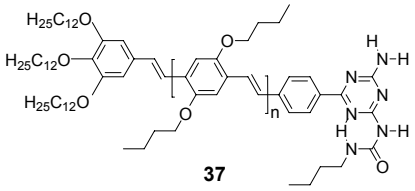

37

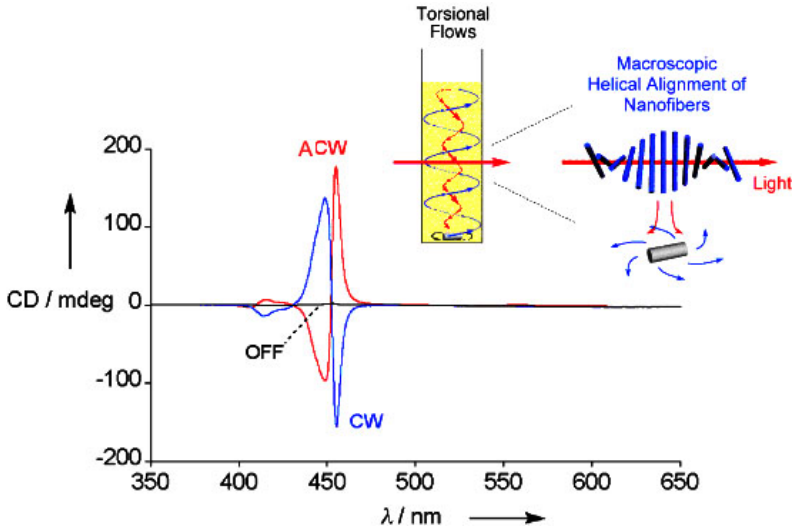

Figure 16. Molecular structures of **36** and **37**. Circular dichroism (CD) spectra of a benzene solution of assemblies of **36** upon rotary stirring in clockwise (CW, blue curve) and anticlockwise (ACW, red curve) directions, and without stirring (OFF, black curve). The inset shows a schematic illustration of torsional flows and macroscopic helical alignment of nanofibers generated upon anticlockwise rotary stirring. Reprinted with permission from ref. 69. Copyright 2008 WILEY-VCH Verlag GmbH & Co. KGaA, Weinheim.

2.4 References and Notes

1 N. M. Sangeetha, U. Maitra, *Chem. Soc. Rev.* **2005**, *34*, 821-836.

2 D. Jordon Lloyd, *Colloid Chemistry*; Alexander, J., Ed.; The Chemical Catalog Co.: New York, 1926; Vol. 1, p 767.

3 D. J. Abdallah, R. G. Weiss, *Adv. Mater.* **2000**, *12*, 1237-1247.

4 J. H. van Esch and B. L. Feringa, *Angew. Chem. Int. Ed*. **2000**, *39*, 2263-2266.

5 H. Maeda, *Chem. Eur. J.,* **2008**, *14*, 11274-11282.

6 L. L. Hench, J. K. West, *Chem. Rev*. **1990**, *90*, 33-72.

7 P. Terech, R. G. Weiss, *Chem. Rev.* **1997**, *97*, 3133-3159.

8 K. Sugiyasu, N. Fujita, S. Shinkai, *Angew. Chem. Int. Ed.* **2004**, *43,* 1229-1233.

9 *Supramolecular Dye Chemistry*, F. Würthner, Ed., *Top Curr Chem* 2005, **258**.

10 (a)U. Maitra, P. V. Kumar, N. Chandra, L. J. D'Souza, M. D. Prasanna, A. R. Raju, *Chem. Commun.* 2009, 595-596; (b) P. Babu, N. M. Sangeetha, P. Vijaykumar, U. Maitra, K. Rissanen, A. R. Raju, *Chem. Eur. J.* **2003**, *9*, 1922-1932.

11 K. Murata, M. Aoki, T. Nishi, A. Ikeda, S. Shinkai, *Chem. Commun.* **1991**, 1715-1718.

12 H.-J. Kim, J.-H. Lee, M. Lee, *Angew. Chem. Int. Ed*. **2005**, *44*, 5810-5814.

13 F. Fages, F. Vögtle, M. Žinić, *Top Curr Chem* **2005**, *256*, 77-131.

14 X.-Q. Li, X. Zhang, S. Ghosh, F. Würthner, *Chem. Eur. J.* **2008**, *14*, 8074-8078.

15 M. Kaftory, M. Kapon, M. Botoshansky, *Chem. Mater.* 1994, 6, 1245-1249

16 K. Sugiyasua, N. Fujitaa, M. Takeuchia, S. Yamadab, S. Shinkai, *Org. Biomol. Chem.* **2003**, *1*, 895-899.

17 (a) K. Murata, M. Aoki, T. Nishi, A. Ikeda, S. Shinkai, *J. Chem. Soc. Chem. Commun.* **1991***,* 1715-1718; (b) K. Murata, M. Aoki, T. Suzuki, T. Hrada, H. Kawabata, T. Komori, F. Ohseto, K. Ueda, S. Shinkai, *J. Am. Chem. Soc.* **1994**, *116*, 6664-6676; (c) M. De Loos, J. Van Esch, R. M. Kellogg, B. L. Feringa, *Angew. Chem. Int. Ed*. **2001**, *40*, 613-616. (d) M. Moriyama, N. Mizoshita, T. Yokota, K. Kishimoto, T. Kato, Adv. Mater. **2003**, *15*, 1335-1338.

18 (a) H. Hachisako, H. Ihara, T. Kamiya, C. Hirayama, K. Yamada, *Chem. Commun.* **1997**, 19-20; (b) A. Schumburo, M. C. Biewer, *Chem. Mater.* **2002**, *14*, 3745-3750.

19 (a) J. J. D. De Jong, L. N. Lucas, R. M. Kellogg, J. H. Van Esch, B. L. Feringa, *Science* **2004**, *304*, 278-281; (b) M. Akazawa, K. Uchida, J. J. D. de Jong, J. Areephong, M. Stuart, G. Caroli, W. R. Browne, B. L. Feringa, *Org. Biomol. Chem*. 2**008**, *6*, 1544-1547.

20 K.-Y. Law, *Chem. Rev*. **1993**, *93*, 449-486.

21 F. Würthner, R. Wortmann and K. Meerholz, *ChemPhysChem* **2002**, *3*, 17-31.

22 C. J. Brabec, N. S. Sariciftci and J. C. Hummelen, *Adv. Funct. Mater.* **2001**, *11*, 15-26.

23 (a) D. T. McQuade, A. E. Pullen and T. M. Swager, *Chem. Rev*. **2000**, *100*, 2537-2574; (b) T. M. Swager, *Acc. Chem. Res*. **1998**, *31*, 201-207.

24 S. Murdan, G. Gregoriadis, A. T. Florence, *Eur. J. Pharm. Sci.***1999**, *8*, 177-186.

25 J. H. Jung, S. Shinkai, *Top Curr Chem* **2004**, *248,* 223-260.

26 (a) B. Simmons, S. Li, V. T. John, G. L. McPherson, C. Taylor, D. K. Schwartz, K. Maskos, *Nanoletters* **2002**, *2*, 1037-1042; (b) M. Kimura, S. Kobayashi, T. Kuroda, K. Hanabusa and H. Shirai, *Adv. Mater*. **2004**, *16*, 335-338.

27 S. Srinivasan, V. K. Praveen, R. Philip, A. Ajayaghosh, *Angew. Chem. Int. Ed*. **2008**, *47*, 5750-5754.

28 L. A. Estroff, A. D. Hamilton, *Chem. Rev*. **2004**, *104*, 1201-1217.

29 (a) G. W. Fiero, *J. Am. Pharm. Assoc.* **1940**, *29*, 502; (b) C. J. Boner, *Manufacture and Application of Lubricating Greases* Reinhold Publishing Corp.: New York, 1960.

30 S. Hoffmann, *Mol. Cryst. Liq. Cryst.* **1984**, *110*, 277-292.

31 (a) Y.-C. Lin, B. Kachar, R. G. Weiss, *J. Am. Chem. Soc.* **1989**, *111*, 5542-5551; (b) R. Mukkamala, R. G. Weiss, *Langmuir* **1996**, *12*, 1474-1482; (c)L. Lu, T. M. Cocker, R. E. Bachman, R. G. Weiss, *Langmuir* **2000,** *16,* 20-34.

32 S. Shinkai, K. Murata, *J. Mater. Chem.* **1998**, *8*, 485-495.

33 O. Gronwald, S. Shinkai, *Chem. Eur. J.* **2001**, *7*, 4328-4334.

34 T. Ishi-I, S. Shinkai, *Top Curr Chem* 2005, **258**, 119-160.

35 H. J. Tian, K. Inoue, K. Yoza, T. Ishi-i, S. Shinkai, *Chem. Lett*. **1998**, 871-872.

36 (a) M. Shirakawa, S. Kawano, N. Fujita, K. Sada, S. Shinkai, *J. Org. Chem.* **2003**, *68*, 5037-5044; (b) M. Shirakawa, N. Fujita, S. Shinkai, *J. Am. Chem. Soc.* **2003**, *125*, 9902-9903; (c) T. Kishida, N. Fujita, K. Sada, S. Shinkai, *Chem. Lett.* **2004**, *33*, 1002-1003; (d) T. Kishida, N. Fujita, K. Sada, S. Shinkai, *J. Am. Chem. Soc.* **2005**, *127*, 7298-7299.

37 M. Shirakawa, N. Fujita, S. Shinkai, *J. Am. Chem. Soc.* **2005**, *127*,4164-4165.

38 (a) B. Strehmel, A. M. Sarker, J. H. Malpert, V. Strehmel, H. Seifert, D. C. Neckers, *J. Am. Chem. Soc.* **1999**, *121*, 1226-1236; (b) H. Meier, *Angew. Chem., Int. Ed.* **2005**, *44*, 2482-2506.

39 A. Ajayaghosh, S. J. George, *J. Am. Chem. Soc.* **2001**, *123*, 5148-5149.

40 A. Ajayaghosh, V. K. Praveen, *Acc. Chem. Res.* **2007**, *40*, 644-656.

41 (a) C. F. van Nostrum, S. J. Picken, A.-J. Schouten, R. J. M. Nolte, *J. Am. Chem. Soc.* **1995**, *117*, 9957-9965; (b) H. Engelkamp, S. Middelbeek, R. J. M. Nolte, Science, 1999, 284, 785-787.

42 F. Würthner, *Chem. Commun.* **2004**, 1564-1579.

43 F. Würthner, B. Hanke, M. Lysetska, G. Lambright, G. S. Harms, *Org. Lett.* **2005**, *7*, 967-970.

44 X.-Q. Li, V. Stepanenko, Z. Chen, P. Prins, L. D. A. Siebbeles, F. Würthner, *Chem. Commun.* **2006**, 3871-3873.

45 S. Ghosh, X.-Q. Li, V. Stepanenko, F. Würthner, *Chem. Eur. J.* **2008**, *14*, 11343-11357.

46 (a) F. Würthner, C. Bauer, V. Stepanenko, S. Yagai, *Adv. Mater.* **2008**, *20*, 1695-1698. (b) A. Wicklein, S. Ghosh, M. Sommer, F. Würthner, M. Thelakkat, *ACS Nano* **2009**, *3*, 1107-1114.

47 X.-Q. Li, X. Zhang, S. Ghosh, F. Würthner, *Chem. Eur. J.* **2008**, *14*, 8074-8078.

48 (a) S. Yagai, Y. Monma, N. Kawauchi, T. Karatsu, A. Kitamura, *Org. Lett.* **2007,** *9,* 1137-1140; (b) T. Seki, S. Yagai, T. Karatsu, A. Kitamura, *J. Org. Chem*.

2008, *73*, 3328-335.

49 S.-i. Kawano, N. Fujita, S. Shinkai, *Chem. Eur. J.,* **2005**, *11*, 4735-4742.

50 J. Mamiya, K. Kanie, T. Hiyama, T. Ikeda, T. Kato, *Chem. Commun.* **2002**, 1870-1871.

51 M. Ikeda, M .Takeuchi, S. Shinkai, *Chem. Commun.* **2003**, 1354-1355.

52 X. Dou, W. Pisula, J. Wu, G. J. Bodwell, K. Müllen, *Chem. Eur. J.* **2008**, *14*, 240-249.

53 R. F. Service, *Science* **2005**, *309*, 95-95.

54 C. C. Lee, Christophe. Grenier, E. W. Meijer, A. P. H. J. Schenning, *Chem. Soc. Rev.* **2009**, *38*, 671-683, and the references thereby.

55 K. Maeda, E. Yashima, *Top Curr Chem* **2006**, *265*, 47-88.

56 J. Schellman, H. P. Jensen, *Chem. Rev.* **1987***, 87,* 1359-1399.

57 S. J. George, Ž. Tomović, M. M. J. Smulders, T. F. A. de Greef, P. E. L. G. Leclère, E. W. Meijer, A. P. H. J. Schenning, *Angew. Chem. Int. Ed.* **2007**, *46*, 8206-8211.

58 A. R. A. Palmans, E. W. Meijer, *Angew. Chem., Int. Ed.* **2007**, *46*, 8948-8968, and references therein.

59 H. Cui, T. K. Hodgdon, E. W. Kaler, L. Abezgauz, D. Danino, M. Lubovsky, Y. Talmon, D. Pochan, *Soft Matter.* **2007**, *3*, 945-955.

60 P. Jonkheijm, F. J.M. Hoeben, R. Kleppinger, J. van Herrikhuyzen, A. P. H. J. Schenning, E. W. Meijer, *J. Am. Chem. Soc.* **2003**, *125*, 15941-15949.

61 T. Yamamoto, T. Fukushima, A. Kosaka, W. Jin, Y. Yamamoto, N. Ishii, T. Aida, *Angew. Chem., Int. Ed.* **2008**, *47*, 1672-1675.

62 (a) M. M. Green, M. P. Reidy, R. J. Johnson, G. Darling, D. J. O'Leary, G. Wilson, *J. Am. Chem. Soc.* **1989**, *111*, 6452-6454; (b) M. M. Green, J.-W. Park, T. Sato, A. Teramoto, S. Lifson, R. L. B. Selinger, J. V. Selinger, *Angew. Chem., Int. Ed.* **1999**, *38*, 3138-3154; (c) A. Ajayaghosh, R. Varghese, S. J. George, C. Vijayakumar, *Angew. Chem. Int. Ed.* **2006**, *45*, 1141-1144; (d) T. E. Kaiser, V. Stepanenko, F. Würthner, *J. Am. Chem. Soc.* **2009**, *131*, 6719-6732.

63 T. Ishi-i, R. Kuwahara, A. Takata, Y. Jeong, K. Sakurai, S. Mataka, *Chem. Eur.*

J. **2006**, *12*, 763-776.

64 H. Fenniri, B. Deng, E. Ribbe, *J. Am. Chem.Soc.* **2002**, *124*, 11064-11072.

65 H. von Berlepsch, S. Kirstein, C. Böttcher, *J. Phys. Chem. B* **2003**, *107*, 9646-9654.

66 (a) U. De Rossi, S. Dähne, S. C. J. Meskers, H. P. J. M. Deckers, *Angew. Chem. Int. Ed.* **1996**, *35*, 760-763; (b) A. Pawlik, S. Kirstein, U. De Rossi, S. Dähne, *J. Phys. Chem. B* **1997**, *101*, 5646-5651; (c) C. Spitz, S. Dähne, *J. Phys. Chem. B* **2000**, *104*, 8664-8669; (d) S. Kirstein, H. von Berlepsch, C. Böttcher, C. Burger, A. Ouart, G. Reck, S. Dähne, *ChemPhysChem*, **2000**, *3*, 146-150.

67 (a) J. M. Ribó, J. Crusats, F. Sagues, J. M. Claret, R. Ruvires, *Science* **2001**, *292*, 2063-2066; (b) R. Rubires, J.-A. Farrera, J. M. Ribó, *Chem. Eur. J.* **2001**, *7*, 436-446.

68 T. Yamaguchi, T. Kimura, H. Matsuda, T. Aida, *Angew. Chem., Int. Ed.* **2004**, *43,* 6350-6355.

69 A. Tsuda, Md. A. Alam, T. Harada, T. Yamaguchi, N. Ishii, T. Aida, *Angew. Chem. Int. Ed.* **2007**, *46*, 8198-8202.

70 M. Wolffs, S. J. George, Ž. Tomović, S. C. J. Meskers, A. P. H. J. Schenning, E. W. Meijer, *Angew. Chem. Int. Ed.* **2007**, *46*, 8203-8205.

71 G. P. Spada, *Angew. Chem. Int. Ed.* **2008**, *47*, 636-638.

Chapter 3

Functional Organogels from Highly Efficient Organogelator based on Perylene Bisimides

3.1 Introduction

In recent years, significant efforts have been devoted toward well-organized π-conjugated organic materials because proper ordering of the functional molecular building blocks is essential for the realization of organic electronic and photonic materials with competitive performance to their inorganic counterparts.[1-3] Among the diverse areas of applications, those seem to be particularly attractive for π-functional organic compounds that rely on multifunctionality emerging from mixtures of molecular building blocks, which provide different functionalities. Typical examples are given by photofunctional composites as applied in xerographic photoreceptors,[4] photorefractive materials,[5] bulk *p*-*n*-heterojunction solar cells[6] as well as light-responsive sensory systems.[7] From the conceptual point of view, dye-based organogels[8] should be highly promising materials for all of these photofunctional applications if one or even more desired functionalities could be provided by the organogelator and additional ones are embedded in the gelated material.[9]

However, towards this goal, robust organogelators are needed that are able to gelate a broad variety of media (e.g., solvents, liquid crystals, etc.) and exhibit favourable functional properties. In recent years such versatile organogelators have been derived from several strongly absorbing as well as *p*-type semiconducting

π-systems, including porphyrins, phthalocyanines, oligophenylenevinylenes and oligothiophenes.[10,11] However, for their *n*-type counterparts no organogelators could be obtained to date that can gelate a broad range of solvents of different polarity. Perylene bisimide (PBI) based organogelators appear to be the most promising candidates for this purpose due to their unrivalled combination of absorption, emission and n-type semiconducting properties.[12] However, all of the recently reported PBI organogelators can only gelate few solvents or optimized solvent mixtures and, accordingly, lack the desired versatility.[13] In this chapter, we describe a PBI organogelator with extended gelation capabilities and discuss its optical and semiconducting properties.

3.2 Result and discussion

3.2.1 Synthesis and Gelation Test

As shown in Scheme 1, perylene bisimide **3** was synthesized by imidisation of

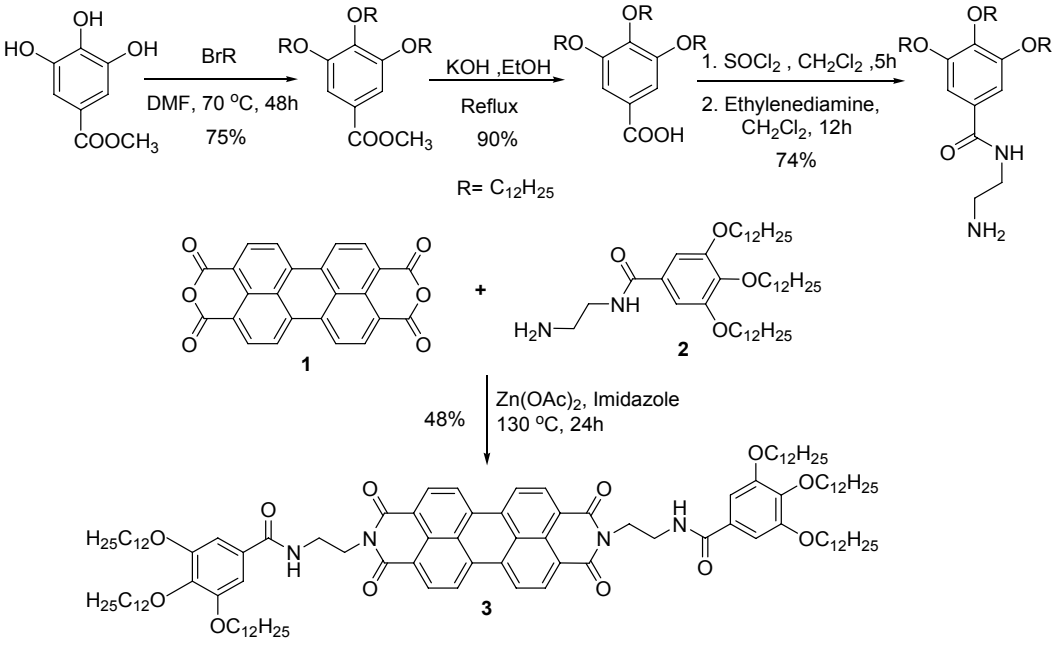

Scheme 1. Synthesis of PBI organogelator **3**.

perylene tetracarboxylic acid bisanhydride **1** with aminoethylbenzamide **2**[14] in imidazole using $Zn(OAc)_2$ as catalyst and isolated as a red powder in 48% yield. Interestingly, this dye is able to gelate a multitude of organic solvents at rather low concentration. The gelation property of perylene bisimide **3** was assessed in 20 different organic solvents. For this purpose, the gelator and the solvent were put together in a screw-capped sample vial and it was heated until everything was dissolved. After leaving the sample over night at ambient temperature, the formation of gel was defined by the "stable-to-inversion of a vial" method. Transparent gels were formed in methylcyclohexane, cyclohexane, n-hexane, n-pentane, benzene, thiophene and toluene. In dioxane, THF, dibutylether and triethylamine opaque gels were formed. For the solvents chloroform, dichloromethane, acetone, ethanol, methanol, 1-octanol, diethylether, DMF and DMSO no gel was observed. The gels formed already at the concentration ≤ 2 mM. The critical gelation concentration (CGC) was determined in MCH, benzene and cyclohexane, which was 0.8 - 1.1 mM (< 0.2 wt%).

3.2.2 Spectroscopic Characterization

The observed gelation properties of PBI **3** can be attributed to the presence of hydrogen bonds between the benzamide functional groups that enforce the strong π-π-stacking interactions given between PBI dyes[15,16].

As shown from Figure 1, The FT-IR spectra of **3** in CH_2Cl_2 solution show a broad N-H stretching band at 3412 cm^{-1} that indicates the absence of hydrogen-bonding. The benzamide carbonyl group vibration band overlaps with the carbonyl group vibration of the perylene imide groups at 1660 cm^{-1}. Contrastively, in the gel phase, **3** shows a sharp N-H stretching band at 3271 cm^{-1} and a benzamide carbonyl group vibration at 1653 cm^{-1}. Both displacements to lower frequency are indicative for hydrogen-bonding interactions among the amide moieties that contribute to the formation of the gel. In contrast, the symmetrical

carbonyl group vibration of the perylene imide groups remain located at 1697 cm^{-1}. This indicates that the imide carbonyl groups are not involved in hydrogen-bond formation.

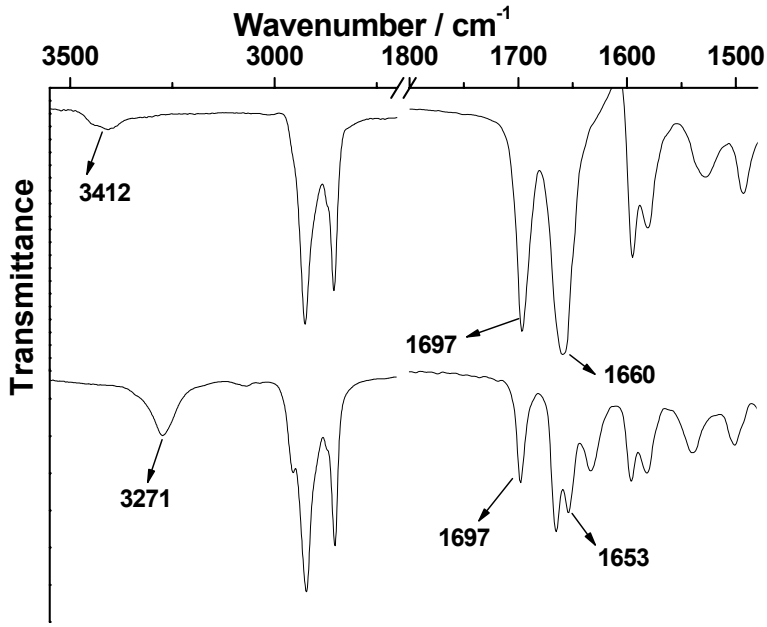

Figure 1. IR spectra of PBI **3**: (top) In CH_2Cl_2 solution (ca. 1 mM) and (bottom) for a xerogel of **3** prepared from MCH.

Interestingly, PBI **3** is able to form intermolecular hydrogen bonds even in some hydrogen bond breaking solvents such as THF and dioxane. Figure 2 shows the FT-IT spectrum of **PBI 3** in THF, which is know as hydrogen bond acceptor solvent. The spectrum shows a sharp N-H stretching band at 3266 cm^{-1} and a benzamide carbonyl group vibration at 1655 cm^{-1}, which are indicative for the formation of hydrogen bonds between the individual gelator molecules. This phenomenon may be attributed to the strong π–π aggregation of the core planar PBI molecules.

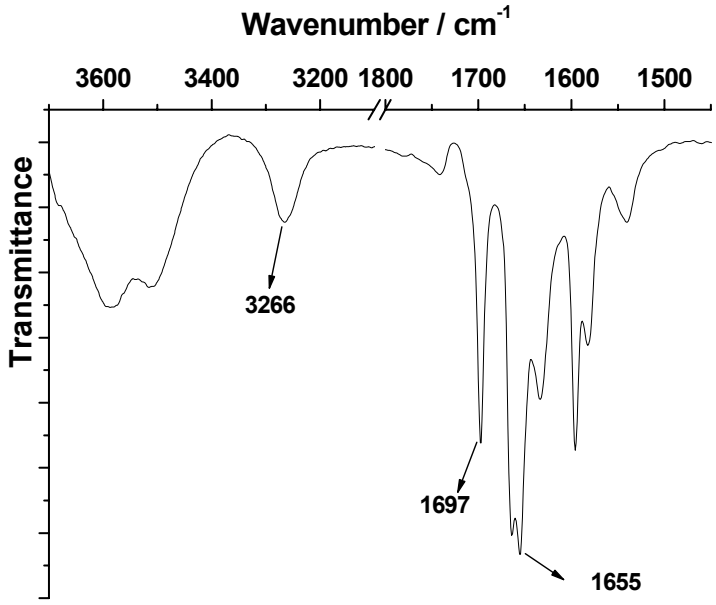

Figure 2. IR spectrum from a gel of **3** in THF (1mM). The spectrum was obtained by subtracting the spectrum of blank THF.

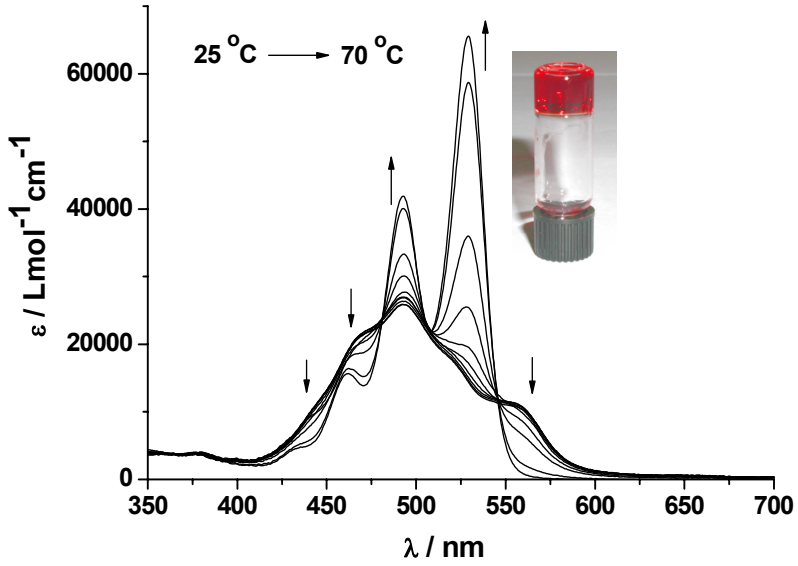

Figure 3. Variable-temperature UV/Vis absorption spectra of **3** (5.1×10^{-5} M, in toluene) and toluene organogel (inset) formed at 1.5 mM concentration. The arrows indicate spectral changes with increasing temperature.

The optical properties of dye **3** in the monomeric and aggregated state were investigated by temperature-dependent UV/vis spectroscopy (Figure 3). At high temperature (non-aggregated state), the spectrum displayed an absorption band between 400 and 550 nm of the $S_0 \rightarrow S_1$ transition of the perylene bisimide with well-resolved vibronic structure that can be attributed to breathing vibration of the perylene skeleton. Upon cooling, aggregation took place and the absorption coefficients decreased drastically with a concomitant blue-shift (ca. 30 nm) of the absorption maximum as well as a pronounced shoulder at longer wavelength. These spectral features are characteristic for perylene bisimide aggregates and indicative for a close face-to-face stacking of rotationally displaced chromophores.[17] However, in contrast to PBIs lacking additional functional groups, for dye **3** aggregation occurs at significantly lower concentration, pinpointing the decisive contribution of additional hydrogen bonds.

3.2.3 Microscopic Studies

Whilst the IR and UV/Vis spectroscopic studies provided information on the local interactions between the individual molecules, atomic force microscopy (AFM) is the method of choice to explore the morphology on the nano- and mesoscopic scale that directs the network formation and the concomitant gelation capabilities. Remarkably, well-defined fibrous structures could be observed upon spin-coating of diluted gel solutions. In addition, the structures are insignificantly influenced by the substrate.As shown in Figure 4, these fibers adopt both left-handed (*M*) and right-handed (*P*) helicities. The observed helicities of gel obtained from achiral **PBI 3** molecules can be explained by the hydrogen-bond directed stacking (Figure 4F). Gel fibers arise upon a strong preference of anisotropic unidirectional growth. As a consequence, long range chiral order can originate by nucleation from a small chiral supramolecular unit, e.g., a hydrogen-bonded dimeric or oligomeric π-stack of *M* or *P* helicity.[18] On both

highly oriented pyrolytic graphite (HOPG) and mica, the mean height of the helical fibers were 3.1 ± 0.3 nm with the width of 8.0 ± 2.0 nm, helical pitch of 15.0 ± 2.0 nm and several micrometers in length. There are few fibers without helicity on HOPG which might observed on the less strongly interacting mica substrate. Similar well-defined helical fibers, however from chiral precursors, have recently been observed for *p*-type semiconductive oligophenylenevinylene organogelators[19] but are unprecedented for achiral perylene bisimides.

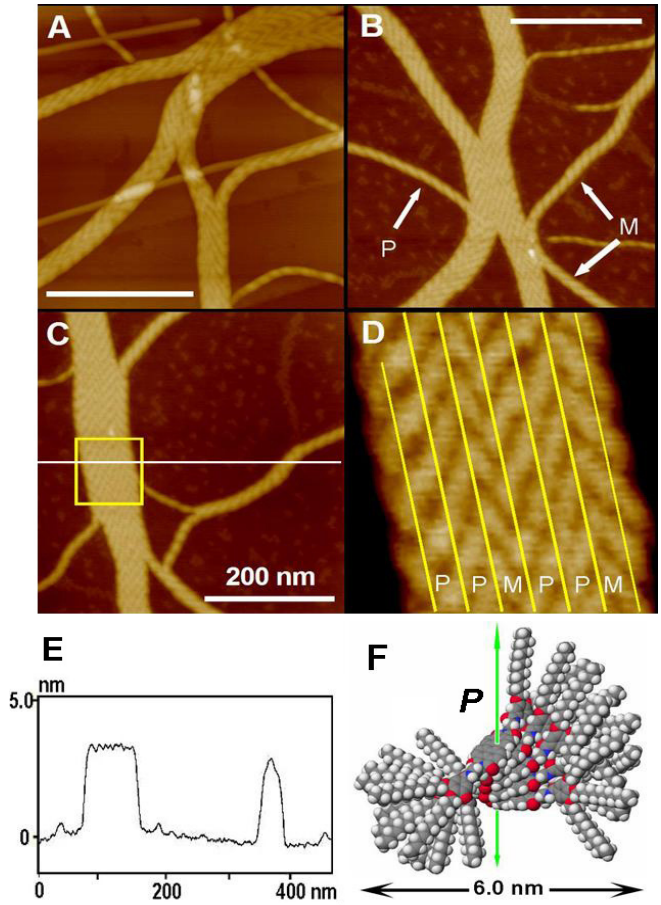

Figure 4. AFM height images of films spin-coated from diluted gel solutions of **3** in toluene (1×10^{-4} M) onto HOPG (A) and mica (B and C); (D) is zoomed region image from (C). In images (A), (B) and (C) the scale bar corresponds to 200 nm and the z scale is 10 nm. (E) shows the cross-section analysis corresponding to the white line of (C) and (F) depicts a suggested packing model for self-assembled *P*-configured hydrogen-bonded aggregate with a diameter of 6.0 nm.

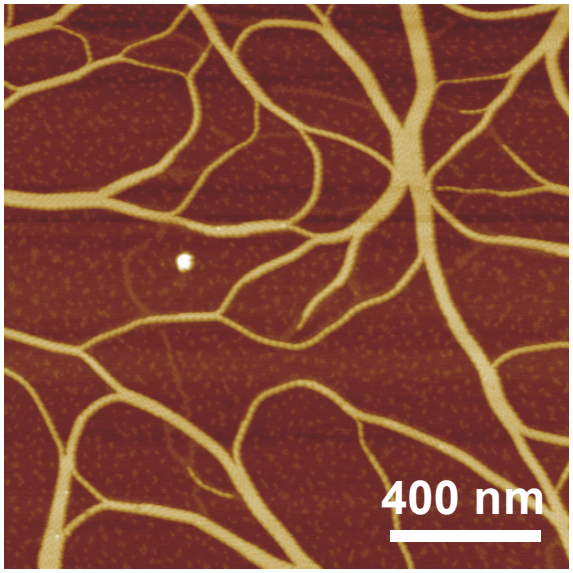

Figure 5. AFM image of a spin-coated film from a diluted gel solution of **3** in toluene (1×10^{-4} M) onto freshly cleaved mica.

For the efficient entrapment of the solvent, it is of importance that these initially formed fibers interconnect to establish a continuous network (see large-scaled AFM images in Figure 5). In the given system this happens most likely by interpenetration of the extended alkyl chains[20] because the height of the fibers does not change upon further self-assembly into larger structures (Figure 4E). As shown by high-resolution AFM in Figure 4D, there is little or no preference for the interpenetration of the alkyl chains of *M*- or *P*-configured helical fibers.

For comparison, the aggregated fibers in THF are shown in Figure 6. Although the fibers are shorter and less defined (no helicity could be resolved) in the hydrogen acceptor solvent, bundle formation as a prerequisite for gel formation is still present. The fiber formation in hydrogen bond breaking solvent such as THF suggests strong π–π interaction among planar PBI **3** chromophores rules out the possibility of solvent insertion irrespective of the nature of the solvent,

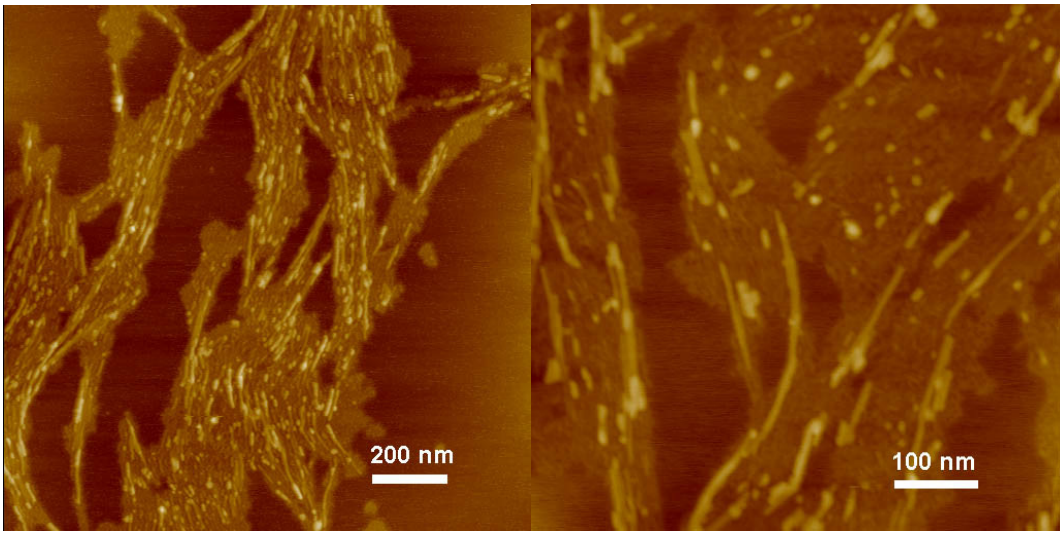

Figure 6. AFM images of a spin-coated film from a diluted gel solution of **3** in THF (2×10^{-4} M) onto freshly cleaved mica.

3.2.4 Thermal Behavior

Differential scanning calorimetry (DSC, Figure 7) of PBI dye **3** reveals several enantiotropic phase transitions in the heating and cooling cycles. First, a crystal-to-crystal phase transition takes place at 96 °C. Subsequently the compound enters into a soft plastic crystalline phase at 126°C and finally an isotropic liquid is formed at 235°C with a melting enthalpy of ΔH = 47.3 kJ mol^{-1}. Remarkably, well-defined macroscopic fibers can be observed upon slow cooling from the isotropic liquid (Figure 7) under the polarized optical microscope (POM). These structures remain even intact upon cooling to room temperature. They adopt a uniform diameter of 3.8 ± 0.2 μm and can extend to beyond 1 mm in length.

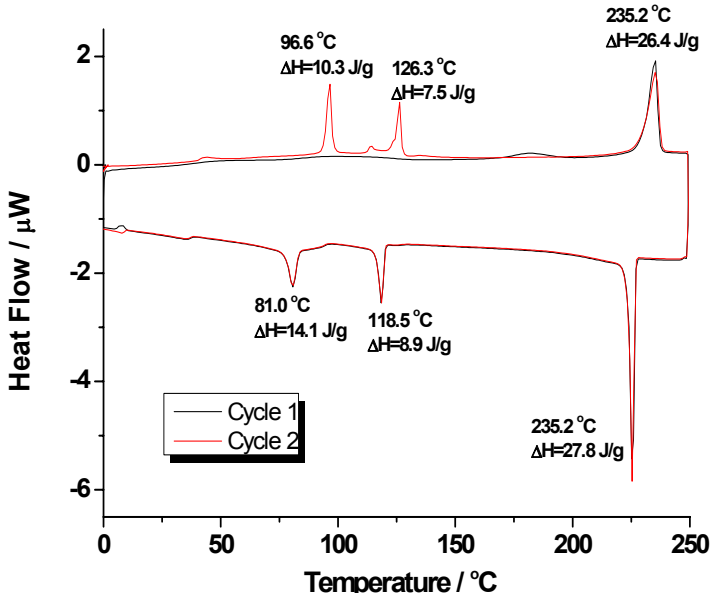

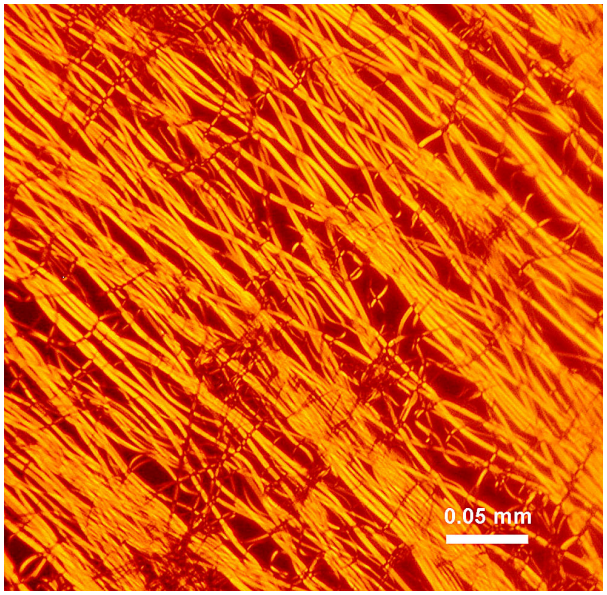

***Figure** 7.* (top) Differential scanning calorimetry (DSC) traces of compound **3**. The black line indicates the first and the red line the second cycle of the DSC measurement, which were performed at heating and cooling rates of 10 °C / min. (bottom) Polarized optical microscopy image (crossed polarizer) of **3** after cooling from the melt at a temperature of 228 °C.

3.2.5 Charge Carrier Mobility

Such well-organized fibers and bundles that are composed of extended π-stacks of the electron poor dye **3** should provide efficient pathways for mobile n-type charge carriers. Therefore, the semiconductive properties of **3** in solid state were investigated by using the pulse-radiolysis time-resolved microwave conductivity (PR-TRMC) technique, which offers the intrinsic charge carrier mobility of the material with minimized effects of grain boundaries as shown for a large number of organic materials in the past.[21] At room temperature, the sum of the isotropic electron and hole mobility is $\Sigma\mu_{TRMC} = 0.052$ $cm^2V^{-1}s^{-1}$ for dye **3**.[22] This value is significantly higher than the values measured with the same method for liquid crystalline phases of related PBIs with tridodecyloxyphenyl[17a] (0.008 $cm^2V^{-1}s^{-1}$)[23a] or with tridodecyloxybenzyl[24] substituents at imide positions (0.011 $cm^2V^{-1}s^{-1}$)[23a]. Likewise, this charge carrier mobility is about one order of magnitude higher than the mobility measured for p-type semiconductive hydrogen-bond directed oligothiophene organogelators.[11]

3.3 Summary

In conclusion, the results presented here show that PBI organogelator **3** exhibits pronounced gelation capabilities leading to interpenetrating networks of PBI stacks in a broad variety of solvents, including electron-rich aromatic solvents such as thiophene. Based on the remarkably high *n*-type charge carrier mobility[22] and the broad absorption range from 400-600 nm, this gelator might provide efficient organic solar cells upon mixing with *p*-type organic semiconductors such as pentacene or polythiophene.

3.4 Experimental Details

General methods. All solvents and reagents were purchased from commercial sources and used as received without further purification. The solvents for spectroscopic studies were of spectroscopic grade and used as received. ^{1}H NMR spectra were recorded on a 400 MHz spectrometer and all the spectra were calibrated against TMS. UV/Vis spectra were measured on a Perkin-Elmer Lambda 40P spectrometer equipped with a Peltier system as temperature controller. FT-IR spectra were measured on a Jasco FT/IR-410 instrument. Differential scanning calorimetry (DSC) measurements were performed by using a TA Q1000 calorimeter. Optical textures at crossed polarizers were obtained with an Olympus BX-41 polarization microscope equipped with a Linkam THMS 600 hot stage and a temperature controller unit.

Atomic force microscopy (AFM). AFM measurements were performed under ambient conditions using a MultiMode Nanoscope IV system operating in tapping mode in air. Silicon cantilevers (OMCL-AC160TS) with a resonance frequency of ~300 kHz were used. Solutions of perylene bisimide **3** were spin-coated onto HOPG (highly oriented pyrolytic graphite) or mica under 7000 rpm.

***N*-(2-aminoethyl)-3,4,5-tris(dodecyloxy)benzamide 2**

Compound **2** was prepared starting from 3,4,5-trihydroxy methylbenzoate in 3 synthetic steps as described before.[14] In the final step we revised the synthesis procedure compared to the reported one in order to achieve higher yield (74%). To a dry dichloromethane (30 ml) solution of 3,4,5-tris(dodecyloxy)benzoic acid (1.5g, 2.25 mmol), thionyl chloride (15 ml, 0.21 mol) was added at room temperature under argon atmosphere. The reaction mixture was allowed to stir at room temperature for 5 h and then the solvent was removed under reduced pressure. The resultant light yellow oil was re-dissolved in dry dichloromethane. The solution

was added dropwise over 30 minutes to ehylenediamine (15 ml) in an ice cold environment and the reaction mixture was further stirred for 12 h at room temperature. The stirring was stopped and the solution was extracted by dichloromethane (50 ml, 3 times). The combined organic layer was washed with water (150 ml, 3 times) and dried over Na_2SO_4. The solvent was evaporated to get the crude product which was purified by recrystallization from ethanol to get the desired compound as a white solid. ^{1}H NMR (400 MHz, $CDCl_3$, 300 K, TMS): δ = 6.99 (s, 2H, Ar-H), 6.62 (t, 1H, J = 5.4 Hz, NH), 4.04 - 3.95 (m, 6H, Ar-OCH_2), 3.50 (q, 2H, J = 5.7, CH_2), 2.95 (t, 2H, J = 5.6, CH_2), 1.80-1.15 (m, 60H, CH_2), 0.88 (m, 9H, CH_3).

_N,N_'-Di[3,4,5-tris(dodecyloxy)benzoylaminoethyl]-perylene-3,4:9,10-tetracarboxylic acid bisimide 3

Perylene-3,4:9,10-tetracarboxylic acid bisanhydride (39 mg, 0.1 mmol), benzamide **2** (150 mg, 0.21 mmol) and zinc acetate (40 mg, 0.22 mmol) were mixed in 3 g of imidazole. The reaction mixture was stirred at 130 °C for 24 h. After cooling to room temperature, 100 ml MeOH was added and the precipitate was collected and washed with additional MeOH. After drying in vacuum, the crude product was purified by silica gel column chromatography (20/1 $CHCl_3$/MeOH) to give a red solid. Yield: 48%. Mp: 233 °C. ^{1}H NMR (400 MHz, $CDCl_3$, 300 K, TMS): δ = 8.50 (d, 4H, J = 7.6 Hz, H_{pery}), 8.36 (d, 4H, J = 8.0 Hz, H_{pery}), 7.08 (s, 2H, NH), 7.00 (s, 4H, Ar-H), 4.53 (m, 4H, CH_2), 3.98 (m, 12H, Ar-OCH_2), 3.88 (m, 4H, CH_2), 1.80-1.15 (m, 120H, CH_2), 0.88 (m, 18H, CH_3). MS (MALDI-TOF, matrix: DCTB): calculated for $C_{114}H_{172}N_4O_{12}$ (m/z) 1789.30, found 1790.28 $[M+H]^+$; elemental analysis (%) calculated for $C_{114}H_{172}N_4O_{12}$ (1790.6): C 76.47, H 9.68, N 3.13; found: C 76.58, H 9.92, N 2.97. UV/vis (CH_2Cl_2): $\lambda_{max}(\varepsilon)$ = 528 (85300), 491 (51600), 460 (18500 M^{-1} cm^{-1}).

Gelation test of PBI 3 in various organic solvents

The gelation property of perylene bisimide **3** was assessed in 20 different organic solvents. For this purpose, the gelator and the solvent were put together in a screw-capped sample vial and it was heated until everything was dissolved. After leaving the sample over night at ambient temperature, the formation of gel was defined by the "stable-to-inversion of a vial" method. Transparent gels were formed in methylcyclohexane, cyclohexane, n-hexane, n-pentane, benzene, thiophene and toluene. In dioxane, THF, dibutylether and triethylamine opaque gels were formed. For the solvents chloroform, dichloromethane, acetone, ethanol, methanol, 1-octanol, diethylether, DMF and DMSO no gel was observed. The gels formed already at the concentration ≤ 2 mM. The critical gelation concentration (CGC) was determined in MCH, benzene and cyclohexane, which was 0.8-1.1 mM (< 0.2 wt%).

Charge carrier mobility measurement

The conductive properties were studied with the pulse-radiolysis time-resolved microwave conductivity (PR-TRMC) technique. Pressed pellets (25 mg, fill factor 0.75) of the material were irradiated with 10 nanosecond pulses of 3 MeV electrons from a Van de Graaff accelerator, which results in the creation of a uniform micromolar concentration of electron-hole pairs. The resulting change in conductivity was monitored as the microwave power absorbed by the mobile charge carriers in the material at an electro-magnetic field frequency of 33 GHz. The mobility values are determined from the conductivity at the end of the electron pulse. The lower limit to the mobility is obtained by assuming that all generated charges contribute to the conductivity (survival parameter W_{eop} = 1) and a pair formation energy of 16 eV as described elsewhere.[25]

3.5 References and Notes

1 A. C. Grimsdale, K. Müllen, *Angew. Chem. Int. Ed*. **2005**, *44*, 5592-5629.

2 (a) A. P. H. J. Schenning, E. W. Meijer, *Chem. Commun* **2005**, 3245-3258; (b) F. J. M. Hoeben, P. Jonkheijm, E. W. Meijer, A. P. H. J. Schenning, *Chem. Rev*. **2005**, *105*, 1491-1546.

3 *Supramolecular Dye Chemistry* F. Würthner, Ed., *Top Curr Chem,* **2005**, *258*.

4 K.-Y. Law, *Chem. Rev*. **1993**, *93*, 449-486.

5 F. Würthner, R. Wortmann, K. Meerholz, *ChemPhysChem* **2002**, *3*, 17-31.

6 C. J. Brabec, N. S. Sariciftci, J. C. Hummelen, *Adv. Funct. Mater.* **2001**, *11*, 15-26.

7 (a) D. T. McQuade, A. E. Pullen, T. M. Swager, *Chem. Rev*. **2000**, *100*, 2537-2574; (b) T. M. Swager, *Acc. Chem. Res*. **1998**, *31*, 201-207.

8 (a) U. Beginn, *Prog. Polym. Sci*. **2003**, *28*, 1049-1105; (b) T. Ishi-I, S. Shinkai, *Top Curr Chem* **2005**, *258*, 119-160.

9 T. Kato, N. Mizoshita, M. Moriyama, T. Kitamura, *Top Curr Chem* **2005**, *256*, 219-236.

10 (a) A. Ajayaghosh, S. J. George, *J. Am. Chem. Soc.* **2001**, *123*, 5148-5149; (b) M. Shirakawa, S.-i. Kawano, N. Fujita, K. Sada, S. Shinkai, *J. Org. Chem.* **2003**, *68*, 5037-5044; (c) J. van Esch, F. Schoonbeek, M. de Loos, H. Kooijman, A. L. Spek, R. M. Kellogg, B. L. Feringa, *Chem. Eur. J.* **1999**, *5*, 937-950; (d) H. Engelkamp, S. Middelbeek, R. J. M. Nolte, *Science* **1999**, *284*, 785-788; (e) K. Hanabusa, M. Yamada, M. Kimura, H. Shirai, *Angew. Chem. Int. Ed.* **1996**, *35*, 1949-1951.

11 F. S. Schoonbeek, J. H. van Esch, B. Wegewijs, D. B. A. Rep, M. P. de Haas, T. M. Klapwijk, R. M. Kellogg, B. L. Feringa, *Angew. Chem. Int. Ed.* **1999**, *38*, 1393-1397.

12 (a) F. Würthner, *Chem. Commun.* **2004**, 1564-1579; (b) W. Herbst, K. Hunger, *Industrial Organic Pigments: Production, Properties, Applications* 2nd ed., WILEY-VCH, Weinheim, **1997**.

13 (a) K. Sugiyasu, N. Fujita, S. Shinkai, *Angew. Chem. Int. Ed.* **2004**, *43*, 1229-1233; (b) F. Würthner, B. Hanke, M. Lysetska, G. Lambright, G. S. Harms, *Org. Lett.* **2005**, *7*, 967-970.

14 (a) P. Mukhopadhyay, Y. Iwashita, M. Shirakawa, S.-i. Kawano, N. Fujita, S. Shinkai, *Angew. Chem. Int. Ed.* **2006**, *45*, 1592-1595; (b) V. Percec, C.-H. Ahn, T. K. Bera, G. Ungar, D. J. P. Yeardley, *Chem. Eur. J.* **1999**, *5*, 1070-1083.

15 (a) S. Yagai, T. Iwashima, T. Karatsu, A. Kitamura, *Chem. Commun.* **2004**, 1114-1115; (b) S. Yagai, T. Karatsu, A. Kitamura, *Langmuir* **2005**, *21*, 11048-11052; (c) T. Kitamura, S. Nakaso, N. Mizoshita, Y. Tochigi, T. Shimomura, M. Moriyama, K. Ito, T. Kato, *J. Am. Chem. Soc.* **2005**, *127*, 14769-14775; (d) F. Camerel, L. Bonardi, M. Schmutz, R. Ziessel, *J. Am. Chem. Soc.* **2006**, *128*, 4548-4549; (e) S. Bhuniya, B. H. Kim, *Chem. Commun.* **2006**, 18421844; (f) C. Bao, R. Lu, M. Jin, P. Xue, C. Tan, T. Xu, G. Liu, Y. Zhao, *Chem. Eur. J.* **2006**, *12*, 3287-3294; (g) T. Ishi-i, R. Kuwahara, A. Takata, Y. Jeong, K. Sakurai, S. Mataka, *Chem. Eur. J.* **2006**, *12*, 763-776.

16 For a recent review on amide and urea-based organogelators, see: F. Fages, F. Vögtle, M. Zinic, *Top Curr Chem* **2005**, *256*, 77-131.

17 (a) F. Würthner, C. Thalacker, S. Diele, C. Tschierske, *Chem. Eur. J.* **2001**, *7,* 2245-2253; (b) F. Würthner, Z. Chen, V. Dehm, V. Stepanenko, *Chem. Commun.* **2006**, 1188-1190.

18 A. Brizard, R. Oda, I. Huc, *Top Curr Chem* **2005**, *256*, 167-218.

19 (a) A. Ajayaghosh, C. Vijiayakumar, R. Varghese, S. J. George, *Angew. Chem. Int. Ed.* **2006**, *45*, 456-460; (b) A. Ajayaghosh, R. Varghese, S. J. George, C. Vijiayakumar, *Angew. Chem. Int. Ed.* **2006**, *45*, 1141-1144; (c) S. J. George, A. Ajayaghosh, P. Jonkheijm, A. P. H. J. Schenning, E. W. Meijer, *Angew. Chem. Int. Ed.* **2004**, *43,* 3422-3425.

20 F. Würthner, S. Yao, U. Beginn, *Angew. Chem. Int. Ed.* **2003**, *42*, 3247-3250.

21 J. M. Warman, M. P. de Haas, G. Dicker, F. C. Grozema, J. Piris , M. G. Debije, *Chem. Mater.* **2004**, *16*, 4600-4609.

22 Notably, the PR-TRMC method cannot distinguish between p- and n-type charge carrier mobility. However, there are many reports where the n-type semiconductive properties of PBI dyes have been confirmed, whilst no p-type mobility for these electron-poor compounds has ever been observed.

23 (a) Z. An, J. Yu, S. C. Jones, S. Barlow, S. Yoo, B. Domercq, P. Prins, L. D. A. Siebbeles, B. Kippelen, S. R. Marder, *Adv. Mater.* **2005**, *17*, 2580-2583. PR-TRMC charge carrier mobilities have also been reorted for other PBI based materials: (b) C. W. Struijk, A. B. Sieval, J. E. J. Dakhorst, M. van Dijk, P. Kimkes, R. B. M. Koehorst, H. Donker, T. J. Schaafsma, S. J. Picken, A. M. van de Craats, J. M. Warman, H. Zuilhof, E. J. R. Sudholter, *J. Am. Chem. Soc.* **2000**, *122***,** 11057-11066; (c) Z. Chen, M. G. Debije, T. Debaerdemaeker, P. Osswald, F. Würthner, *ChemPhysChem* **2004**, *5*, 137-140.

24 J. van Herrikhuyzen, A. Syamakumari, A. P. H. J. Schenning, E. W. Meijer, *J. Am. Chem. Soc.* **2004**, *126*, 10021-10027.

25 (a) P. G. Schouten, J. M. Warman, M. P. de Haas, *J. Phys. Chem.* **1993**, *97*, 9863-9870; b) P. G. Schouten, J. M. Warman, M. P. de Haas, C. F. van Nostrum, G. H. Gelinck, R. J. M. Nolte, M. J. Copyn, J. W. Zwikker, Mc. K. Engel, M. Hanack, Y. H. Chang, W. T. Fords, *J. Am. Chem. Soc.* **1994**, *116*, 6880-6894.

Chapter 4

Recognition of Micro- and Macroscopic Chiral Assembly in Non-Equilibrium Environments

4.1 Introduction

Helical architectures such as DNA and proteins are ubiquitously found in nature for the performance of complicated functions. The design of helical architectures is accordingly of great interest for scientists and may ultimately lead to artificial species with advanced functionality.[1] Over the past decade, several non-covalent interactions such as hydrogen bonding, metal-ion to ligand coordination, electrostatic interaction, π-π-stacking, dipole-dipole interaction, hydrophobic interaction, etc., have been identified to generate various superstructures from synthetic small molecule building blocks.[2]

In particular, a number of artificial self-assembled helical nanofibers have been created from chiral building blocks by virtue of non-covalent interactions.[3] Nevertheless, chiral supramolecular architectures obtained from achiral molecular units are still rare.[3c, 4] Chiral self-assembled nanofibers composed of achiral candidates are commonly a mixture of both left-handed and right-handed helicities in equal amount, and the systems are overall racemic.[5, 6] The purposive selection of one-handed helicity is of paramount interest to supramolecular scientists, because it may explain the origin of homochirality in natural biomacromolecules and lead to new catalytic templates for the asymmetric synthesis of homochiral compounds. Dähne's and Kirstein's group reported a formation of chiral

J-aggregates from achiral cyanine dyes, in which the enantiomeric symmetry is spontaneously broken at a primary state of nucleation.[7] In the recent past, another achiral carbocyanine dye was found to form optically active superhelical J-aggregates in aqueous solution when chiral alcohol participated in the system.[8] This indicated the possibility of preferential population of one handed helices by external chiral bias imparted by a suitable chiral solvent.

More recently, however, it has been reported that bisignate CD spectra can also result upon rotary stirring, shacking, etc. owing to a macroscopic alignment of extended fibers.[9,10] Ribó' group reported on the controllable self-assembly of achiral porphyrin dye into homochiral J-aggregates by the means of vortex motion caused by either stirring or rotary evaporation.[9] Aida and co-workers have reported remarkable vortex effects on the CD signal of zinc porphyrin nanofibers, which was attributed to the alignment of the nanofibers macroscopically along the direction of the vortex flow.[10a] At the same time, Meijer and co-workers observed similar behavior of supramolecular fibrous aggregates generated from oligo(*p*-phenylenevinylene) derivatives.[10b] Such chiral alignment effects are well-established for biomacromolecules like DNA and applied, e.g. to distinguish between intercalating and groove-building chromophores by LD spectroscopy.[11]

In the last chapter we have demonstrated that amide functionalized perylene bisimides (**PBI 1** in Figure 1) self-assemble into one-dimensional helical fibers by synergic effects of π-π-stacking and hydrogen-bonding interaction. In some apolar solvents such as toluene the fine fibers further intercross to form three dimensional network structures, by which the solvents are immobilized resulting in organogels.[12] Microscopy studies revealed that the fibrous aggregates from **PBI 1** exhibit a defined helical pitch and the left-handed and right-handed helicity appears at equal amounts. In this chapter we will study the impact of chiral solvents and vortex flow created by a rotary stirring on the CD spectra of these aggregates.

4.2 Structural Features and Aggregation Behaviors

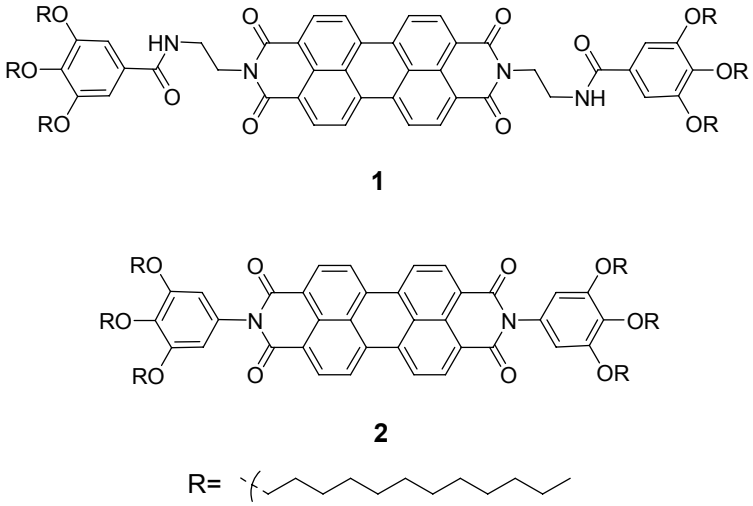

Figure 1. Molecular structures of **PBI 1** and **PBI 2**, that are distinguished by the presence and absence of amide function groups.

Figure 1 shows the molecular structures of **PBI 1** and **PBI 2**. The distinct structural difference is the ethyl-amide spacer unit between the rigid chromophores core and trialkoxyphenyl groups. The amide functional groups can assist the π–π-stacking of the PBI cores by amide-amide hydrogen bond which triggers the formation of fibrous aggregates and organogels. In contrast, no gelation phenomena are observed in any solvents for **PBI 2** due to the much smaller aggregate size in the absence of hydrogen bonding ability.

The intermolecular interactions of these dyes were investigated readily by UV/Vis spectroscopy. Figure 2a and 2b show the temperature-dependent UV/Vis spectra of **PBI 1** in *R*- and *S*-limonene, respectively. The aggregation/ de-aggregation behavior of **PBI 1** in limonene can be readily tuned by changing the temperature at a certain concentration. The absorption spectra of **PBI 1** in *R*- and *S*-limonene are almost identical to those in toluene,[12] i.e., at high temperature it

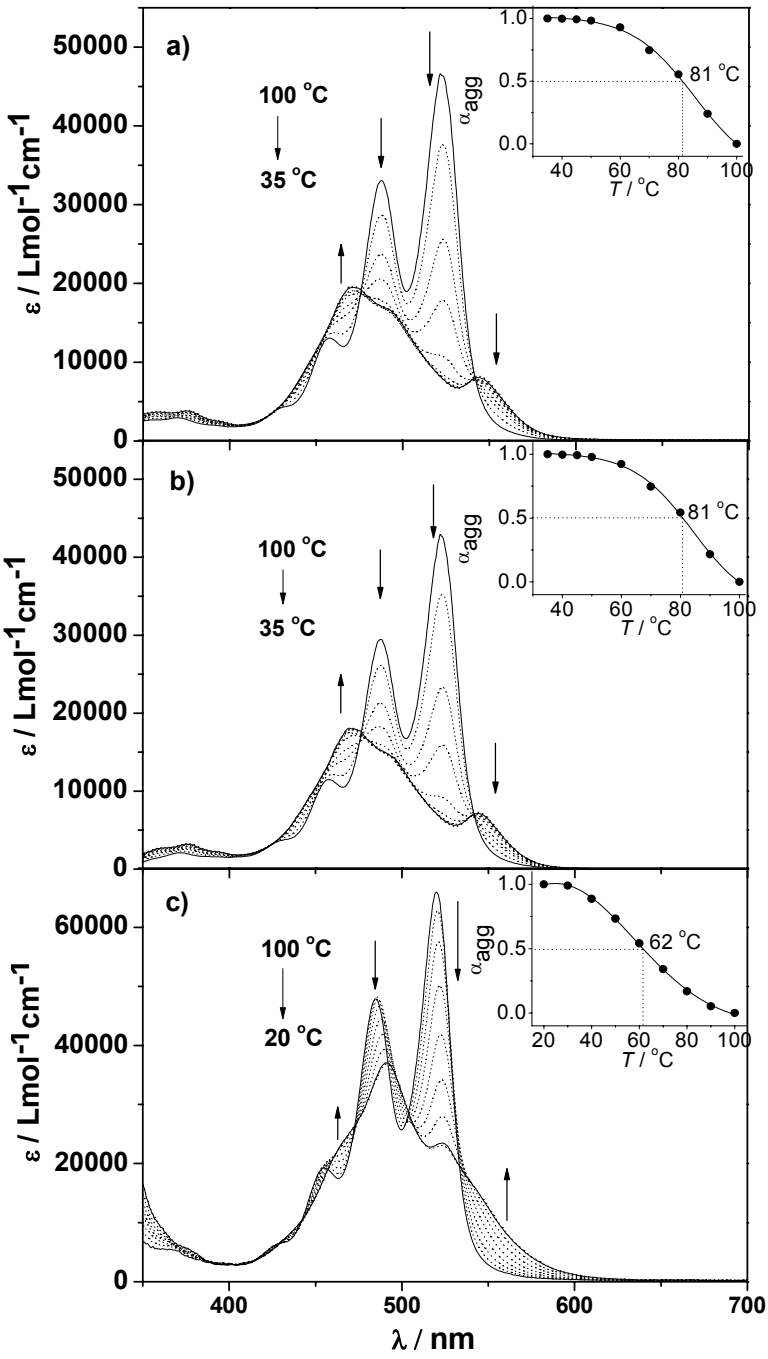

Figure 2. Temperature dependent absorption spectra of (a) **PBI 1** in *R*-limonene (5.1×10^{-5} M), (b) **PBI 1** in *S*-limonene (5.0×10^{-5} M), and (c) **PBI 2** in *R*-limonene (5.0×10^{-5} M), respectively. The arrows indicate spectral change with decreasing temperature. Inset shows the plots of α_{agg} as a function of temperature. The sigmoidal fit for the data points were obtained by using the Boltzmann function.

gives monomer spectrum at λ = 522 nm, upon cooling π-π-stacking takes place with a blue shifted absorption maximum as well as depressed absorption coefficient value. According to exciton coupling theory, such hypsochromic shifts (H-band) can be attributed to a sandwich-type packing of the chromophores. A second less intensive band around 545 nm of the aggregate spectrum indicates a helical packing fashion of the PBI chromophores. These identical spectral features observed of **PBI 1** in *R*- and *S*-limonene suggest the equal propensity of aggregate formation in both isomers of the apolar solvent used.

For comparison, Figure 2c shows the variable-temperature absorption spectra of **PBI 2** in *R*-limonene. At high temperature the dye molecules prevail as non-aggregated monomers which is reflected by a characteristic monomer absorption band; upon cooling, π-π-stacking takes place with a decrease of the absorption coefficient at λ = 520 nm (monomer), a concomitant blue-shift of the absorption maximum and a pronounced shoulder at longer wavelength of around 560 nm. These spectral features are indicative for the typical face-to-face stacking mode of perylene bisimide species with rotationally displaced chromophores.[13]

Noteworthily, the π-π-stacking of **PBI 1** starts at considerably lower concentration (5×10^{-8} M, in both *R*-limonene and *S*-limonene) at room temperature, which could be attributed to the assistance by hydrogen bond formation. In contrast, the aggregation of **PBI 2** molecules require higher concentrations of about 1×10^{-6} M in *R*-limonene because of the inefficient strength of π-π-stacking without hydrogen bonding. Note that the critical gelation concentration of **PBI 1** in *R*- and *S*-limonene is far higher, i.e. 0.8×10^{-3} M.

Insets in Figure 2 show the mole fraction of aggregate at each temperature estimated using Equation (1):

$$\alpha_{agg\,(T)} \approx \frac{A(T) - A_{mon}}{A_{agg} - A_{mon}} \qquad (1)$$

where $\alpha_{agg}(T)$ is the mole fraction of aggregated dye at temperature T, A_{mon}, $A(T)$ and A_{agg} are the absorbance at 522 nm for the monomer, the solution at temperature T and the pure aggregate solutions, respectively. The $\alpha_{agg}(T)$ values were plotted as a function of temperature and fitted by using the Boltzmann function. From such a plot the $\alpha_{50}(T)$ (temperature at which $\alpha_{agg}= 0.5$) could be estimated. As indicated in the insets of Figure 2a-c, the α_{50} value of **PBI 1** was determined as 81°C in *R*- and *S*-limonene, which is higher than that of **PBI 2** in *R*-limonene (62 °C). The significantly higher α_{50} values of **PBI 1** again confirms the higher binding strength due to additional hydrogen bonds.

Whilst the spectroscopic studies give primary information on the intermolecular interaction of the π-systems, structural evidence is obtained from atomic force microscopy (AFM). Unlike **PBI 2** and other structurally similar PBI derivatives which adopt short rod-like aggregates,[14] **PBI 1** forms well-defined extended fibers that further intercross to network structures in apolar solvents. Figure 3 shows the AFM images of a diluted **PBI 1** gel in toluene, in which well-defined long fibers (several microns in length) and 3D network structures can be observed. The mean height of the helical fibers were 3.1 ± 0.3 nm with the width of 8.0 ± 2.0 nm, helical pitch of 15.0 ± 2.0 nm. The fine fibers can further interdigitate into broad ropes, with width varying from 20-80 nm. The zoomed images show that the fibers adopt clear helicities and both left-handed (*M*) and right-handed (*P*) helices can be found simultaneously in the present network matrix. Note that there is no preference for the two kinds of helices and that even conversion points are formed in a single fiber (the transition points are labeled as *TP* in Figure 3c). The well-defined helical pitch of these nanofibers can be explained by the hydrogen bond-directed π-π-stacking. Molecular modeling studies (Figure 4) show two possibilities of the hydrogen bond-directed chromophore packing into *M*- and *P*-

helical π-stacks. Considering that the precursors are intrinsically achiral, it is reasonable that the two enantiomers should be presented in equal amount at the present conditions (Figure 3c-d). The two hydrogen-bonding "pillars" are highlighted to play an important role in the formation of helicity because they can efficiently direct a one-handed helical sense (see enlarged area in Figure 4). In contrast, for simple PBI π-stacks without such hydrogen-bonding functionality the helical sense can easily change within a π-stack because of equal interaction energies between individual *M*- or *P*-type PBI dimeric unit.[14a,15]

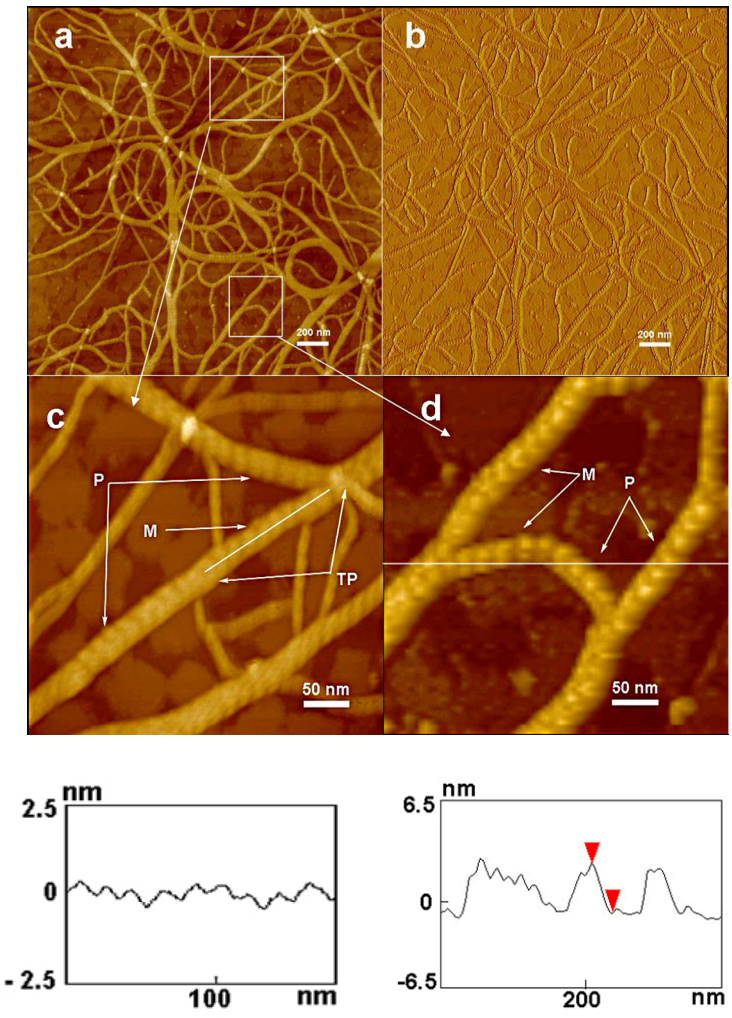

Figure 3. AFM height (a) and phase (b) images of films spin-coated from a diluted gel solution of **PBI 1** in toluene (c = 1×10^{-4} M) on HOPG surface; (c) and d) are zoom region images from (a); bottom figures show the cross-section analyses corresponding to the white lines of (c) and (d) respectively.

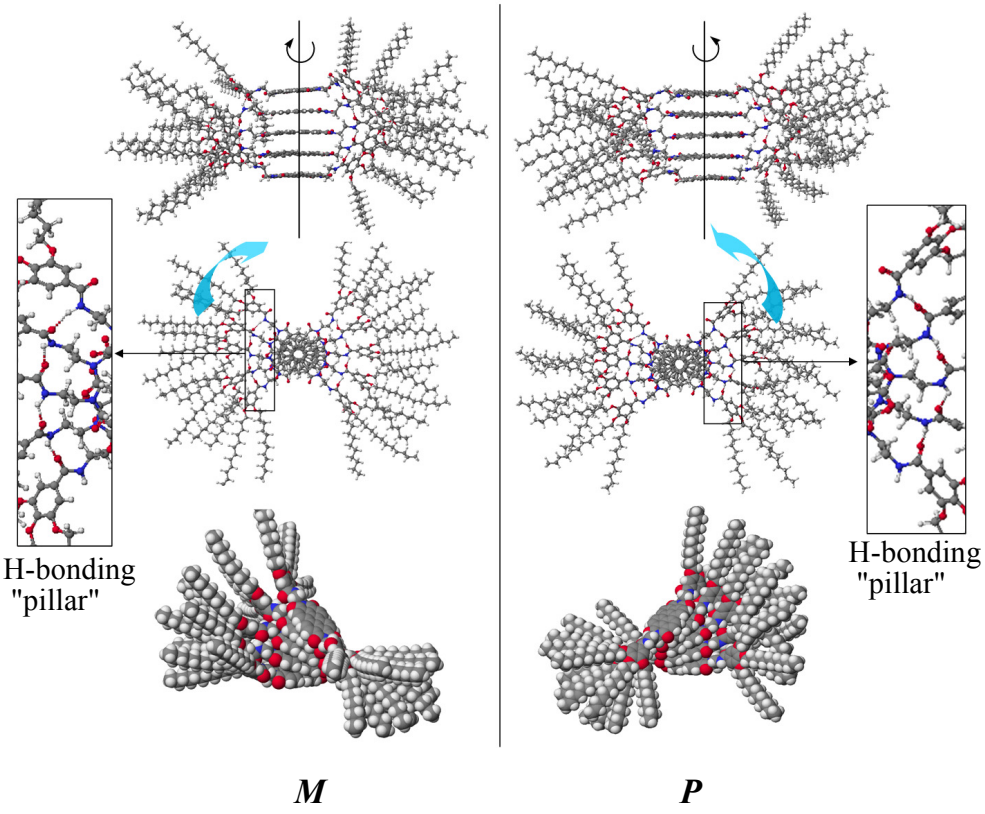

Figure 4. Suggested packing models for self-assembled *P*- and *M*-configured hydrogen-bonded aggregates of PBI **1**. The enlarged area shows the hydrogen bond chains formed between the amide groups. Atom assignment: gray: carbon; white: hydrogen; red: oxygen; blue: nitrogen.

4.3 Change of Helical Bias by Chiral Solvents

4.3.1 CD-spectroscopic Monitoring of Chiral Assembly

The network formed by **PBI 1** in toluene comprises well-organized helical fibers and bundles, however the system is overall racemic, which is reasonable since the building blocks and the exterior environment are achiral. This situation changes as already reported when the peripheral alkyl chains of **PBI 1** are replaced by chiral analogues.[14b,16] Another source of chiral bias might be provided by chiral solvents.

Hereon we chose chiral *R*-limonene and *S*-limonene (Figure 5), because they exhibit chirality centers and their structures are similar to methylcyclohexane and toluene, in which the self-assembly of **PBI 1** chromophore has been intensively studied before.[14]

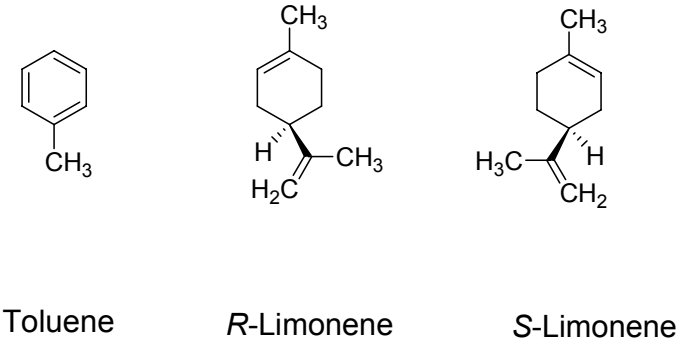

Figure 5. Structures of solvents used in this chapter

To monitor the helical arrangement of the chromophores upon self-assembly, temperature-dependent CD spectroscopic studies were carried out in *R*- and *S*-limonene, respectively (Figure 6a). At elevated temperature no Cotton effect was observed, suggesting the absence of any aggregated structure; as the temperature was decreased, a significant induced bisignate Cotton effect was observed with a positive maximum at 458 nm and a negative maximum at 499 nm. In addition, a shoulder at 546 nm was observed corresponding to the lowest energy exciton band of UV/vis spectrum (Figure 2a). The shape and intensity of CD spectra appears similar to those observed for PBI chromophores with chiral side chains,[17] which suggests a comparable helical bias imparted by the chiral side chain and the chiral solvent. The bisignate shape of the CD spectra in *R*-limonene (red lines) indicates the preferential formation of left-handed (*M*-configured) aggregates according to the exciton chirality method.[18]

When similar temperature variable studies were carried out in *S*-limonene, the CD spectra observed were perfect mirror-images of those found in case of

R-limonene (Figure 6a, black lines: 458 nm, negative; 499 nm, positive; 546 nm, positive), which indicate a right-handed (*P*-configured) helicity of the aggregates. The observation of reversed CD spectra of **PBI 1** in *R*- and *S*-limonene reveals that the chiral environment directs the helical sense of the chromophore packing, which results in a chiral bias towards homochiral aggregates.

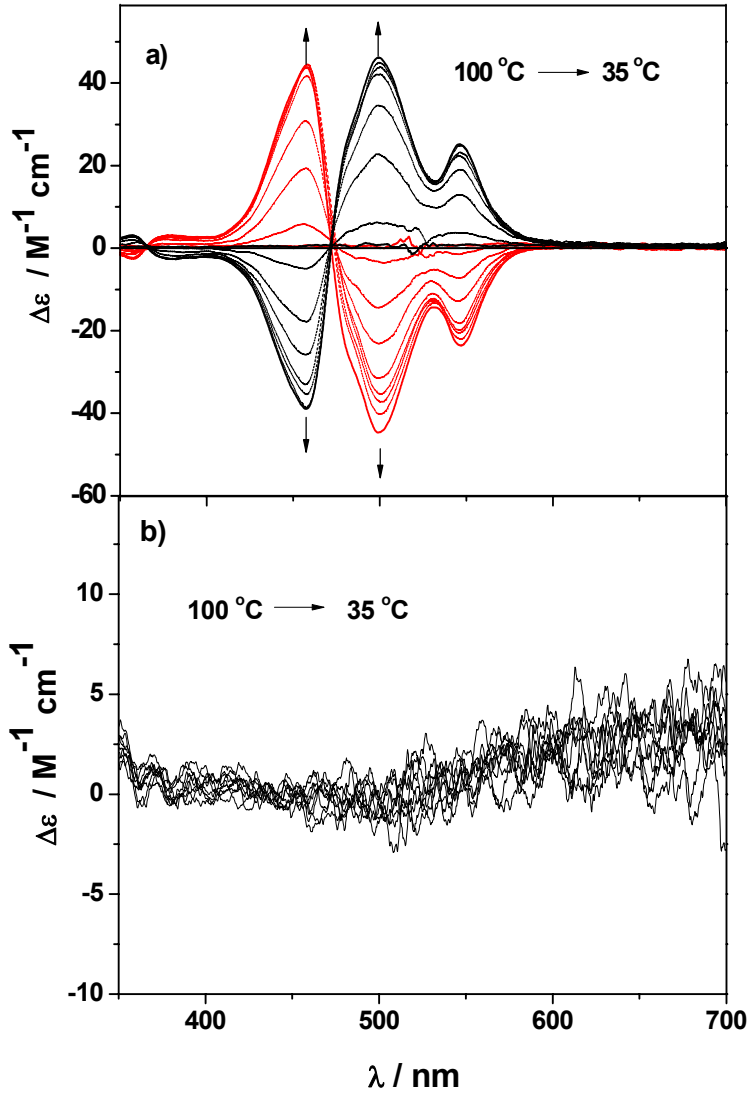

Figure 6. Temperature dependent CD spectra of (a) **PBI 1** in *R*-limonene (red, 5.0×10^{-5} M) and *S*-limonene (black, 5.0×10^{-5} M) and (b) **PBI 2** in *R*-limonene (5.1×10^{-5} M), respectively. For all the measurement the equilibrating time between each spectrum was ~ 18 minutes. Arrows indicate the spectral changes upon decreasing temperature from 100 °C to 35 °C.

For comparison, the solution of **PBI 2** in *R*-limonene was cooled in a similar fashion and the CD spectra were monitored. Unlike gelator **PBI 1**, in this case no Cotton effect could be observed upon cooling, although aggregation took places under this condition as indicated by the UV/vis spectra (Figure 2c). This is assigned to lack of hydrogen-bonding functionality of **PBI 2**, in which the π–π-stacking can not be orientated by external chiral environment.

Recent studies showed that self-assembly processes may be governed by both thermodynamic and kinetic control.[19] Thus we were also interested in investigating the impact of different cooling rates on the formation of these helical fibers. The solution of **PBI 1** was cooled from 100°C to 35°C at two different cooling speeds (Figure 7). When cooled at slower rate (15 °C/h), an intense bisignate CD signal was observed compared to cooling at a faster rate (60 °C/h). The observed effect suggests that fast cooling leads to the formation of kinetically trapped aggregated stacks whereas a more ordered nanostructure is formed when the cooling rate is slower.

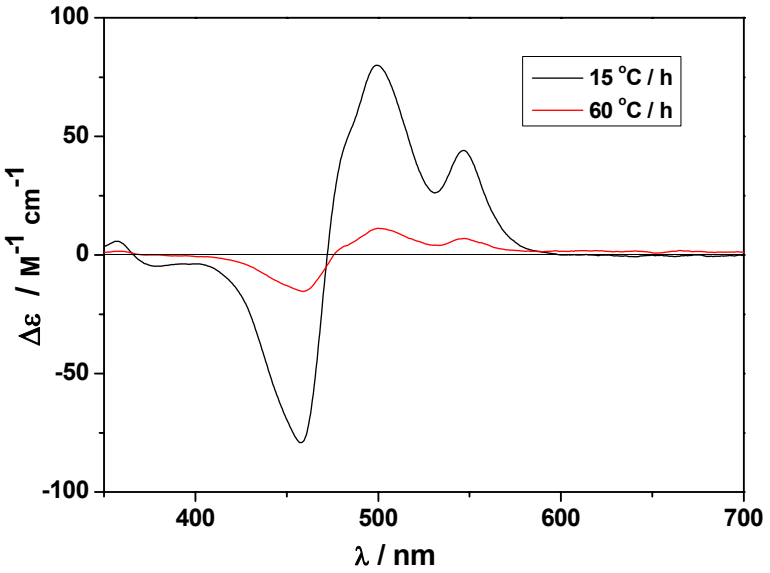

Figure 7. Cooling speed dependent CD spectra of **PBI 1** (5.0×10^{-5} M) in *S*-limonene. The sample was cooled from 100°C to 35°C.

4.3.2 Morphology of the Chiral Aggregates

The morphology of the **PBI 1** gels in chiral solvents were examined by atomic force microscopy (AFM). Gels were prepared from a 1×10^{-3} M solution of **PBI 1** in *S*-limonene by cooling, diluted to a concentration of 1×10^{-4} M and subsequently spin-casted on highly oriented pyrolytic graphite (HOPG) with a spin speed of 2000 rpm. The AFM images of these gels are shown in Figure 8. Two types of fibres were recognized: without and with helicity (labelled as 1 and 2 in Figure 8B). The smaller fibers without helicity on HOPG might be created by a template effect of HOPG due to the well-known strong interactions between alkyl chains and this substrate. The height of the larger helical structures is 2.6 ± 0.2 nm and the mean helical pitch is 19.0 ± 1.0 nm. Whilst CD spectroscopic studies revealed a preferential population of one-handed helices in chiral solvents, they do not provide any quantitative information on the enantiomeric excess. In contrast, AFM images of the gels with well-resolved helicity can provide this information. At first glance **PBI 1** gels made in *S*-limonene were found to consist of both types of helices.[20] It should be noted, however, that gelation is a very fast process under the given conditions (fast cooling, high chromophore concentration), thus, the chiral induction from external sources may be governed by kinetic effects (compare Figure 7). Even for a similar PBI organogelator which has one chiral alkyl group as a peripheral substituent (**PBI r2** in ref. 21), helices of both handedness are formed, which indicates a weak influence of the remote chiral center in the alkyl side chain on the chromophore packing in the fast gelation process. However, for the PBI which all of the three alkyl substituents are chiral, only *P*-type helices were found in AFM studies (**PBI r1**, see structures in ref. 21).[17, 21]

However, close inspection of the left-handed (*M*) and right-handed (*P*) helicity in large-scale AFM image in Figure 8A revealed 51 legible helical fibers, 30 right-handed (*P*) ones populate a majority of 59%, whereas 21 left-handed (*M*) ones

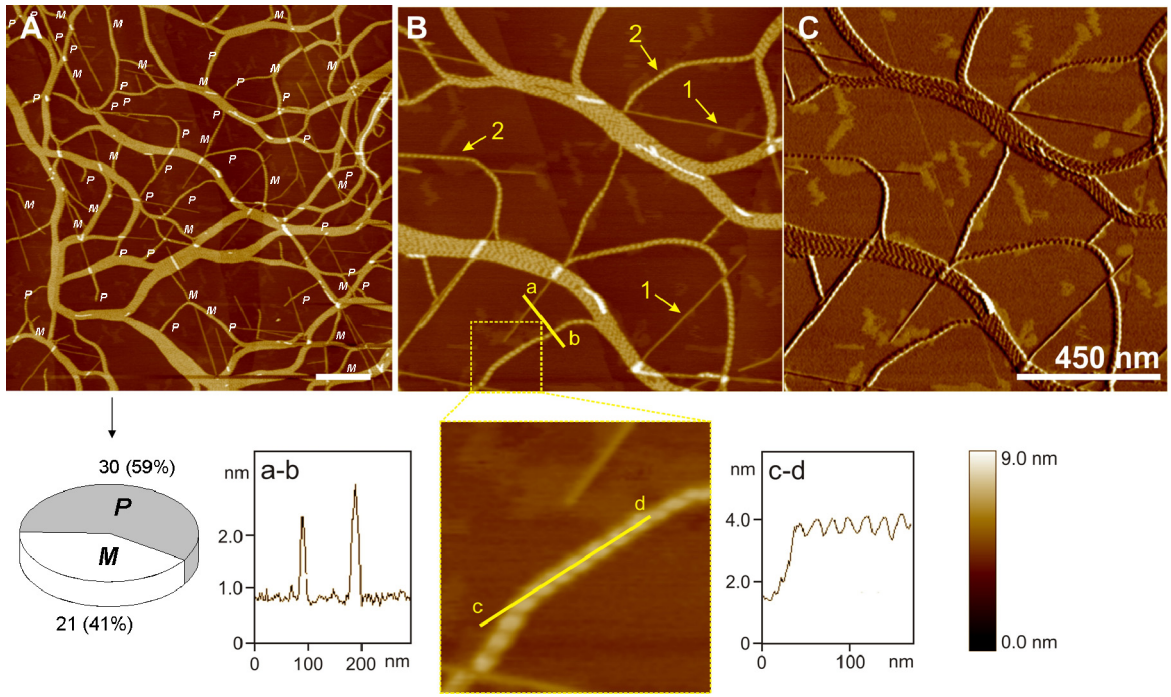

Figure 8. AFM images of a film spin-coated (2000 rpm) from a solution of **PBI 1** in *S*-limonene (1×10^{-4}M, room temperature) onto HOPG. A, B are height images and C is phase image. The scale bar in A, C corresponds to 450 nm and the z scale in A and B is 9 nm. The statistical graph of *M* and *P* helix are derived A. a-b and c-d are cross-section analysis of the fibers.

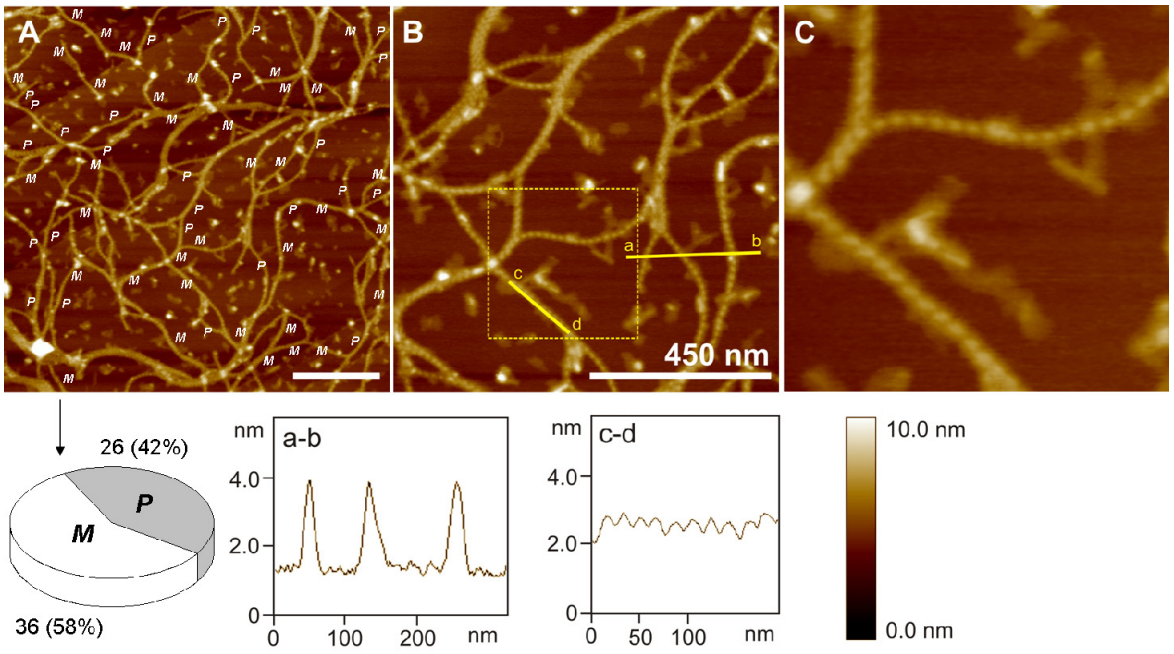

Figure 9. AFM images of a film spin-coated (2000 rpm) from a solution of **PBI 1** in *S*-limonene (1×10^{-4}M, room temperature) onto HOPG. he scale bar of A and B t is 450 nm and the z scale is 10 nm. C is zoomed region image of B. The statistical graph of *M* and *P* helix are derived A. a-b and c-d are cross-section analysis of the fibers.

populate a minority of is 41%, as shown in the statistical graph of Figure 8.

Similar AFM studies were also performed on **PBI 1** aggregates in *R*-limonene. As shown in Figure 9, network structures can be observed and the mean height of the fibrous components is 3.6 nm and the length is of several microns. These fibers show again nice helicities, in which both *M* and *P* configuration are adopted. Conversely to the case in *S*-limonene, 36 helical fibers in Figure 9a suggest a left-handed helical sense domination (58%) whilst only 26 (42%) are right-handed.

Thus, the excess of *P*-configured helical fibers in *S*-limonene, and *M*-configured helical fibers in *R*-limonene observed in AFM, is in accordance with the observed helical bias in solution recorded by CD spectroscopy. We conclude that homochiral fibers of **PBI 1** can be generated by applying chiral solvents upon the aggregation process.

4.4 Macroscopic Alignment of the Aggregates in Vortex Flow

The macroscopic alignment of self-assembled nanofibers was recently reported by Aida and co-workers for zinc porphyrin dyes as well as Meijer and Schenning's group for oligo(*p*-phenylenevinylene) derivatives, respectively.[10] It was found that extended aggregates of chromophores are an important prerequisite for this observation. In order to further explore this phenomenon, we performed similar studies on helical fibers generated from hydrogen-bond functionalized perylene bisimide dye **PBI 1**.

Firstly, we studied the impact of vortex flow on the CD spectra upon aggregation of achiral **PBI 1** in toluene. To do this, a diluted solution of **PBI 1** was cooled down from 75^{o}C to 35 ^{o}C in order to obtain extended fibrous aggregates. Then, a teflon-coated magnetic stirring bar (ca. Φ3×7 mm) was put into a 10 × 10 × 40 mm cuvette and the solution was under stirring when the spectra were recorded. In the absence of stirring no CD signal was observed. However, upon clockwise (CW) stirring a very strong bisignated CD signal with a positive band at 458 nm and two

negative bands at 498 and 546 nm were observed (Figure 10a). Upon anticlockwise (ACW) stirring a mirror image CD spectrum was recorded with a negative band at 458 nm and two positive bands at 498 and 546 nm.

Evidence for the dynamic nature of this process is given by the instantaneous on/off switching of the CD signal upon switching on/off the magnetic stirrer (the CD intensity was recorded at 452 nm, see inset in Figure 10a). When the stirrer was on, a strong CD couplet could be observed but as soon as it was switched off, the CD signal intensity reduced to zero. This experiment was repeated for several cycles and identical results were obtained, suggesting the complete reversibility of this process by external stirring. According to Aida and Meijer these CD signals are not related to true chiroptical effects by enantiomeric enrichment of *M*- or *P*-type helices as observed in chiral solvents, but originate from a macroscopic alignment of the fibers in the cuvette.[10]

Likewise, the helical fibers generated in chiral solvents can also be aligned by virtue of vortex flow. The CD spectra of **PBI 1** in chiral limonene reveal a synergic effect of micro-scale helical packing of the chromophores and the macroscopic orientation of the extended fibers. As shown in Figure 10b, in *R*-limonene a very strong bisignated CD signal is observed upon stirring and the sign of the spectra reverses when altering the stirring directions. Quite interestingly, while **PBI 1** gave almost perfect mirror images under reversal stirring directions in toluene (Figure 10a), in chiral solvents the spectra were not symmetrical, i.e., in *R*-limonene, the magnitude of the spectrum recorded with clockwise stirring was more prominent than that with anticlockwise stirring (Figure 10b), and in *S*-limonene the spectrum recorded with anticlockwise stirring was more intensive than that with clockwise stirring (Figure 10c). The intensities of CD signals recorded at 450 nm, 480 nm, and 545 nm are summarized in Table 1. Taking into account that the *M/P*-ratio of **PBI 1** helices is biased in this chiral solvent, the unsymmetrical CD sign of **PBI 1** in chiral solvents upon altering the stirring direction indicates a combined effect of both supramolecular chirality and macroscopic alignment (Figure 11).

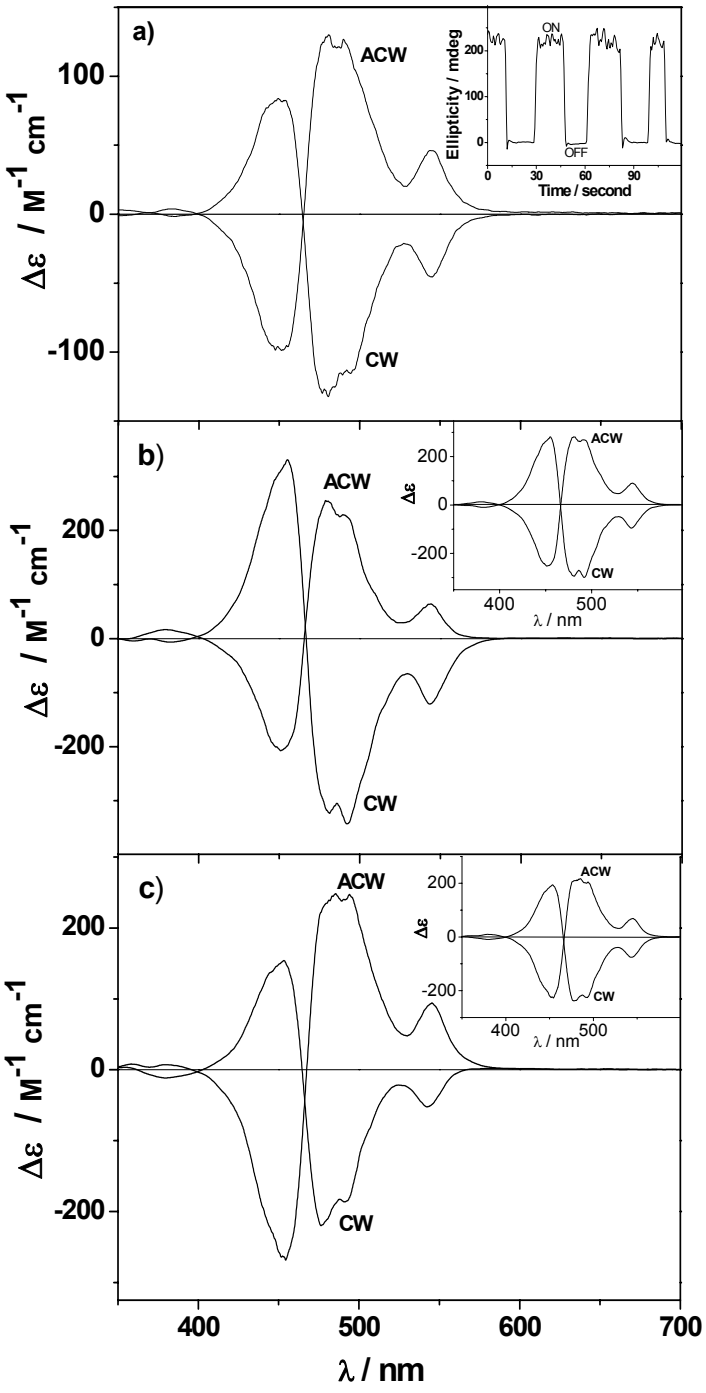

Figure 10. Evolution of CD signal upon stirring (1300 rpm) in clockwise and anticlockwise direction for **PBI 1** solution (5.0×10^{-5} M) at 35 °C in toluene (a), *R* -(b) and *S*-limonene (c), respectively. All the solutions were cooled from 100 ^{o}C within 3 hours in order to obtain well-organized aggregates. Inset in (a) is showing the CD intensity at 452 nm with successive on-off cycles of stirring at 1300 rpm. Inset in (b) and (c) are the spectra after subtraction of CD values for unstirred solutions (Figure 6a).

	At 450 nm ($\Delta\varepsilon/M^{-1}\ cm^{-1}$)			At 480 nm ($\Delta\varepsilon/M^{-1}\ cm^{-1}$)			At 545 nm ($\Delta\varepsilon/M^{-1}\ cm^{-1}$)		
	Quiet	CW	ACW	Quiet	CW	ACW	Quiet	CW	ACW
Toluene	2	85	-97	2	-130	130	0	-45	47
R-limonene	44	310	-206	-29	-323	255	-26	-121	62
S-limonene	-38	150	-257	27	-206	241	25	-48	92

Table 1. Intensity of CD spectra of **PBI 1** recorded at different wavelength under various conditions.

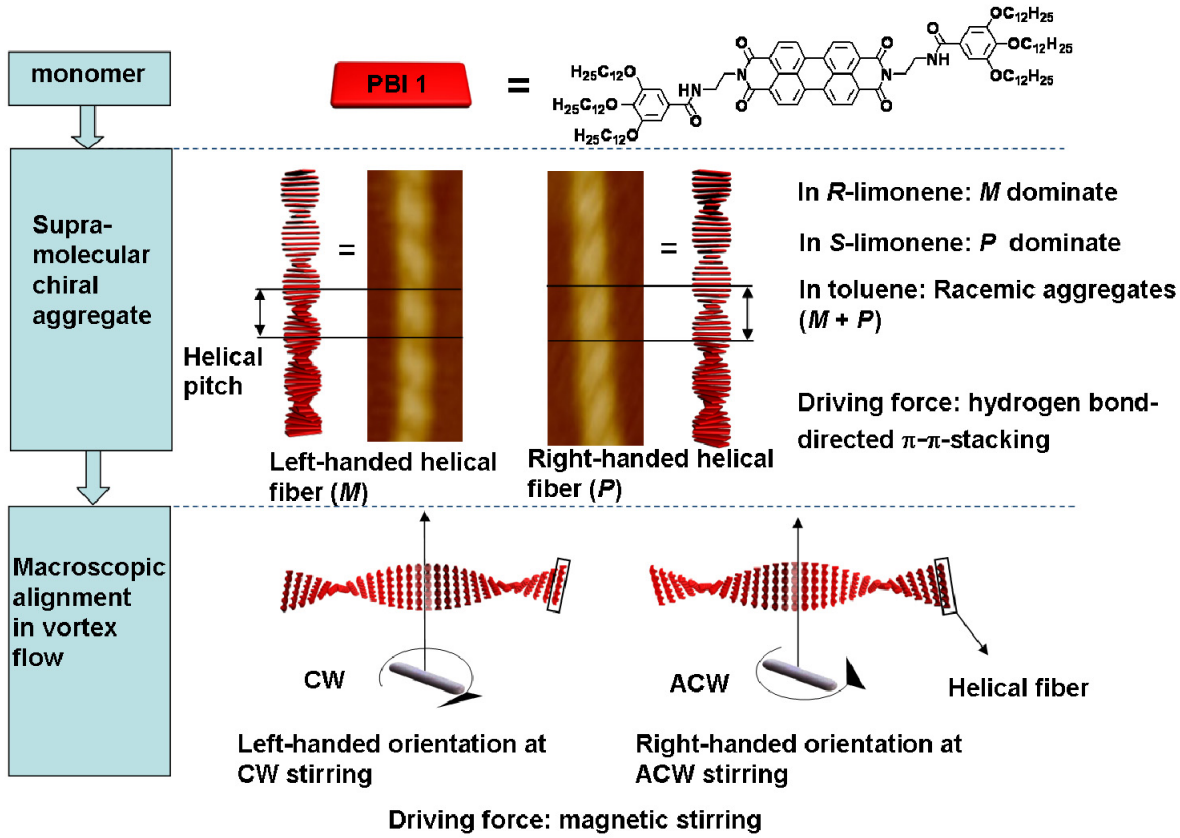

Figure 11. Schematic explanation for the origin of CD signals for **PBI 1** aggregates in chiral solvents and under vortex flow.

When we subtract the CD values of un-stirred solution (Figure 6a) from those of stirred solutions (Figure 10b and Figure 10c) in *R*- and *S*-limonene, mirror-imaged CD spectra were obtained, as shown in the insets of Figure 10b and 10c. This observation again confirms the independent effects of the chiral solvents and magnetic stirring, the former being related to a helical packing of the chromophores in *M*- or *P*-type direction, and the latter to macroscopic orientation of the fibers.

Similar investigations for **PBI 2** did not reveal any CD signal upon stirring in either clockwise or anticlockwise direction. This suggests that the presence of long fibers is essential for macroscopic alignment under vortex flow.

Further support for a macroscopic alignment of the fibers is given by Linear Dichroism (LD).[22] Thus, pronounced LD signal were observed in toluene, *R*- and *S*-limonene under vortex flow. The LD patterns do not alter the sign upon reversal of stirring direction (Figure 12a-c), and are almost identical in all three solvents although the intensity is more or less different. The remarkable similarity of our results with those recently published in the literature for two other dye aggregates indicates that extended dye aggregates can be oriented macroscopically by vortex flow which might be a particularly appealing technique for the orientation of functional materials based on organogelators.[10]

Further investigations include stirring speed dependent CD studies in toluene, *R*- and *S*- limonene. In order to simplify the investigation, only clockwise stirring was chosen. As show in Figure 13, the CD intensities respond strongly upon variation of stirring speed. In toluene, there was no CD sign when the solution was quiet; as stirring started, the CD signal showed up. With gradual increase of the stirring speed, the intensity of the CD signal increased steadily before it reached to saturation at about 1000 rpm (Figure 13d). In *R*-limonene, when the solution was quiet, the shape of CD spectrum was [(-)/(-)/(+) for longer to shorter wavelengths] as shown in Figure 13b. Upon clockwise stirring, the intensity of the spectra increased remarkably while the shape was remained. In the mean while, the absorption maximum shift to lower wavelength gradually (ca. 7 nm for the positive peak, 19 nm for the negative peak and 3 nm for the negative shoulder peak).

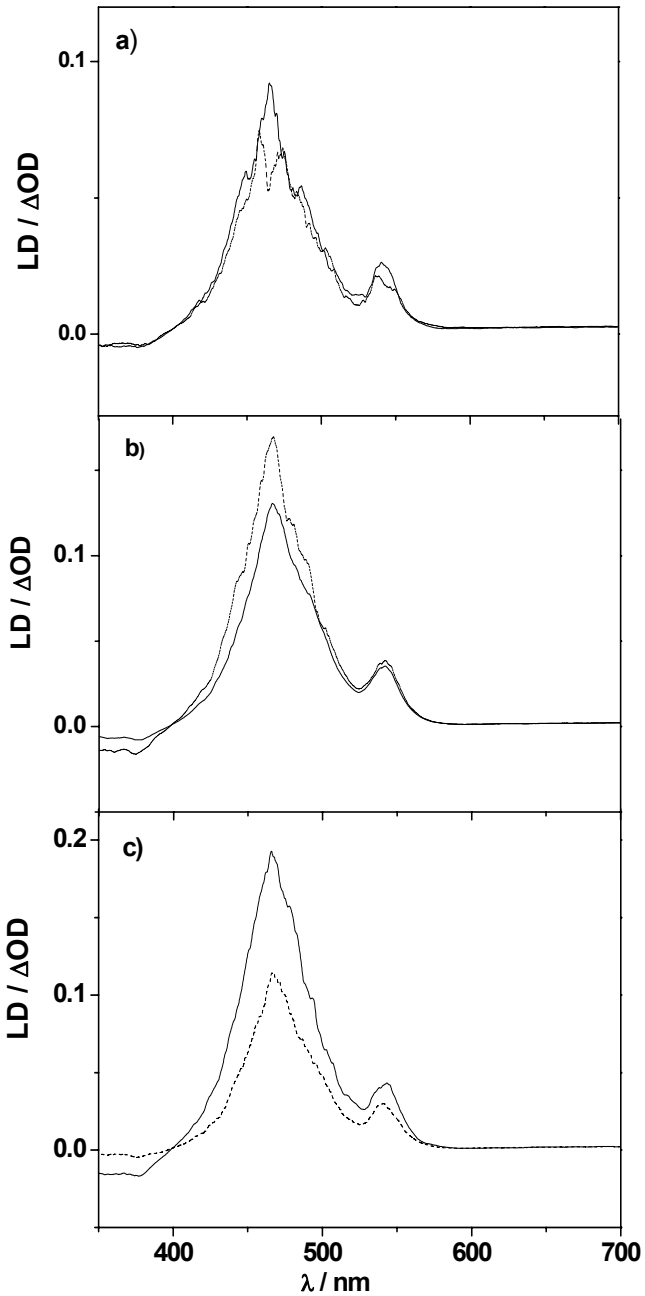

Figure 12. LD spectra of **PBI 1** measured at 35 °C under stirring (1300 rpm) in (a) toluene, (b) *R*-limonene, and (c) *S*-limonene. The solutions were cooled from 100 °C in about 3 h at 5.0×10^{-5} M. The solid line and dash line indicate CW and ACW stirring directions respectively.

More interesting phenomenon was found in *S*-limonene, as seen in Figure 14c, upon clockwise stirring, the [(+)/(+)/(-)] shaped CD spectrum was gradually inverted and finally led to opposite [(-)/(-)/(+)] shape upon increasing the stirring speed. In due time, if the stir was switch off, the spectra went back to original

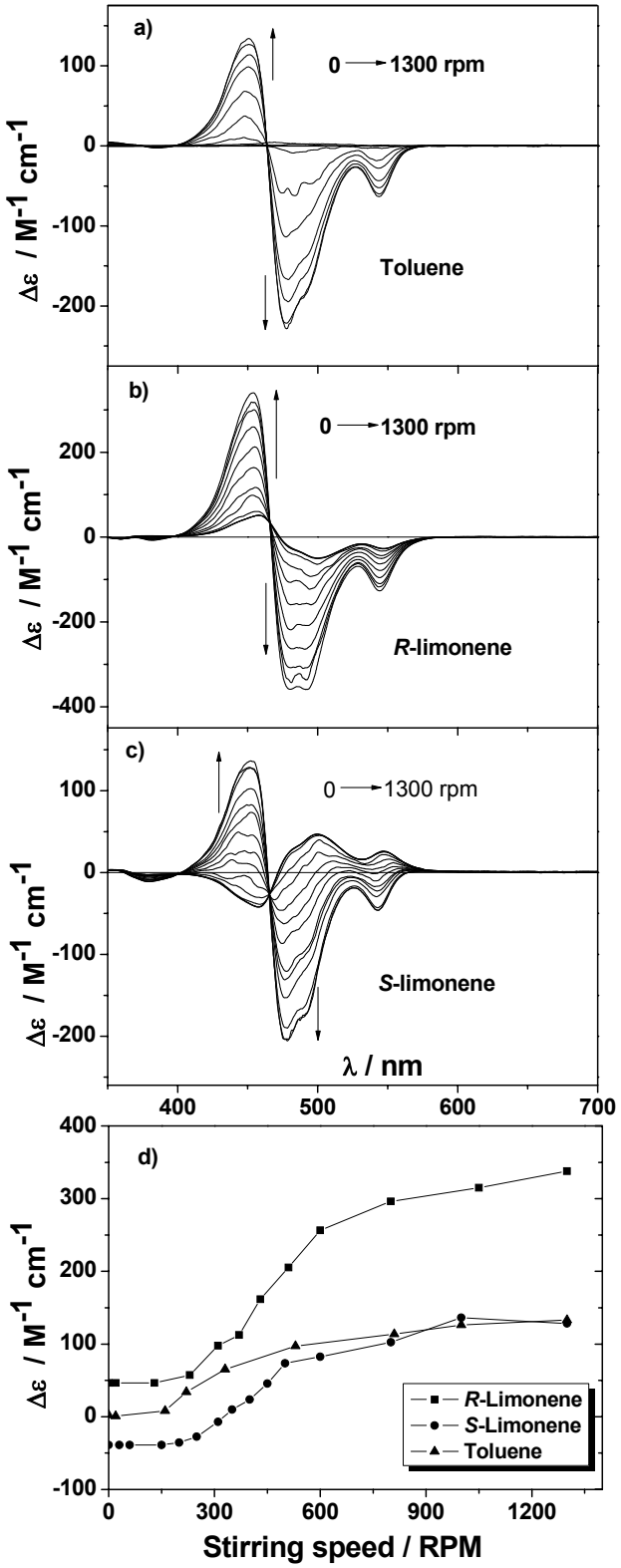

Figure 13. Evolution of CD signal upon gradual increase the stirring (clockwise direction) speed for **PBI 1** solution (5.0×10^{-5} M) at 35 °C (a) in toluene, (b) in *R*-limonene, and (c) in *S*-limonene. (d) is the variation of CD intensity at 452 nm as a function of stirring speed. All the solutions were cooled from 100 ^{o}C within 3 hours in order to obtain well-organized aggregates.

[(+)/(+)/(-)] shape immediately. Figure 14d shows the variation of CD intensity at 452 nm as a function of stirring speed. These observations illustrate legibly that the aggregated nanofibers of **PBI 1** can be aligned by rotator stirring, while the helicity of the individual fibers do not change in the vortex flow, and the crosscorrelation of macroscopic and supramolecular chirality can be readily visualized from the sharp change of CD spectra upon changing the stirring speed.

4.5 Conclusions

In this chapter, we have investigated the impact of chiral solvents and vortex flow on the self-assembly of **PBI 1** molecules by UV/Vis and CD spectroscopy and AFM microscopy. In solution **PBI 1** molecules form long helical fibers by π-π-stacking and hydrogen bonding interactions. In achiral solvent such as toluene, both left-handed and right-handed helicity co-exist in equal amounts and the system is overall chiroptically silent. However, in chiral environments the *M*/*P* ratio is biased and a preferential helicity can be selected by choosing a chiral solvent such as *R*- and *S*-limonene. Interestingly, these long helical fibers can align at macroscopic level under vortex flow. The microscopic helical sense originating from chiral environment is independent to the macroscopic orientation of the fibers generated by vortex flow.

4.6 Experimental Details

Materials and methods: All solvents and reagents were purchased from commercial sources. The solvents for spectroscopic studies were of spectroscopic grade and used as received. *R*- and *S*-limonene were purchased from Merck & Co., Inc. UV/Vis spectra were measured in a Perkin-Elmer Lambda 950 spectrometer equipped with a Peltier system as temperature controller. All the solutions were measured in conventional quartz cell of 0.1 cm - 1 cm path length to cover a suitable concentration range.

Circular Dichroism (CD) and Linear Dichroism (LD) spectroscopy. The CD and LD spectra were recorded with a Jasco J-810 spectropolarimeter equipped with Jasco CDF 426S temperature/stirring controller. The stirring direction can be altered reversely. All the solutions were measured in conventional quartz cell of 1 cm path length.

Atomic force microscopy (AFM). AFM measurements were performed under ambient conditions using a MultiMode Nanoscope IV system operating in tapping mode in air. Silicon cantilevers (OMCL-AC160TS) with a resonance frequency of ~300 kHz were used. For AFM studies, the gel in toluene, *R*- and *S*-limonene were diluted (concentration 0.1 mM) and then were spin-coated onto HOPG under 2000 rpm rotating speed.

4.7 References and Notes

1 (a) M. Albrecht, *Chem. Rev.* **2001**, *101*, 3457-3497; (b) K. R. MacKenzie, *Chem. Rev.* **2006**, *106*, 1931-1977.

2 (a) F. M. Hoeben, P. Jonkheijm, E. W. Meijer, A. P. H. J. Schenning, *Chem. Rev.* **2005**, *105*, 1491-1546.

3 (a)T. Shimizu, M. Masuda, H. Minamikawa, *Chem. Rev.* **2005**, *105*, 1401-1443; (b) L. A. Estroff, A. D. Hamilton, *Chem. Rev.* **2004**, *104*, 1201-1217; (c) C. C. Lee, Christophe. Grenier, E. W. Meijer, A. P. H. J. Schenning, *Chem. Soc. Rev.* **2009**, *38*, 671-683.

4 (a) A. R. A. Palmans, J. A. J. M. Vekemans, E. E. Havinga, E. W. Meijer, *Angew. Chem., Int. Ed.* **1997**, *36*, 2648-2651; (b) G. Dantlgraber, A. Eremin, S. Diele, A. Hauser, H. Kresse, G. Pelzl, C. Tschierske, *Angew. Chem. Int. Ed.* **2002**, *41*, 2408-2412.

5 M. Sua´rez, N. Branda, J.-M. Lehn, A. Decian, J. Fischer, *Hel*v.*Chim. Acta* **1998**, *81*, 1-13.

6 W. Yang, X. Chai, L. Chi, X. Liu, Y. Cao, R. Lu, Y. Jiang, X. Tang, H. Fuchs, T. Li, *Chem. Eur. J.* **1999**, *5*, 1144-1149.

7 (a) U. De Rossi, S. Dähne, S. C. J. Meskers, H. P. J. M. Deckers, *Angew. Chem. Int. Ed.* **1996**, *35*, 760-763; (b) A. Pawlik, S. Kirstein, U. De Rossi, S. Dähne, *J. Phys. Chem. B* **1997**, *101*, 5646-5651; (c) C. Spitz, S. Dähne, *J. Phys. Chem. B* **2000**, *104*, 8664-8669; (d) S. Kirstein, H. von Berlepsch, C. Böttcher, C. Burger, A. Ouart, G. Reck, S. Dähne, *ChemPhysChem*, **2000**, *3*, 146-150.

8 H. von Berlepsch, S. Kirstein, C. Böttcher, *J. Phys. Chem. B* **2003**, *107*, 9646-9654.

9 (a) J. M. Ribó, J. Crusats, F. Sagues, J. M. Claret, R. Ruvires, *Science* **2001**, *292*, 2063-2066; (b) R. Rubires, J.-A. Farrera, J. M. Ribó, *Chem. Eur. J.,* **2001**, *7*, 436-446.

10 (a) A. Tsuda, Md. A. Alam, T. Harada, T. Yamaguchi, N. Ishii, T. Aida, *Angew. Chem. Int. Ed.* **2007**, *46*, 8198-8202; (b) M. Wolffs, S. J. George, Ž. Tomović, S.

C. J. Meskers, A. P. H. J. Schenning, E. W. Meijer, *Angew. Chem. Int. Ed.* **2007**, *46*, 8203-8205; (c) G. P. Spada, *Angew. Chem. Int. Ed.* **2008**, *47*, 636-638.

11 (a) M. Eriksson, M. Härdelin, A. Larsson, J. Bergenholtz, B. Åkerman, *J. Phys. Chem. B* **2007**, *111*, 1139-1148; (b) U. Pindur, M. Jansen, T. Lemster, *Curr. Med. Chem*. **2005**, *12*, 2805-2847.

12 X.-Q. Li, V. Stepanenko, Z. Chen, P. Prins, L. D. A. Siebbeles, F. Würthner, *Chem. Commun*. **2006**, 3871-3873.

13 (a) F. Würthner, C. Thalacker, S. Dielec, C. Tschierske, *Chem. Eur. J.* **2001**, *7*, 2245-2253; (b) Z. Chen, U. Baumeister, C. Tschierske, F. Würthner, *Chem. Eur. J.* **2007**, *13*, 450-465.

14 (a) F. Würthner, Z. Chen, V. Dehm, V. Stepanenko, *Chem. Commun*. **2006**, 1188-1190; (b) V. Dehm, Z. Chen, U. Baumeister, P. Prins, L. D. A. Siebbeles, F. Würthner, *Org. Lett.* **2007**, *9*, 1085-1088.

15 M. R. Hansen, T. Schnitzler, W. Pisula, R. Graf, K. Müllen, H. W. Spiess, *Angew. Chem. Int. Ed.* **2009**, *48*, 4621-4624.

16 F. Würthner, C. Bauer, V. Stepanenko, S. Yagai, *Adv. Mater.* **2008***, 20*, 1695-1698.

17 S. Gosh, X.-Q. Li, V. Stepanenko, F. Würthner, *Chem. Eur. J.* **2008**, *14*, 11343-11357.

18 N. Berova, K. Nakanishi, R. W. Woody, *Circular Dichroism:Principles and Applications* Wiley-VCH: New York, 2000.

19 (a) F. Würthner, S. Yao, U. Beginn, *Angew. Chem. Int. Ed.* **2003**, *42*, 3247-3250; (b) S.Yao, U. Beginn, T. Gress, M. Lysetska, F. Würthner, *J. Am.Chem. Soc.* **2004**, *126,* 8336-8348; (c) A. Lohr, F. Würthner, *Angew. Chem. Int. Ed.* **2008**, *47*, 1232-1236.

20 (a) A. Wu, L. Isaacs, *J. Am. Chem. Soc*. **2003**, *125*, 4831-4835; (b) P. Mukhopadhyay, P. Y. Zavalij, L. Isaacs, *J. Am. Chem. Soc*. **2006**, *128*, 14093-14102; (c) K. Sugiyasu, *S*-i. Kawano, N. Fujita, S. Shinkai, *Chem. Mater*. **2008**, *20*, 2863-2865.

21 Structures of **PBI r1** and **PBI r2** which possess chiral alkyl chains

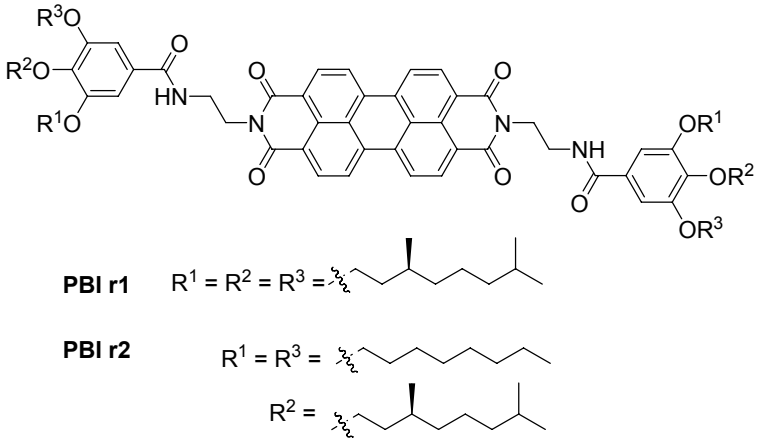

22 (a) B. Nordén, *J. Phys. Chem.* **1978,** *82*, 744-746; (b) A. Davidsson, B. Nordén, S. Seth, *Chem. Phys. Lett*. **1980**, *70*, 313-316; (c) Y. Shindo, M. Nishio, S. Maeda, *Biopolymers* **1990**, *30*, 405-413; (d) R. Kuroda, T. Harada, Y. Shindo, *Rev. Sci. Instrum.* **2001**, *72*, 3802-3810; (e) H. Gillgren, A. Stenstam, M. Ardhammar, B. Nordén, E. Sparr, S. Ulvenlund, *Langmuir* **2002**, *18*, 462-469; (f) A. Ohira, K. Okoshi, M. Fujiki, M. Kunitake, M. Naito, T. Hagihara, *Adv. Mater*. **2004**, *16*, 1645-1650.

Chapter 5

Highly Fluorescent Mesophases and Organogels Based on J-Aggregates of Core-Twisted Perylene Bisimide Dyes

5.1 Introduction

Over the past decade, low molecular weight organogelators have attracted considerable interest because of their diverse applications as supramolecular soft materials.[1] The formation of organogels[2] is facilitated by highly directional self-assembly through non-covalent interactions such as π–π–stacking, hydrogen bonding, metal-ion coordination, dipole-dipole interactions, etc. In the last few years, several functional dye based building blocks have been reported to form organogels and the unique features of the 3D network superstructures have been applied for sensors, optoelectronic devices, light harvesting, nucleation of inorganic materials, etc. [3-8]

Organogelators based on numerous electron-rich aromatic building blocks such as porphyrins, phthalocyanines, oligo(phenylenevinylenes), oligothiophenes and tetrathiafulvalenes have been investigated in the recent past.[7] However, such examples for electron-poor aromatic systems are still rare.[8] Perylene bisimides (PBIs) have been extensively studied as n-type semiconductors in various applications such as optical recording media, organic photo- and semiconductors, and solar cells.[9] Recently, the groups of Shinkai and Yagai as well as our group have reported the first PBI based organogelators.[10-12] In these examples,

well-defined fibrous aggregates were observed by atomic force microscopy (AFM) and their formation has been attributed to π–π–stacking and intermolecular hydrogen bonding between the constituent PBI molecules. However, for these gels broadened UV/Vis absorption bands and inferior emission properties were observed compared to solutions of the monomeric dyes. In this chapter, we introduce a new perylene bisimide based organogelator (**PBI 1**) with an unprecedented sharp J-type absorption band and favorable emission properties. These features can be attributed to strong excitonic coupling as demanded for exciton transport in photonic and photovoltaic applications.

5.2 Results and Discussions

5.2.1 Structural Properties

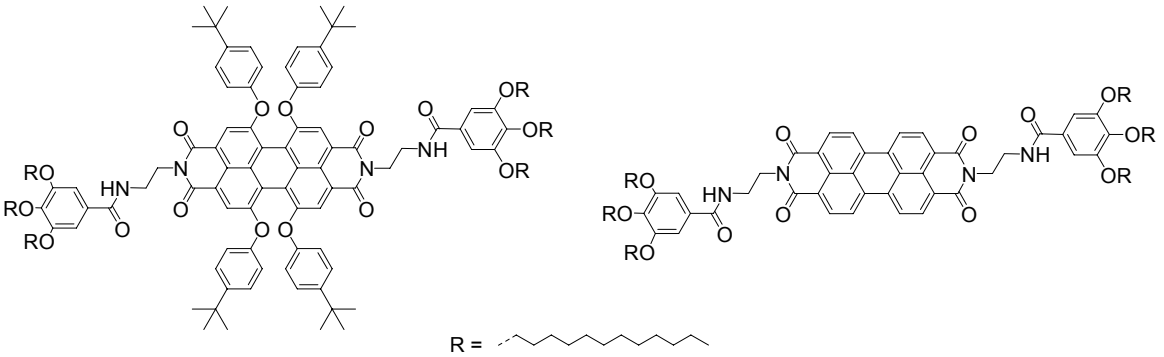

Figure 1. Molecular structures of **PBI 1** and **PBI 2**.

The structures of **PBI 1** and **PBI 2** are shown in Figure 1. **PBI 1** was synthesized by imidization of *tert*-butyl-phenoxy perylene tetracarboxylic acid bisanhydride with aminoethyl-tris(dodecyloxy)benzamide in quinoline using $Zn(OAc)_2$ as catalyst and isolated as a purple powder in 51% yield (details for synthesis and characterization of **PBI 1** are given experiment part). The calculated molecular models as well as several crystal structures for related compounds indicate that **PBI**

2 possesses a planar perylene core, whereas **PBI 1** exhibits a distorted perylene core with a twist angle of about 25-30^{o} due to the presence of four bulky *tert*-butyl-phenoxy substituents at the bay positions[13] (Figure 2). In chapter 3, we showed that **PBI 2** is an efficient gelator, which can gel various types of organic solvents at low critical gelation concentrations (CGC) by virtue of π–π–stacking

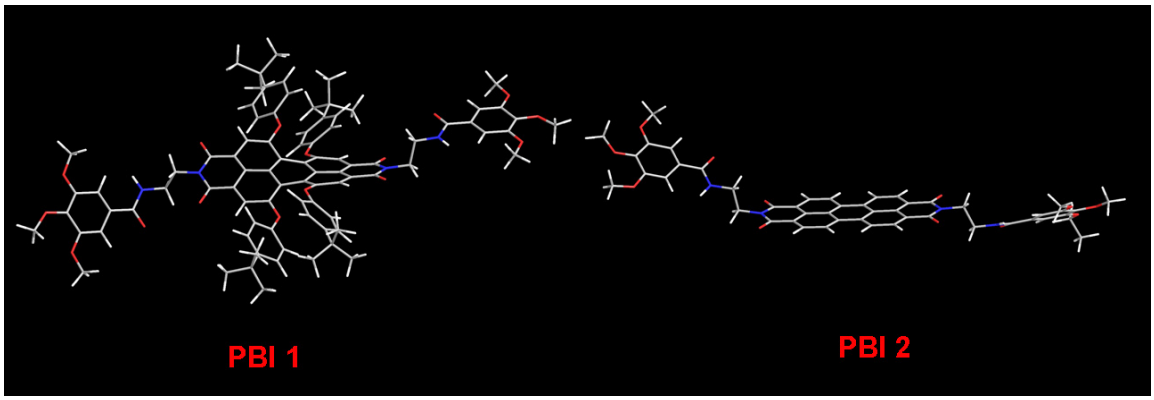

Figure 2. Optimized molecular structures of twisted **PBI 1** and planar **PBI 2** (HyperChem, MM+; the alkyl chains were replaced by methyl groups).

and hydrogen-bonding interactions.[11b] In order to examine whether similar hydrogen-bonding interaction exists among the bay-substituted **PBI 1** chromophores, we performed FT-IR spectroscopy of **PBI 1** in apolar solvent methylcyclohexane (MCH) which revealed the formation of intermolecular hydrogen bonds between the benzamide functional groups (Figure 3). The IR spectrum of **PBI 1** in CH_2Cl_2 shows a broad N-H stretching band at 3410 cm^{-1} which indicates the absence of hydrogen bonding. The benzamide carbonyl group vibration band overlap with the carbonyl group vibration of the perylene imide groups at 1660 cm^{-1}. In concentrated MCH solution, **PBI 1** shows N-H stretching band at 3290 cm^{-1} and a benzamide carbonyl group vibration at 1628 cm^{-1}. Both displacements to lower frequency are indicative for the hydrogen-bonding interactions among the amide moieties.

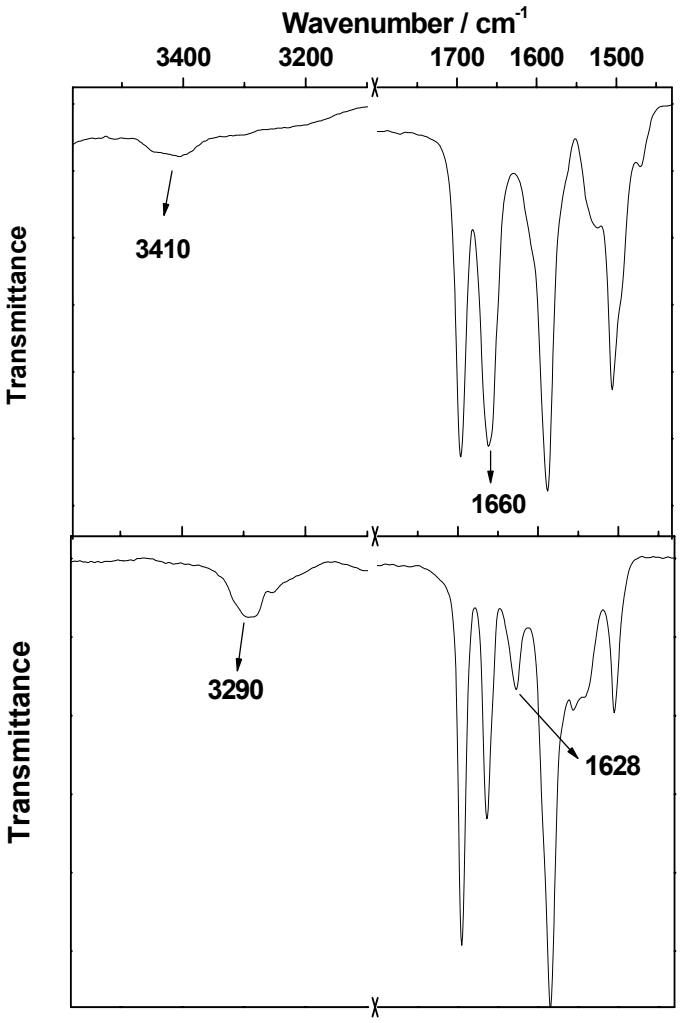

Figure 3. FT-IR spectra of **PBI 1**: (top) In CH_2Cl_2 solution (1.0×10^{-3} M) and (bottom) in MCH solution (1.0×10^{-3} M).

5.2.2 Organogels and Mesophases

Gelation tests were performed for **PBI 1** in 17 different organic solvents. In most of solvent such as methylcyclohexane, cyclohexane, *n*-hexane, *n*-pentane, benzene, thiophene, toluene, THF, chloroform, dichloromethane, 1-octanol, **PBI 1** can be well dissolved (in all the cases, concentration > 5 mM). For the solvents DMF, DMSO, ethanol and methanol precipitates could be observed. The opaque gels

were formed only in acetone and dioxane. The critical gelation concentration (CGC) was determined as 0.9 mM (0.27 wt%) in acetone and 4.6 mM (1.05 wt%) in dioxane at room temperature. It is quite unexpected to us that, no gelation was

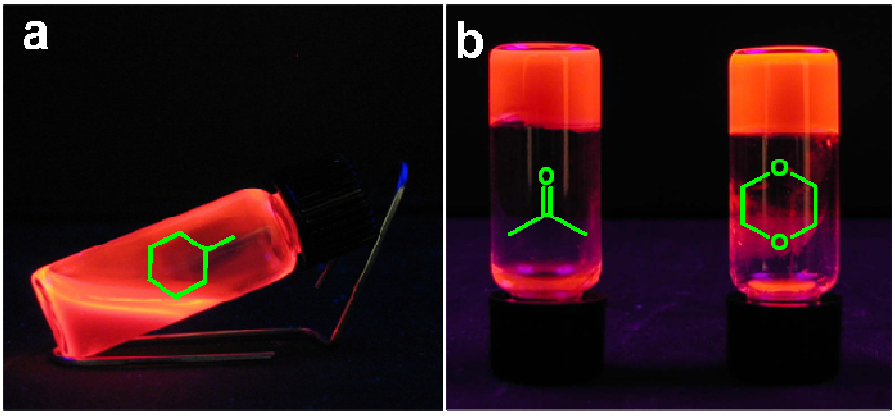

Figure 4. Photographs of **PBI 1** in different solvents under a UV lamp (366 nm): (a) in MCH at *c* = 10 mM (2.9 wt%); (b) in acetone at *c* = 1.5 mM (0.4 wt%) and in dioxane at *c* = 4 mM (1.1 wt%).

observed in aromatic solvents such as toluene, benzene and aliphatic solvents such as methylcyclohexane and cyclohexane, but opaque gels were observed in acetone and dioxane, which are known as hydrogen-bond breaking solvents (Figure 4). Despite their failure to gel apolar organic solvents, the signature of aggregate formation was evident in these aliphatic solvents (e.g., methylcyclohexane, cyclohexane, and *n*-hexane) from the increased viscosity of the solutions at higher concentrations (c > 10 mM). Notably, no precipitation took place at these rather high concentrations but textures that resemble those found for chromonic liquid crystals[14] were observed under the optical polarizing microscope (OPM). As shown in Figure 4, the formation of a nematic (N) phase in a concentrated MCH solution was indicated by a Schlieren texture (Figure 5a, b). In this phase, the mesogens typically stack to form columns, but there is no positional order among the columns. As the sample was concentrated (edge evaporated for 2 hours), a grainy optical texture can be observed, which is characteristic of the columns arranged in a

hexagonal order in the hexagonal (M) phase (Figure 4c).[14b] Similar textures can also be observed in cyclohexane and *n*-hexane that show both N and M phases in concentrated solutions (Figure 5e, f).

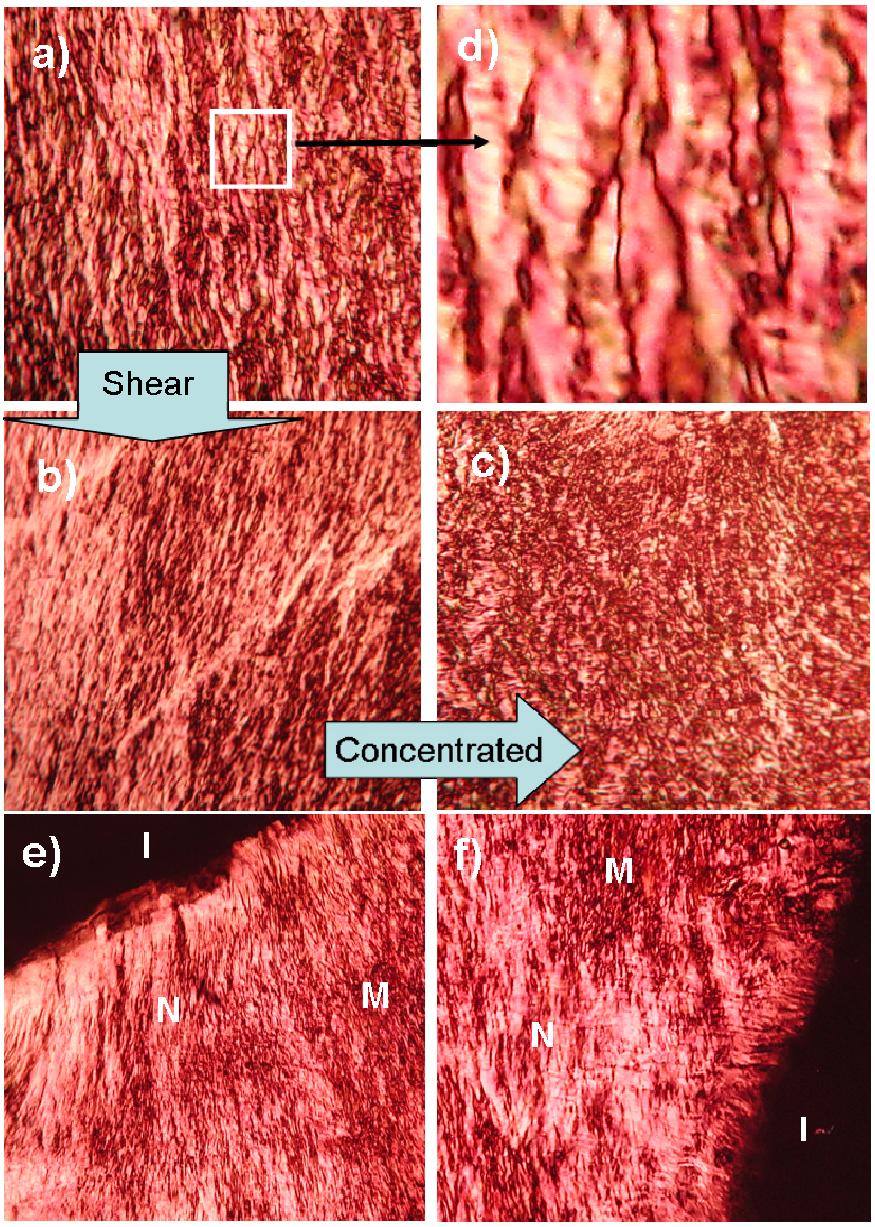

Figure 5. Polarized optical microscopy images (crossed polarizers) of (a) schlieren textures from a viscous solution of **PBI 1** in MCH (8 mM; 2.3 wt%); (b) after shearing, the texture can recover; (c) grainy textures after the film was edge evaporated for 2 hours; (d) is zoomed region from image from (a); (e) and (f) indicate the co-existence of the mesophases (N and M) and isotropic phase (I) of **PBI 1** in cyclohexane (15 mM, 4.3 wt%) and *n*-hexane (15 mM, 5.4 wt%), respectively.

5.2.3 Spectroscopic Properties

To investigate the aggregation properties of **PBI 1** in more detail, we carried out photophysical studies in solution. Firstly, optical properties of **PBI 1** in the monomeric and aggregated states were investigated by temperature-dependent UV/Vis and fluorescent spectroscopy in different solvents (Figure 6). The UV/Vis spectra of **PBI 1** in CH_2Cl_2 (or in MCH at higher temperature) exhibit typical spectroscopic features that are expected for monomeric tetra-aryloxy-substituted PBI chromophores.[15] The absorption maximum at 583 nm indicates a strongly allowed $S_0 \rightarrow S_1$ transition. The fluorescent emission spectrum with a peak maximum at 621 nm is mirror image of the absorption band. The absorption and emission bands are rather broad with full-width-at-half-maximum (fwhm) values of 2311 cm^{-1} and 1780 cm^{-1}, respectively. The broadness of these bands results from the distortion of the chromophore and various conformational states of the four aryloxy groups.

Unlike those in CH_2Cl_2, the absorption spectra of **PBI 1** in MCH exhibit a sharp intense band that is bathochromically shifted by ca. 13 nm from the monomer band (Figure 6a). The fluorescent spectrum has a mirror image relationship to the absorption spectrum with a Stokes shift of only 11 nm. The fwhm values of absorption and emission spectra are significantly reduced to 850 cm^{-1} and 786 cm^{-1}, respectively. Temperature-dependent UV/Vis experiments in MCH testify the reversibility of the self-assembly process. When the temperature is raised from 10 ^{o}C to 90 ^{o}C, the sharp band at 598 nm gradually disappears and the monomeric species is recovered as evidenced by re-appearance of the broad spectrum (Figure 6b). These spectral features clearly indicate the reversible formation of J-aggregates of **PBI 1** in apolar solvent which is in contrast to the H-aggregating **PBI 2** and other PBI based organogelators.[10,11] The very intense J-band of **PBI 1** with relatively small bathochromic shift suggests the presence of tightly aggregated chromophores at a slip angle close to the magic angle of 54.7° that is unprecedented for this class of chromophores.[16,17] These unusual spectral and

packing features are encoded in the unique molecular structure of **PBI 1**: a twisted π-conjugated core and additional amide groups that can assist intermolecular H-bonds.

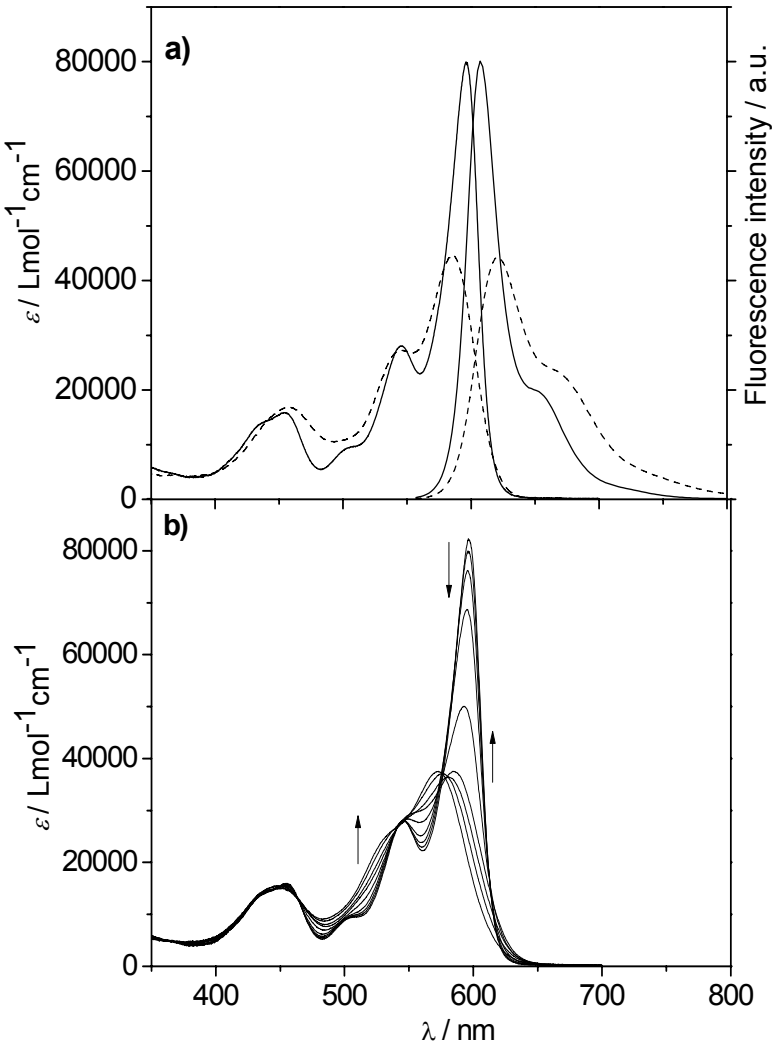

Figure 6. (a) UV/Vis (left) and fluorescence (right) spectra of **PBI 1** in CH_2Cl_2 (dashed lines, 1.1×10^{-5} M) and MCH (solid lines, 1.1×10^{-4} M) at 20 °C; (b) temperature-dependent absorption spectra of **PBI 1** (1.1×10^{-4} M, in MCH) from 10 °C to 90 °C. The arrows indicate spectral changes with increasing temperature.

Similar optical properties of **PBI 1** can also be found in acetone and dioxane, in which organogels were formed. Temperature-dependent UV/Vis spectra of **PBI 1**

in these hydrogen-bond breaking solvents (Figure 7) clearly show J-type aggregating behavior, i.e., upon aggregation the absorption maximum shifts bathochromically. However, in these solvents aggregation took place only at considerably higher concentrations and lower temperatures (in acetone: $c > 1.0$ mM, $T < 30$ °C, and in dioxane: $c > 2.5$ mM, $T < 20$ °C) when compared with that in apolar solvent such as MCH. The relatively lower propensity to aggregate formation of **PBI 1** in acetone and dioxane is conceivable since the solvent molecules in these cases are capable of interacting with the amide functionality of

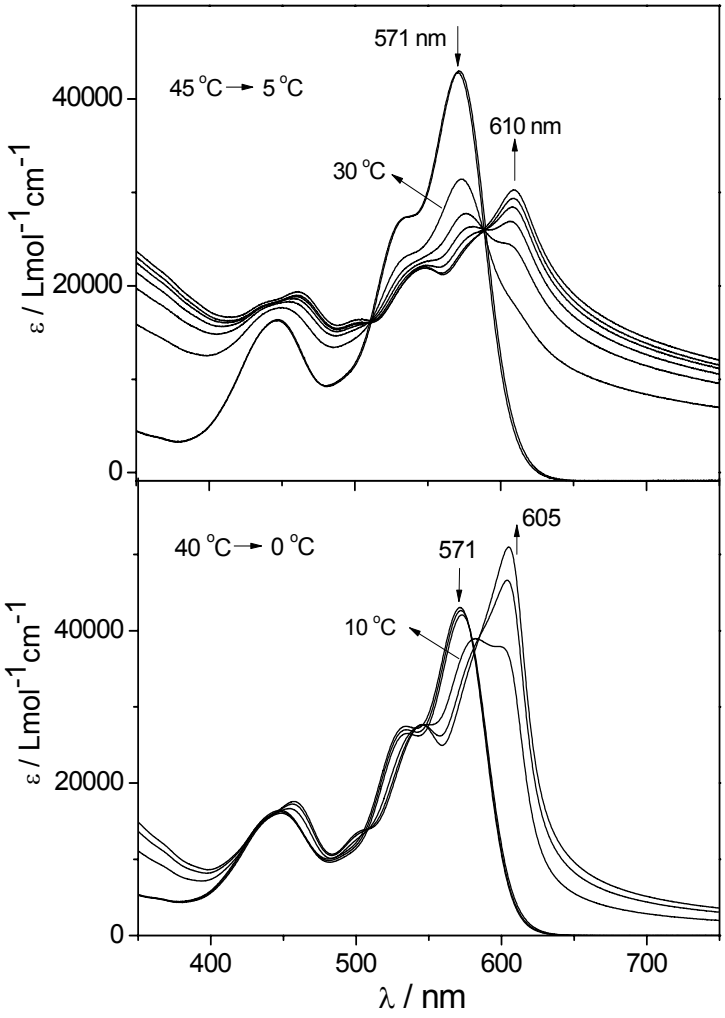

Figure 7. Variable-temperature UV/Vis absorption spectra of **PBI 1** in acetone (top, 1.0×10^{-3} M, from 45 °C to 5 °C) and in dioxane (bottom, 2.5×10^{-3} M, from 40 °C to 0 °C). The arrows indicate spectral changes upon decreasing temperatures.

the dye molecules through hydrogen bonding,[18] and thus can weaken the inter-chromophoric interactions. However, at significantly higher concentration and lower temperature, dye aggregation was evidenced from distinct spectral changes (bathochromic shift of ca. 39 nm in acetone) that are indicative of a packing motif with more displaced dye molecules according to exciton coupling theory[17]

Further evidence of solvent participation in hydrogen bonding with the amide functionality of **PBI 1** was gathered from ^{1}H NMR studies (Figure 8). The amide proton of **PBI 1** (labeled with green dots) was found to be significantly downfield shifted in acetone (either for aggregates gel or for monomers) compared to that in chloroform (monomers) or in benzene (aggregates). This suggests the proposed hydrogen-bonding interaction with the solvent molecule. On the other hand, no obvious change of amide protons could be observed from spectra (a) and (b), which indicates the absence of amide-amide hydrogen bonding between the self-assembled dye building blocks.

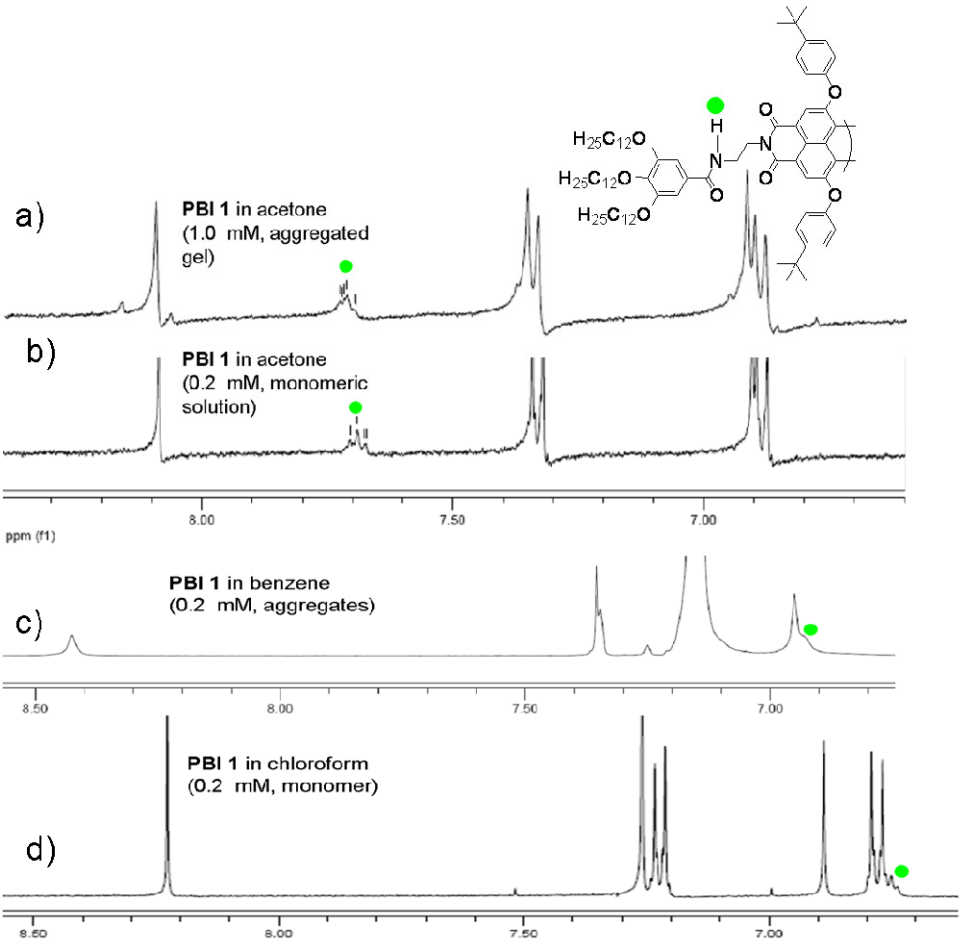

Figure 8. ^{1}H NMR spectra of **PBI 1**: (a) in acetone, c = 1.0 mM, aggregated dyes in gel phase; (b) in acetone, c = 0.2 mM, primarily monomeric dyes; (c) in benzene, c = 0.2 mM, aggregated dyes; (d) in chloroform, c = 0.2 mM, monomeric dyes.

5.2.4 Microscopic Morphology

Whilst the solution spectroscopic studies revealed the aggregate formation in various solvents, transmission electron microscopy (TEM) studies provided direct evidences for the formation of extended networks. Figure 9 shows typical TEM images of aggregated structures of **PBI 1** and **PBI 2** in different solvents. As reported previously, **PBI 2** can form long well-defined fibers and further entangle to network structures in many apolar solvents.[11b] In contrast, for **PBI 1** less regular structures are observed. In MCH loosely connected bundles of aggregate structures are visualized by TEM (Figure 9a, b) as expected for lyotropic mesophases.[14] These aggregates appear much more fluid-like as compared to the entangled fibers observed for gels of **PBI 2**[11b](Figure 9e, f). They are able to cause an increase in viscosity of the medium (Figure 4a) but are unable to gel the solvent.[19] Interestingly, TEM images from a suspension of **PBI 1** gel in acetone revealed distinctly different aggregate morphologies as shown in Figure 9c and 9d. The willow-leaf-like aggregated units appear to be more flexible and they can gradually entangle to each other at the ends to give star-shaped structures. Those "stars" further intercross to form the 3D network structures, which are essential for gelation. Similar spectroscopic and microscopic features of **PBI 1** could also be observed in dioxane (Figure 10). The flexible leaf-like aggregates entangle to network structures forming organogels, however, this process takes place at higher concentration in dioxane (2.5×10^{-3} M), as also verified in temperature-dependent absorption spectra (Figure 7).

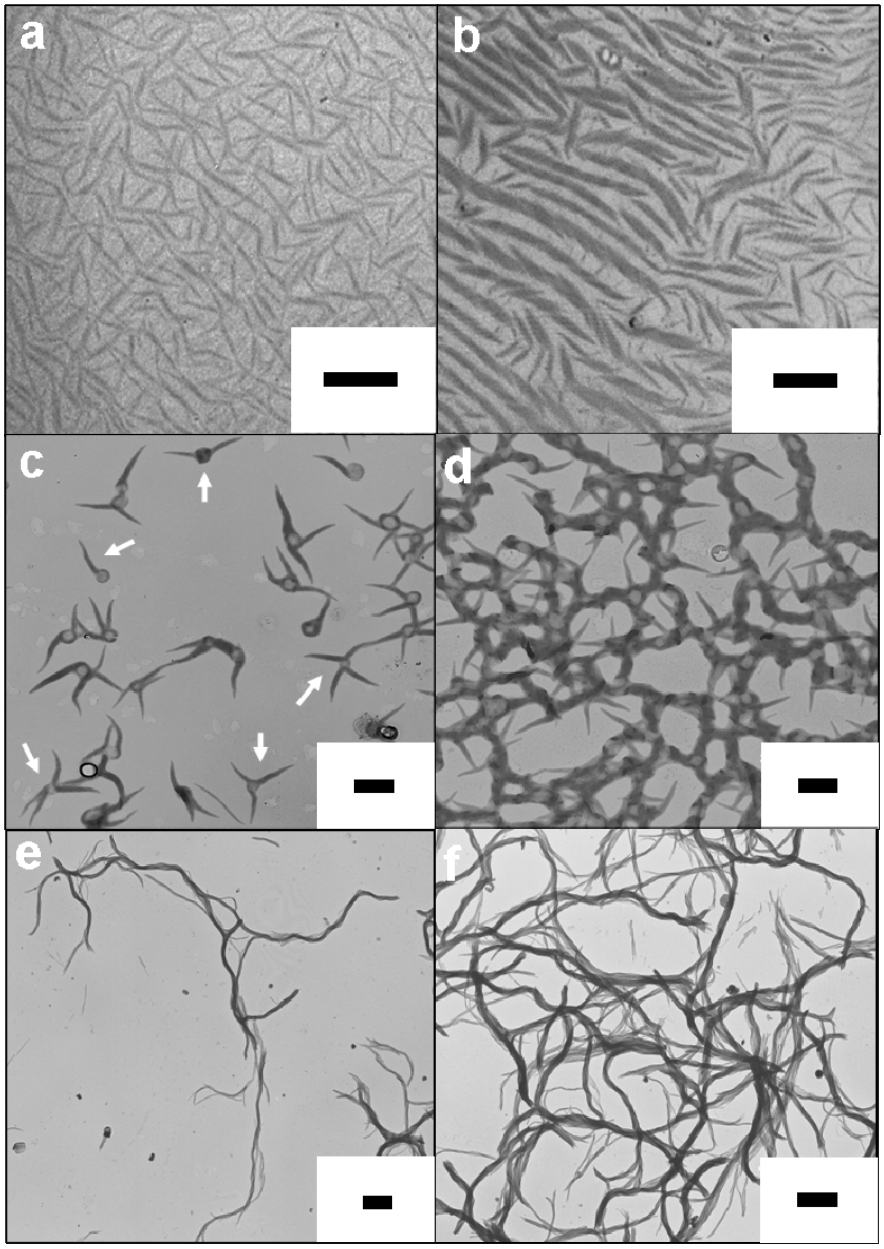

Figure 9. TEM images of **PBI 1** in MCH (1.0×10^{-4} M, a and b) and a suspension of a gel in acetone (ca. 1.0×10^{-3} M, c and d); (e) and (f) show the long aggregated fibers of **PBI 2** from a suspension of a gel in dioxane (ca. 1.0×10^{-3} M). The scale bar in (a)-(d) corresponds to 500 nm and in (e) and (f) corresponds to 1000 nm.

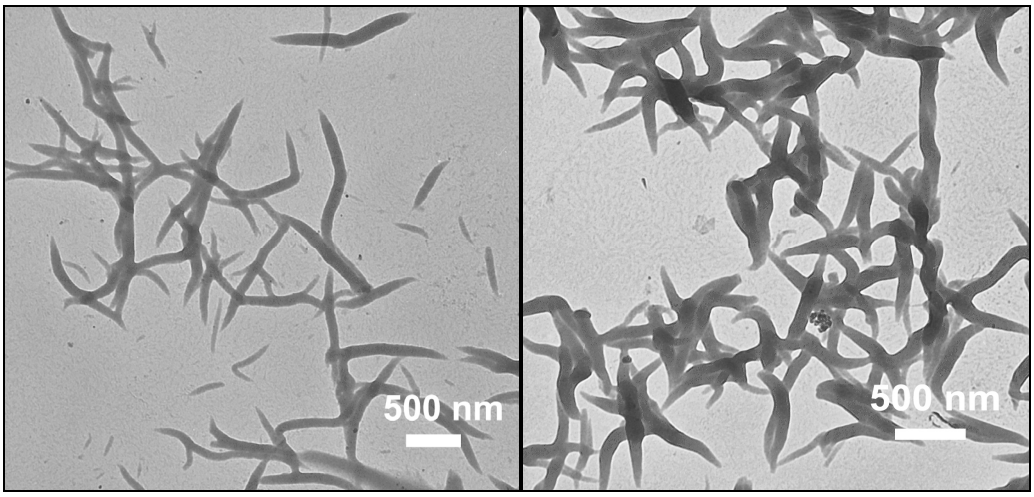

Figure 10. TEM images of a suspension of **PBI 1** gel in dioxane ($c = 2.5 \times 10^{-3}$ M).

5.2.5 Calculation of Excitonic Coupling and the Models

PBI 1 molecules form J-aggregates in MCH and acetone at higher concentration and lower temperature, which was evidenced from distinct spectral changes (bathochromic shift). According to exciton coupling theory (Scheme 1), in MCH

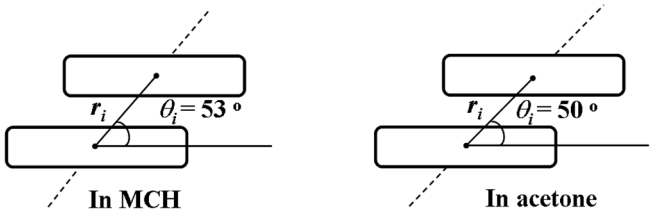

$$\left|\mu_{eg}\right|^2 = \frac{3hc\varepsilon_0 \ln 10}{2\pi^2 N_A} \int_{\tilde{\nu}_1}^{\tilde{\nu}_2} \frac{\varepsilon(\tilde{\nu})}{\tilde{\nu}} d\tilde{\nu} \qquad (1)$$

$$\Delta E_{agg} = \Delta E_{mon} + \Delta E_{vdW} + \sum_i J_i \qquad (2)$$

$$J_i = \frac{|\mu_{eg}|^2}{4\pi\varepsilon_0 r_i^3}(1 - 3\cos^2\theta_i) \qquad (3)$$

$$\Delta\tilde{\nu}_{agg-mon} = \frac{\Delta E_{vdW}}{hc} + \frac{\sum_i J_i}{hc} \Longrightarrow \Delta\tilde{\nu}_{agg-mon} < \frac{\sum_i J_i}{hc}$$

Scheme 1. Arrangement of monomeric **PBI 1** units in a J-type aggregate structure and equations

for estimating the spectral shift. μ_{eg} is the transition dipole moment of the monomer, J_i is the excitonic coupling and r_i the distance of adjacent monomeric units with the slip angle θ_i. ΔE_{agg}, ΔE_{mon}, and ΔE_{vdW} denote the energy differences of ground and excited states of the aggregate, the monomer and the van der Waals energy, respectively. $\Delta\tilde{\nu}_{agg-mon}$ denotes the spectral shift of the aggregate band with respect to the monomer band.

the transition dipole moment of **PBI 1** was calculated as 6.9 D for monomer and 7.8 D for aggregate (equation 1). For a H-bond-fixed aggregate structure, a bathochromic shift of $\Delta\tilde{\nu}_{agg\text{-}mon} < -470\ cm^{-1}$ is calculated for a inter core distance of 4.8 Å and a slip angle of $\theta = 53°$, which is close to the magic angle 54.7°. This value is in good agreement with the experimental value of $-560\ cm^{-1}$, if one considers an additional contribution by the van der Waals energy.

In acetone, the chromophores of **PBI 1** are slightly more displaced in longitudinal direction because of the incorporation of solvent molecules. The transition dipole moment was calculated as 7.0 D for monomer and 8.6 D for aggregate. The molecular modeling study in this case suggests a larger distance between the dyes' centers of 5.2 Å and a slip angle of 50°. The calculated bathochromic shift is determined as $\Delta\tilde{\nu}_{agg\text{-}mon} < -900$, which is in good accordance with the experimental value of $-1080\ cm^{-1}$.[17,21] (see models in Figure 11)

In contrast to the morphology of core-twisted **PBI 1**, the core-planar **PBI 2** gives very long (several microns) 1D fiber in dioxane. This observation strongly indicates that the differences in gelation behavior of these dyes are originated from the structural change of the perylene cores. Possibly, strong π–π interaction among planar **PBI 2** chromophores rules out the possibility of solvent insertion irrespective of the nature of the solvent, while the core-twisted **PBI 1** allows solvent participation in H-bonding because of the relatively weaker inter-chromophoric interactions (Figure 11).

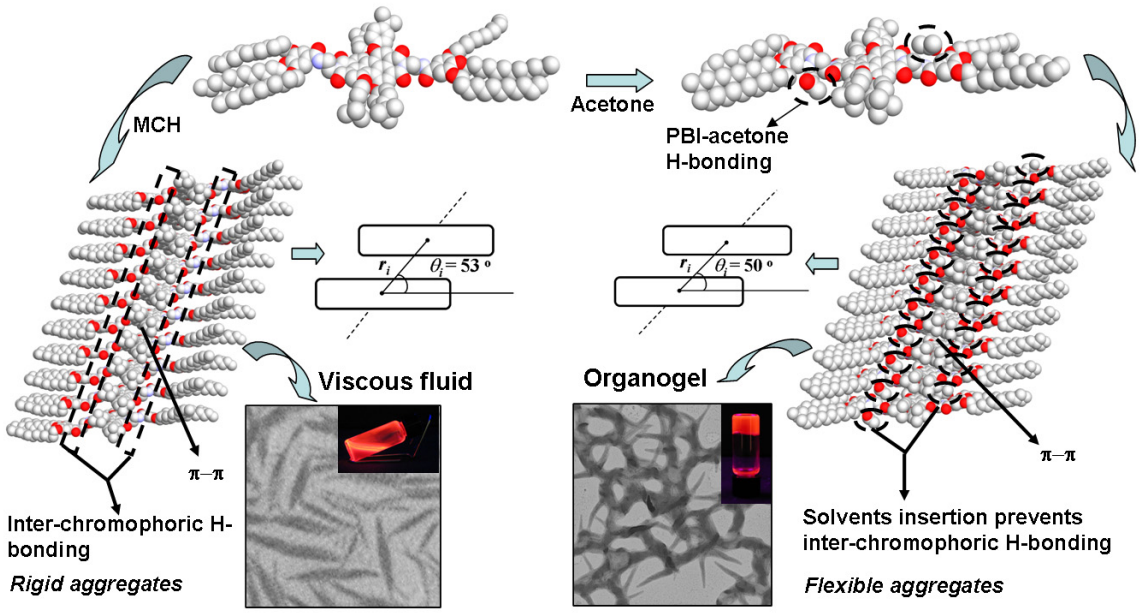

Figure 11. Schematic illustration for the formation of viscous lyotropic fluids and gels from **PBI 1** in MCH and acetone.

5.2.6 Light Emission Ability

It is noteworthy that the fluorescence of **PBI 2** is rather weak due to a photoinduced electron transfer process from the electron-rich trialkoxyphenyl group to the electron poor PBI core.[20] Thus, the fluorescence quantum yield is 0.03 for the monomers in dichloromethane and less than 0.01 for the aggregates in toluene. In contrast, very exciting fluorescence properties for **PBI 1** are given under various conditions that are attributed to a more electron-rich PBI core and a more favorable dye packing. The fluorescence quantum yields for monomeric **PBI 1** were found to be 0.78 ± 0.02, 0.76 ± 0.01, and 1.00 ± 0.01 in dichloromethane, acetone, and dioxane, respectively. For the J-aggregate in MCH, the quantum yield was found to be 0.82 ± 0.01. Such unquenched emission upon dye aggregation in solution is indeed a rare phenomenon.[16] Even in the gel phases, remarkable fluorescence quantum yields were determined: 0.20 ± 0.01 in acetone and 0.39 ±

0.01 in dioxane where the concentrations were 2.0 mM and 5.0 mM, respectively (Table 1).

	Monomeric (optical diluted)			Aggregated		
	DCM	Acetone	Dioxane	MCH	Acetone gel	Dioxane gel
PBI 1	0.78 ± 0.02	0.76 ± 0.01	1.00 ± 0.01	0.82 ± 0.01	0.20 ± 0.01	0.39 ± 0.01
PBI 2	0.03 ± 0.01	/	/	<0.01	/	/

Table 1. Fluorescent quantum yield of **PBI 1** and **PBI 2** in various conditions

5.3 Conclusion

In summary, we have introduced highly fluorescent PBI J-aggregate based lyotropic mesophases and gels of organic solvents. UV/Vis studies revealed more pronounced aggregation in apolar solvents like MCH due to intermolecular π-π-stacking and hydrogen bonding interactions. On the other hand, in polar solvents like acetone and dioxane, participation of the solvent molecules in hydrogen bonding significantly reduced the aggregation propensity but enforced the gel formation at higher concentrations (Figure 11). The outstanding fluorescent properties of the dye in both J-aggregated viscous lyotropic mesophases and bulk gel phases suggest very promising applications in photonics, photovoltaics, security printing, or as fluorescent sensors.

5.4 Experimental Details

General methods All solvents and reagents were purchased from commercial sources and used as received without further purification. The solvents for spectroscopic studies were of spectroscopic grade and used as received. ^{1}H NMR spectra were recorded on a 400 MHz spectrometer and all the spectra were calibrated against TMS. UV/vis spectra were measured on a Perkin-Elmer Lambda 40P spectrometer equipped with a Peltier system as temperature controller. FT-IR spectra were measured on a Jasco FT/IR-410 instrument. Optical textures at crossed polarizers were obtained with an Olympus BX-41 polarization microscope equipped with a Linkam THMS 600 hot stage and a temperature controller unit.

Transmission electron microscope (TEM)

TEM measurements were performed on a Siemens Elmiskop 101 Electron Microscope, operating at an acceleration voltage of 80-100 kV. For the observation of aggregates or gel morphologies, a drop of sample solution or a suspension of diluted gel was placed on 400-mesh formvar copper grids coated with carbon. About 2 min after the deposition, the grid was tapped with filter paper to remove surface water. This step was performed without any staining. The samples are stable on the copper grids and the morphologies can remain at least for 1 week.

Fluorescence measurements

The steady state fluorescence spectra were recorded on a PTI QM4/2003 spectrofluorometer. For all the measurements on the aggregated state (e.g., **PBI 1** in MCH at $c = 1.0 \times 10^{-4}$ M), two Glan-Thomson polarizers under magic angle and front face setup were adopt due to the high optical densities of the samples. All the data were corrected against photomultiplier and lamp intensity.

The fluorescence quantum yields were determined by optical dilute method.[22] Fluorescein (Φ_{fl} = 0.92 in 1N aqueous NaOH, for **PBI 2**) and *N*,*N'*-di(2,6-

diisopropylphenyl)-1,6,7,12-tetraphenoxyperylene-3,4:9,10-tetracarboxylic acid bisimide (Φ_{fl} = 0.96 in $CHCl_3$, for **PBI 1** in solutions) were used as references. The given quantum yields are averaged from values measured at three different excitation wavelengths.

Absolute fluorescence quantum yield determination

The quantum yields for the gel phases were determined using a Hamamatsu Absolute PL Quantum Yield Measurement System CC9920-02. The system is composed of an excitation source that uses a 150 W CW Xenon light source, a monochromator (250-700 nm, FWHM 10 nm), an integrating sphere, and a multi-channel spectrometer capable of simultaneously measuring multiple wavelengths between 300 and 950 nm and counting the number of absorbed and emitted photons. With this system the absolute fluorescence quantum yield of gels from **PBI 1** in acetone ($c = 2.0 \times 10^{-3}$ M) and in dioxane ($c = 5.0 \times 10^{-3}$ M) were determined by excitation at λ = 540 nm under ambient conditions.

For comparison, a dilute solution ($c = 1.0 \times 10^{-6}$ M in $CHCl_3$) of the fluorescence standard *N,N'*-bis(2,6-diisopropylphenyl)-1,6,7,12-(tetraphenoxy) perylene-3,4:9,10-tetracarboxylic acid bisimide was determined under identical conditions and a fluorescence quantum yield of 0.92 ± 0.02 was obtained upon excitation at λ = 540 nm (literature value:[23] 0.96 - 1.01).

Synthesis and characterization of PBI 1

N,N' - Di[*N*-(2-aminoethyl) - 3,4,5 - tris (dodecyloxy)benzamide] - 1,6,7,12 - tetra (4-*tert*-butylphenoxy) perylene - 3,4:9,10-tetracarboxylic acid bisimide (**PBI 1**):
1, 6, 7, 12-Tetra (4-*tert*-butyl phenoxy) perylene- 3,4:9,10-tetracarboxylic acid bisanhydride (150 mg, 0.15 mmol), compound 4 (220 mg, 0.31 mmol) and zinc acetate (33 mg, 0.18 mmol) were mixed in 5 mL dry quinoline. The reaction mixture was stirred at 180 °C for 3 h. After cooling to room temperature, the mixture was poured into 150 mL MeOH. The precipitate was collected by filtration

and washed thoroughly with methanol. The solid was dried in vacuum. After that, the crude product was further purified by silica gel column chromatography (50/1 CH_2Cl_2/MeOH) to give a purple solid. Yield: 51%; m.p.: 177 °C; ^{1}H NMR (400 MHz, $CDCl_3$, TMS, 300 K): δ = 8.23 (s, 4H, H_{pery}), 7.22 (m, 8H, Ar-H), 6.89 (s, 4H, Ar-H), 6.78 (m, 8H, Ar-H), 6.75 (t, *J* = 4.8, 2H, NH), 4.45 (t, 4H, *J* = 5.2, CH_2), 3.91 (m, 12H, Ar-OCH_2), 3.78 (br, 4H, CH_2), 1.8-1.2 (m, 156H, CH_2), 0.87 (m, 18H, CH_3). UV-vis (CH_2Cl_2): $\lambda_{max}(\varepsilon)$ = 583 (47600), 544 (29500), 457 (18200), 421 (21300 M^{-1} cm^{-1}). MS (MALDI-TOF, matrix: DCTB): m/z, calculated for $C_{154}H_{220}N_4O_{16}$: 2383.66, found 2383.58 $[M]^+$; Elemental analysis (%) calculated for $C_{154}H_{220}N_4O_{16}$: C 77.61, H 9.30, N 2.35; found: C 77.50, H 9.00, N 2.35.

5.5 References and Notes

1 (a) P. Terech, R. G. Weiss, *Chem. Rev*. **1997**, *97*, 3133-3159; (b) U. Beginn, *Prog. Polym. Sci*. **2003**, *28*, 1049-1105; (c) T. Ishi-I, S. Shinkai, *Top. Curr. Chem.* **2005**, *258*, 119-160; (d) T. Kato, N. Mizoshita, M. Moriyama, T. Kitamura, *Top. Curr. Chem.* **2005**, *256*, 219-236; e) N. M. Sangeetha, U. Maitra, *Chem. Soc. Rev.* **2005**, *34*, 821-836.

2 (a) L. A. Estroff, A. D. Hamilton, *Chem. Rev*. **2004**, *104*, 1201-1217; (b) J. H. van Esch, B. L. Feringa, *Angew. Chem. Int. Ed*. **2000**, *39*, 2263-2266.

3 (a) R. I. Petrova, J. A. Swift, *J. Am. Chem. Soc.* **2004**, *126*, 1168-1173; (b) G. Wulff, B.-O. Chong, U. Kolb, *Angew. Chem. Int. Ed.* **2006**, *45***,** 2955-2958; (c) C. Thiot, M. Schmutz, A. Wagner, C. Mioskowski, *Angew. Chem. Int. Ed.* **2006**, *45,* 2868-2871.

4 (a) S. Bhuniya, B. H. Kim, *Chem. Commun.* **2006**, 1842-1844; (b) Y. Koshi, E. Nakata, H. Yamane, I. Hamachi, *J. Am. Chem. Soc.* **2006**, *128*, 10413-10422;

(c) P. Mukhopadhyay, Y. Iwashita, M. Shirakawa, S.-I. Kawano, N. Fujita, S. Shinkai, *Angew. Chem. Int. Ed.* **2006***, 45***,** 1592-1595.

5 V. K. Praveen, S. J. George, R. Varghese, C. Vijayakumar, A. Ajayaghosh, *J. Am. Chem. Soc*. **2006**, *128,* 7542-7550.

6 A. Ajayaghosh, S. J. George, V. K. Praveen, *Angew. Chem. Int. Ed.* **2003**, *42*, 332-335.

7 (a) A. Ajayaghosh, S. J. George, *J. Am. Chem. Soc.* **2001**, *123,* 5148-5149; (b) M. Shirakawa, S.-i. Kawano, N. Fujita, K. Sada, S. Shinkai, *J. Org. Chem.* **2003**, *68*, 5037-5044; (c) J. van Esch, F. Schoonbeek, M. de Loos, H. Kooijman, A. L. Spek, R. M. Kellogg, B. L. Feringa, *Chem. Eur. J.* **1999**, *5*, 937-950; (d) H. Engelkamp, S. Middelbeek, R. J. M. Nolte, *Science* **1999**, *284*, 785-788; (e) K. Hanabusa, M. Yamada, M. Kimura, H. Shirai, *Angew. Chem. Int. Ed.* **1996**, *35*, 1949-1951; (f) F. S. Schoonbeek, J. H. van Esch, B. Wegewijs, D. B. A. Rep, M. P. de Haas, T. M. Klapwijk, R. M. Kellogg, B. L. Feringa, *Angew. Chem. Int. Ed.* **1999**, *38*, 1393-1397; (g) T. Akutagawa, K. Kakiuchi, T. Hasegawa, S. Noro, T. Nakamura, H. Hasegawa, S. Mashiko, J. Becher, *Angew. Chem. Int. Ed.* **2005**, *44*, 7283-7287; (h) C. Wang, D. Q. Zhang, D. B. Zhu*, J. Am. Chem. Soc.* **2005**, *127*, 16372-16373; (i) J. Puigmartí-Luis, V. Laukhin, A. P. del Pino, J. Vidal-Gancedo, C. Rovira, E. Laukhina, D. B. Amabilino, *Angew. Chem. Int. Ed.* **2007**, *46*, 238-241.

8 T. Ishi-i, K. Yaguma, R. Kuwahara, Y. Taguri, S. Mataka, *Org. Lett.* **2006**, *8*, 585-588.

9 (a) F. Würthner, *Chem. Commun.* **2004**, 1564-1579; (b) K.-Y. Law, *Chem. Rev.* **1993**, *93*, 449-486; (c) C. W. Tang, *Appl. Phys. Lett.* **1986**, *48*, 183-185; (d) L. Schmidt-Mende, A. Fechtenkötter, K. Müllen, E. Moons, R. H. Friend, J. D. MacKenzie, *Science* **2001**, 2*93*, 1119-1122.

10 K. Sugiyasu, N. Fujita, S. Shinkai, *Angew. Chem. Int. Ed.* **2004**, *43,* 1229-1233.

11 (a) F. Würthner, B. Hanke, M. Lysetska, G. Lambright, G. S. Harms, *Org. Lett.* **2005**, *7*, 967-970; (b) X.-Q. Li, V. Stepanenko, Z. Chen, P. Prins, L. D. A. Siebbeles, F. Würthner, *Chem. Commun.* **2006**, 3871-3873.

12 S. Yagai, Y. Monma, N. Kawauchi N, T. Karatsu, A. Kitamura, *Org. Lett.* **2007**, *9*, 1137-1140.

13 P. Osswald, F. Würthner, *J. Am. Chem. Soc.* **2007**, *129*, 14319-14326.

14 (a) J. Lydon, *Current Opinion in Colloid and Interface Science* **2004**, *8*, 480-490; (b) S.-W. Tam-Chang, J. Helbley, I. K. Iverson, *Langmuir* **2008,** *24*, 2133-2139; (c) For a recent review on PBI based chromonic liquid crystals in water, see: S.-W. Tam-Chang, L. Huang, *Chem. Commun.* **2008**, 1957-1967.

15 (a) G. Seybold, G. Wagenblast. *Dyes Pigm.* **1989**, *11*, 303-317; (b) R. Gvishi, R. Reisfeld, Z. Burshstein, *Chem. Phys. Lett.* **1993**, *213*, 338-344; (c) J. Hofkens, T. Vosch, M. Maus, F. Kohn, M. Cotlet, T. Weil, A. Herrmann, K. Müllen, F. C. De Schryver, *Chem. Phys. Lett.* **2001**, *333*, 255-263; (d) F. Würthner, C. Thalacker, S. Diele, C. Tschierske, *Chem. Eur. J.* **2001**, *7*, 2245-2253; (e) Z. Chen, U. Baumeister, C. Tschierske, F. Würthner, *Chem. Eur. J.* **2007**, *13*, 450-465.

16 Only one structurally related highly fluorescent J-aggregate has been reported so far: T. E. Kaiser, H. Wang, V. Stepanenko, F. Würthner*, Angew. Chem. Int. Ed.* **2007**, *46*, 5541-5544. This J-aggregate has a more pronounced bathochromic shift and does not gelate organic solvents. Note that, most recently we have reported the J-aggregate of a PBI gelator which is nearly non-fluorescent: F. Würthner, C. Bauer, V. Stepanenko, S. Yagai, *Adv. Mater*. **2008**, *20*, 1695-1698.

17 M. Kasha, H. R. Rawls, M. A. El-Bayoumi, *Pure Appl. Chem.* **1965**, *11,* 371-392.

18 (a) M. Kaftory, M. Kapon, M. Botoshansky, *Chem. Mater.* **1994**, *6*, 1245-1249; (b) E. Kokufuta, H. Suzuki, R. Yoshida, K. Yamada, M. Hirata, F. Kaneko, *Langmuir* **1998**, *14*, 788-795; (c) R. Kumaran, P. Ramanurthy, *J. Phys. Chem. B* **2006**, *110*, 23783-23789.

19 H.-J. Kim, J.-H. Lee, M. Lee, *Angew. Chem. Int. Ed.* **2005**, *44*, 5810-5814.

20 For perylene bisimides bearing electron-rich oligo(phenylenevinylene) substituents at the imide nitrogens, it has been experimentally confirmed that fluorescence quenching arises from photoinduced electron transfer: E. H. A. Beckers, S. C. J. Meskers, A. P. H. J. Schenning, Z. Chen, F. Würthner, R. A. J. Janssen, *J. Phys. Chem. A* **2004,** *108*, 6933-6937.

21 (a) F. Würthner, S. Yao, T. Debaerdemaeker, R. Wortmann, *J. Am. Chem. Soc.,* **2002**, *124*, 9431; (b) H. Wang, T. E. Kaiser, S. Uemura, F. Würthner, *Chem. Commun.,* **2008**, 1181.

22 J. N. Demas, G. A. Crosby, *J. Phys. Chem.* **1971**, *75*, 991-1024.

23 (a) G. Seybold, G. Wagenblast, *Dyes Pigments* **1989**, *11*, 303; (b) R. Gvishi, R. Reisfeld, Z. Burshtein, *Chem. Phys. Lett.* **1993**, *213*, 338.

Chapter 6

Synthesis of Thioacetate Functionalized Perylene Bisimides and Construction of PBI/Gold Nanorod Hybrids

6.1 Introduction

Metal nanoparticles have attracted considerable interests in recent years due to their shape- and size-dependent optical properties originating from the localized surface plasmon resonance.[1] Among various shapes of nanoparticles reported so far, gold nanorods (NRs) are particularly attractive, because the localized surface Plasmon resonance can be readily tuned by adjusting their aspect ratio (the ratio of length to width of the rods)[2]. One of the most challenging tasks for scientist is to align the rods or to organize them into desired device[3]. Selective modification of the rods with functional organic groups is a reasonable way to build up new nanorods-based structures by various chemical interactions. Several reports have described the formation of linear gold nanochains by using bi-thiol derivatives as "joints", because the gold NRs prefer to assemble end to end when thiol groups are added.[4] However, the introduction of chromophores onto gold nanorods and the creation of rods-dye systems are still rare.[5]

Perylene tetracarboxylic acid bisimide (PBI)[6] represents a unique class of chromophores that can be applied in organic light-emitting diodes[7], organic field effect transistors[8] or solar cells.[9] In this chapter, we describe the synthesis of gold nanorods and a series of thioacetate functionalized perylene bisimides. Further, we show our preliminary result on the construction of chromophore-nanorods chains using PBI dyes as joint, which are characterized by UV/Vis spectroscopy and

transmission electron microscope (TEM). The closely packed chromophore-nanorods hybrids might be applied as guides of electromagnetic radiation (waveguides) based on optical antenna technology.[10]

6.2 Synthesis and Structural Properties of Gold Nanorods

In recent years, the metallic nanorods/wires are synthesized via several procedures such as electrochemical deposition on shaped templates, [11] electrochemical synthesis in solutions,[12] seed-mediated growth method,[13] as well as photochemical synthesis.[14] By using these approaches, gold nanorods can be prepared with the range of aspect ratios from 2 to 25.[15] In the present work, we used photochemical method to synthesize gold nanorods, by which the aspect ratio (AR) of the rods can be readily tuned from 2.8 to 4.8 by changing the concentration of silver ion and the irradiation time.[14]

The synthesis procedures are described as following (Figure 1): Cetyltrimethylammonium bromide (CTAB, 240 mg) and tetraoctylammonium bromide (TOAB, 4.5 mg) were dissolved in distilled water (15 ml). The mixture was ultrasonicated until the reagents dissolved completely (ca. 20 minutes). To this solution, 1.25 ml of 0.024 M $HAuCl_4$ solution was added along with 325 μl of acetone and 225 μl of cyclohexane. 450 μl of 0.01 M $AgNO_3$ was added to the above solution under stirring. The mixed solution was stirred for another 20 minutes. After that, the solution was transferred to the reaction vessel (1 mm path length, as shown in Figure 1) and irradiated with 300 nm light in a Rayonet Photochemical Reactor for 150 minutes (see details in experiment part). Upon irradiation, the color of the mixture changed from yellow to dark brown. Above solution was treated under a centrifuge (ca. 10 minutes, 12000 rpm) and the deposit was re-dissolved in 1 ml water. This procedure was repeated 3 times to remove the superfluous surfactants.

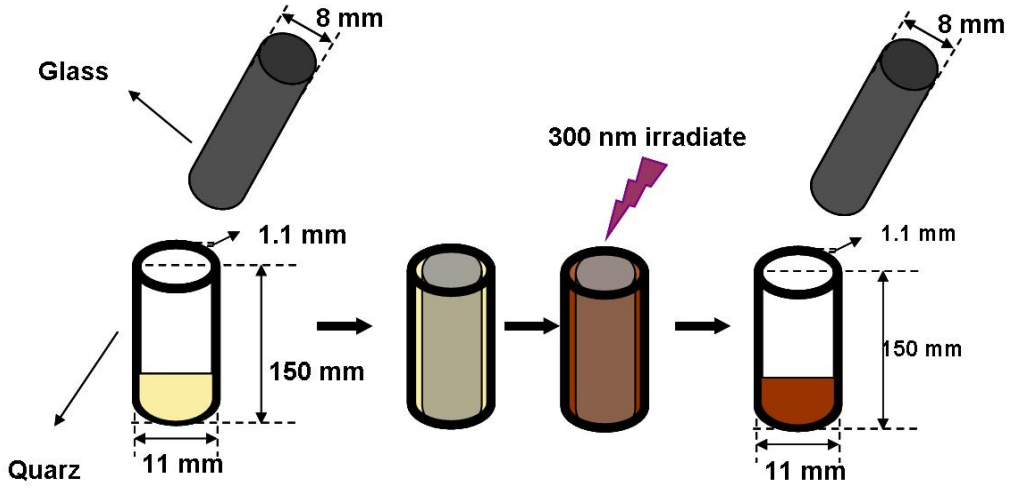

Figure 1. Schematic illustration of reaction vessels for the preparation of gold nanorods

Note that, the mechanism for the growth of gold nanorods is still elusive.[16] In many synthetic approaches, the surfactants used are deemed to be an important "soft template" for directing the nano particle growth and can additionally provide colloidal stability for the synthesized nanorods.[17] In the mean while, the presence of small amounts of silver nitrate was found to effect the final shape and size of the rods dramaticly.[14,16] For the photochemical method, the role of silver (or AgBr) is particularly crucial to control/facilitate the formation of the particles.[14a]

Figure 2 shows a proposed model of the gold nanorods synthesized photochemically. CTAB molecules adsorb onto the rod surface in a bilayer fashion, i.e., the trimethylammonium headgroups of the first layer face to the rod surface and the second layer faces outside. Crystallography study of gold nanorods from Murphy's group reveals that the rods are capped with five triangular facets (Au [111]), while the sides of the rods are not well-defined, which are either Au[100] or Au[110] facet (Figure 2).[2b]

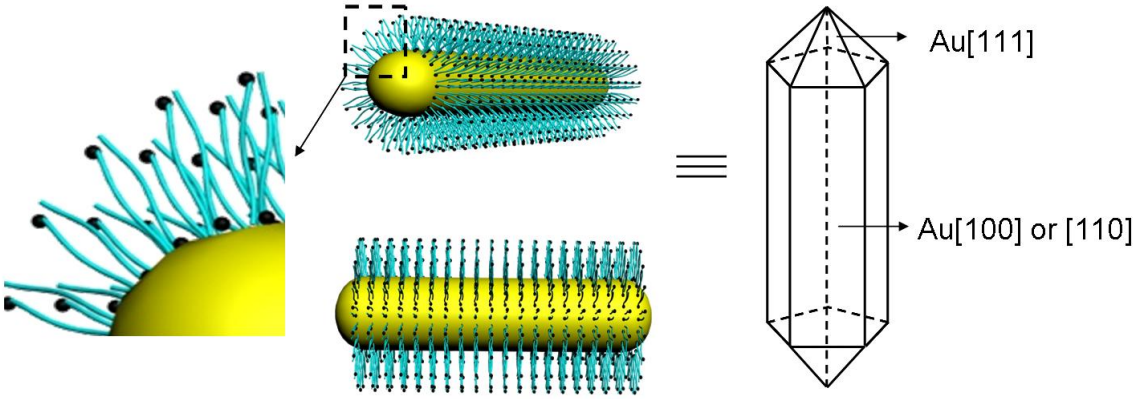

Figure 2. Proposed model of CTAB double layer coated gold nanorods.

Based on these facts that: a) the bilayer structure of gold nanorods leave their end relative "naked", and b) the CTAB bilayer on the side of rods is consistently difficult to be displaced,[2] some bifunctional molecules should in principle be able to link the rods end to end.[4a] Recently, Thomas' group has reported several examples of one dimensional linked gold nanorods by either bi-thiol functionalized molecules[5a, 18] or hydrogen bonding molecules.[14c] Another nice example for the linear connection of gold nanorods was reported by Kumacheva and coworkers, in which the polymer-terminated amphiphilic rods self-assemble linearly by virtue of supramolecular driving forces.[19] Such 1D alignment of gold nanorods can enhance the electric field in the gap of the chains upon plasmon excitation, thus paves ways towards several applications such as surface-enhanced Raman or fluorescence sensors[20] and photonic devices.[21]

The absorption spectra of gold nanorods synthesized photochemically are shown in Figure 3. The stock solution before irradiation gives singlet absorption at 402 nm, which corresponds to $AuCl_4^-$ ions. Upon irradiation with 300 nm UV light, the free gold chloride ions absorption disappears and two absorption bands can be observed. The peak at 517 nm with less intensity corresponds to the transverse plasmon absorption of the gold nanorods, which is independent to different aspect ratio of the rods. The more intense absorption band at 710 ± 25 nm comes from the longitudinal plasmon absorption of the rods. By addition of different amount silver

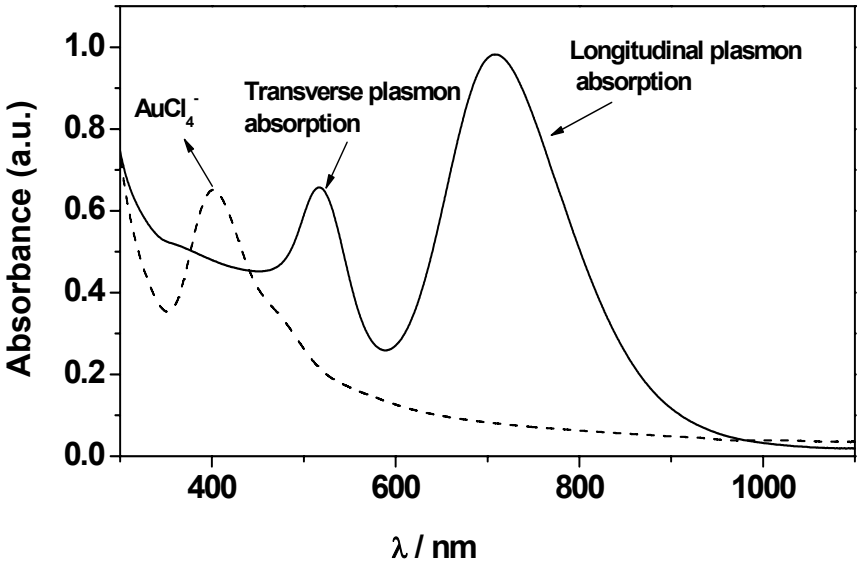

Figure 3. Absorption spectra of gold nanorods (solid line) and stock solution before irradiation (dashed line). The rods were obtained from the stock solution after 150 minutes irradiation. The concentration of the rods was determined to be 2.0×10^{-9} M. All the spectra were recorded in a 1 mm quartz cuvette.

nitrate, the longitudinal absorption band can vary from 600 nm to 800 nm, which reflect different aspect ratio of the rods achieved, as reported by Yang and coworkers.[14a] Our experiments show an error of about ± 25 nm for the longitudinal absorption wavelength, by using the same amount of silver nitrate. This is reasonable since the formation of the gold nanorods is a rather complex process, which can be influenced by various unknown factors.[2]

The morphology and size distribution of the gold nanorods were further studied by transmission electron microscopy (TEM), which is one of the most important method for the characterization of nanoparticles[1,2]. The fresh synthesized nanorods as an aqueous solution was dropped on a copper grid coated with carbon. As shown in Figure 5, the rods are distributed without any preferential orientation. The length of the rods varies from 20 nm to 54 nm with a width of about 12 nm. Calculated for 200 individual rods, the average aspect ratio (Figure 4) of the rods was 2.9, with the mean length of 34 nm and the width of 12 nm.

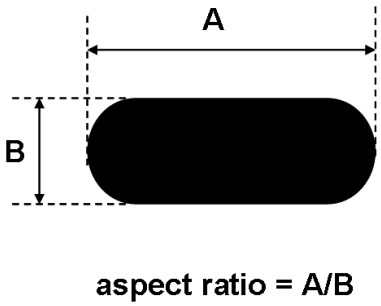

Figure 4. Calculation of the aspect ratio of gold nanorods.

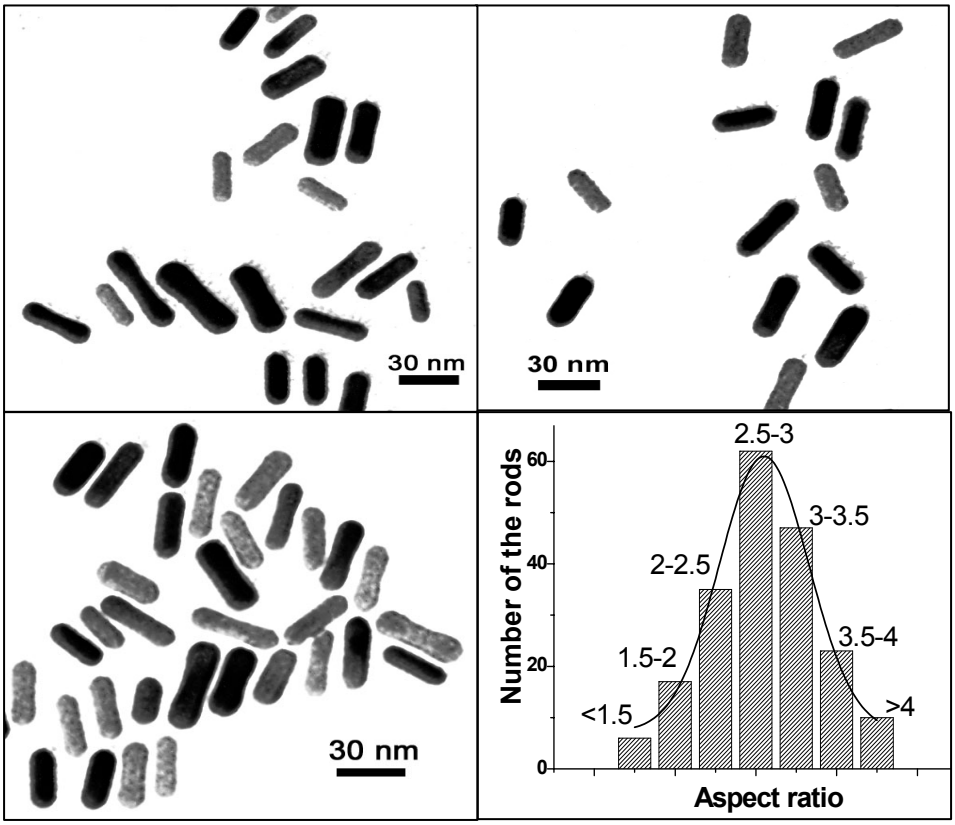

Figure 5. TEM images of gold nanorods and distribution of the aspect ratios (calculated from 200 dispersed rods).

6.3 Construction of rod/PBI Nanochains

6.3.1 Synthesis of the Linker Molecules

As discussed above, gold nanorods prefer to connect end to end by mixing with bi-thiol molecules. We synthesized a series of bis- and mono-thioacetate functionalized perylene bisimides (**PBI 1 - PBI 5**, Figure 6) as joints to connect gold nanorods. The design of the molecules is based on the high stability of thioacetate group compared with free thiol group, thus the compounds are facile to be prepared and to reach a high purity. Moreover, the acetyl group can be cleaved spontaneously when exposed to Au surface, or be readily de-protected to form free thiol group by using base-promoted method.[22] **PBI 1** and **PBI 2** possess tetra-phenoxy substitutes at the bay areas of the aromatic cores, which ensure the solubility of the dye in the solvents used. In **PBI 3** and **PBI 4**, more bulky tritylphenoxy groups were introduced in order to prohibit dye aggregation. **PBI 2** and **PBI 4** are unsymmetrical molecules, which possess thioacetate phenyl group at one side, and alkyl substitute at another imide position. In **PBI 5** the chlorine atoms can alter the electron affinity, which may induce different interactions between the dye molecules and the rods.

The synthesis of the thioacetate functionalized PBI was summarized in Scheme 1 - Scheme 3. Scheme 1 shows the synthesis procedure for **PBI 1**. 4-methoxymethyl-aniline **8** were obtained within 2 steps reaction from 4-nitrobenzylalcohol **6**. After imidization of **8** with tetra-chloro perylene bisanhydride **9**, crude PBI **10** was obtained as a solid, which was not further purified because of its bad solubility. *t*-Butyl phenoxy groups were then introduced to the bay position of **10** to get PBI **11**. The next two steps were more straightforward, that PBI **11** was bromized and then treated with KSAc to get **PBI 1** as a dark red powder, with a moderate yield of 57% for the last step.

The synthesis of **PBI 2** is shown in Scheme 2. The intermediate PBI **14** was synthesized from tetra-chloro perylene bisanhydride **9** by imidisation and

bay-substitution. During reduction of PBI **14**, perylene bisanhydride **15** and monoanhydride **16** were obtained as a mixture, which could not be separated by column chromatography due to the strong adsorption of PBI anhydride to silica gel. The reactions were followed as bromination and sulfuration, and **PBI 2** was separated as dark red powder. The yield for the last step is 33%. As shown in Scheme 2, **PBI 1** can also be isolated as a by-product in the meanwhile with a yield of 21%.

The more bulky **PBI 3** and **PBI 4** was synthesized using similar strategy for **PBI 2**. As shown in scheme 3, tritylphenoxy groups were introduced at the bay positions of the PBIs. Intermediate PBI **19** were synthesized from perylene bisanhydride **9**. The reaction for bay-substitution (step 2 in Scheme 3) and the consequent reduction (step 3 in Scheme 3) was not sufficient due to the steric hindrance of bulky tritylphenoxy groups, resulting in yields of 20% and 9%, respectively. The mixture of PBI **20** and **21** are further treated by bromination and sulfuration, after which **PBI 3** and **PBI 4** were isolated with yields of 21% and 18%, respectively.

AS shown in Scheme 3, **PBI 5** was synthesized from tetra-chloro perylene bisanhydride **9** in 3 steps followed by imidisation, bromination, and sulfuration. The final compound **PBI 5** was purified by column chromatography to get powders with light red color. However, the overall yield was only 3%, due to the bad solubility of intermediates **10**, **14** as well as **PBI 5**.

Figure 7 shows the calculated molecular models of **PBI 1**. The overall longitudinal length of **PBI 1** is 3.1 nm and the distance between two sulfur atoms is 2.4 nm. The width of the molecule is ca. 1.9 nm. Four *t*-butyl phenoxy groups at the bay position distort perylene core, and the twist angel is determined to be 25^{o}-30^{o}. Consequently, the dye molecules are not prone to form aggregates, which is considered advantageous for their interaction with gold nanorods.

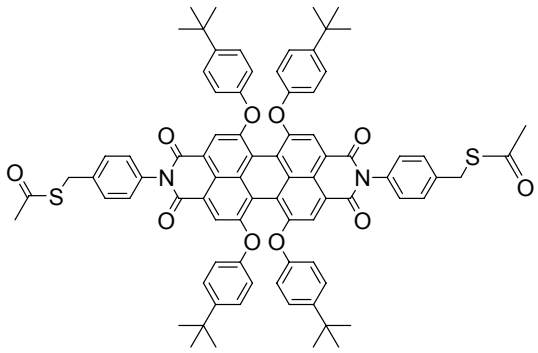

PBI 1

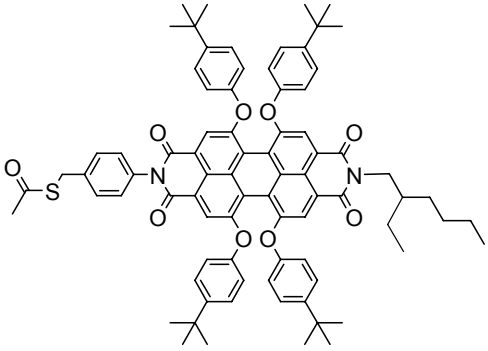

PBI 2

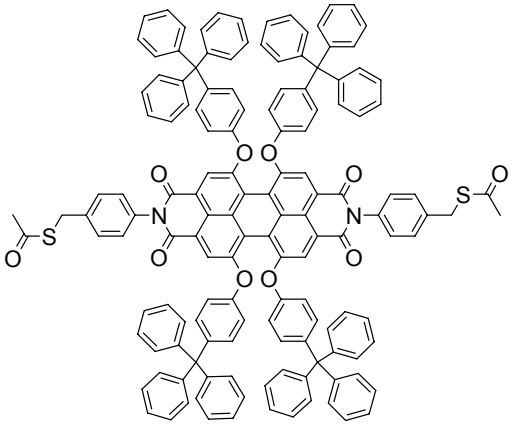

PBI 3

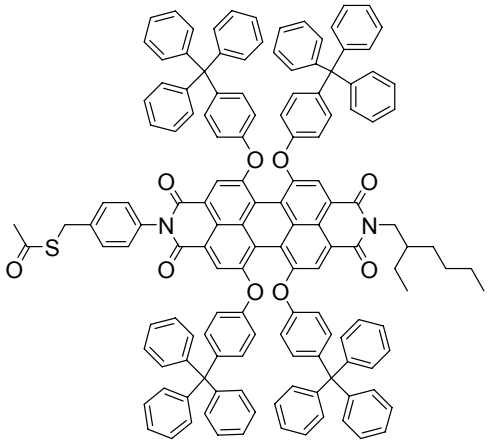

PBI 4

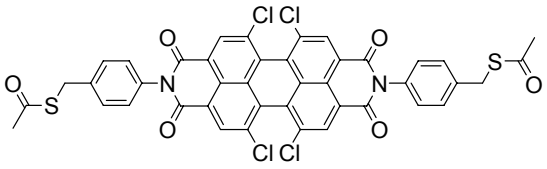

PBI 5

Figure 6. Molecular structures of **PBI 1** to **PBI 5**

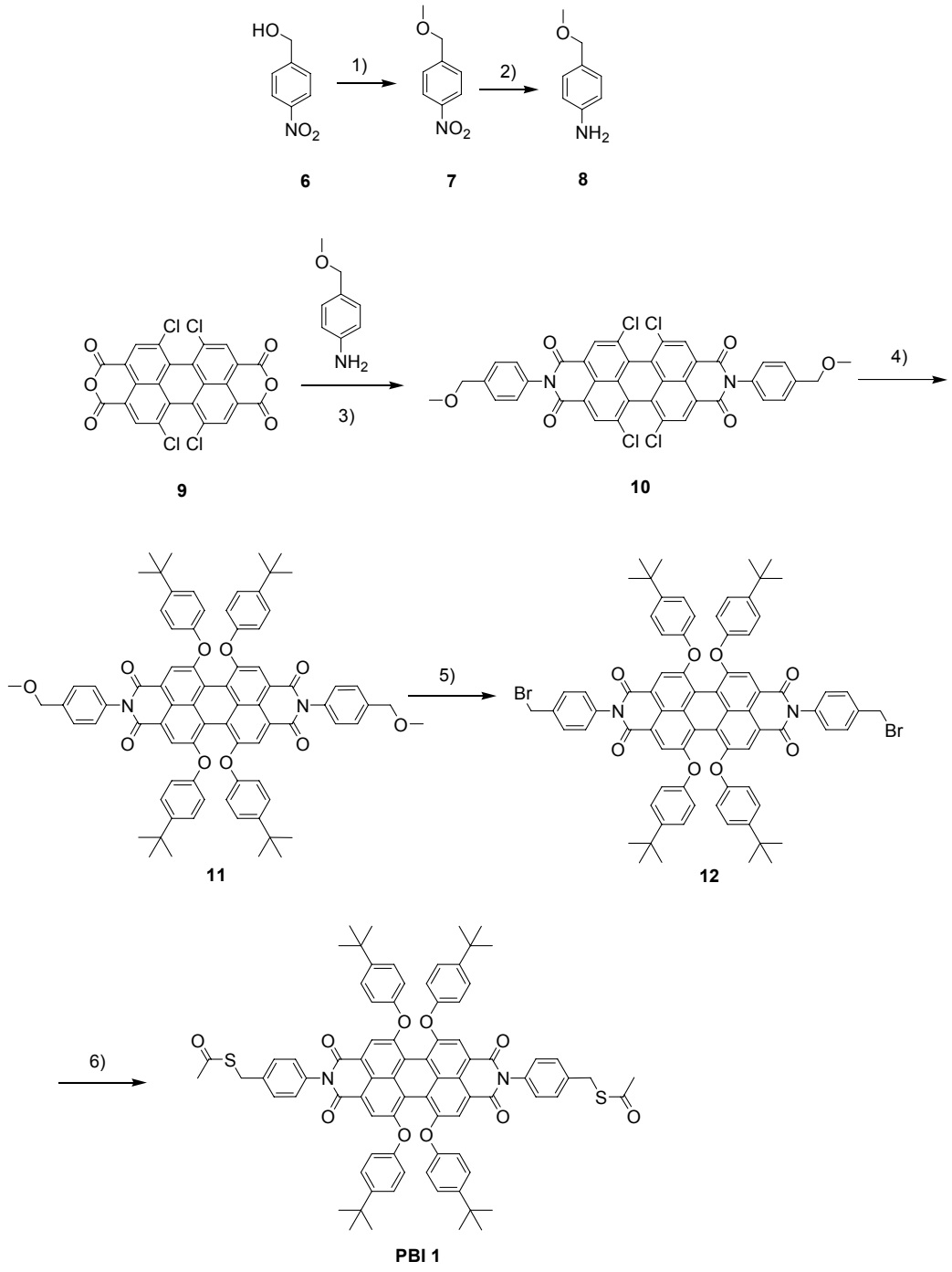

Scheme 1. (1) Methyl iodide, KOH, DMSO, rt, 4h, 72%; (2) Fe, NaCl, H_2O, reflux, 3h, 32%. (3) $Zn(OAc)_2$, imidazole, argon, 140 ^oC, 3.5 h, 79%; (4) 4-*tert*-butylphenol, K_2CO_3, NMP, argon, 120 ^oC, 16 h, 37%; (5) HBr/HOAc, DCM, argon, rt, 64 h, 81%; (6) KSAc, NMP, argon, 60 ^oC, 3 h, 57%.

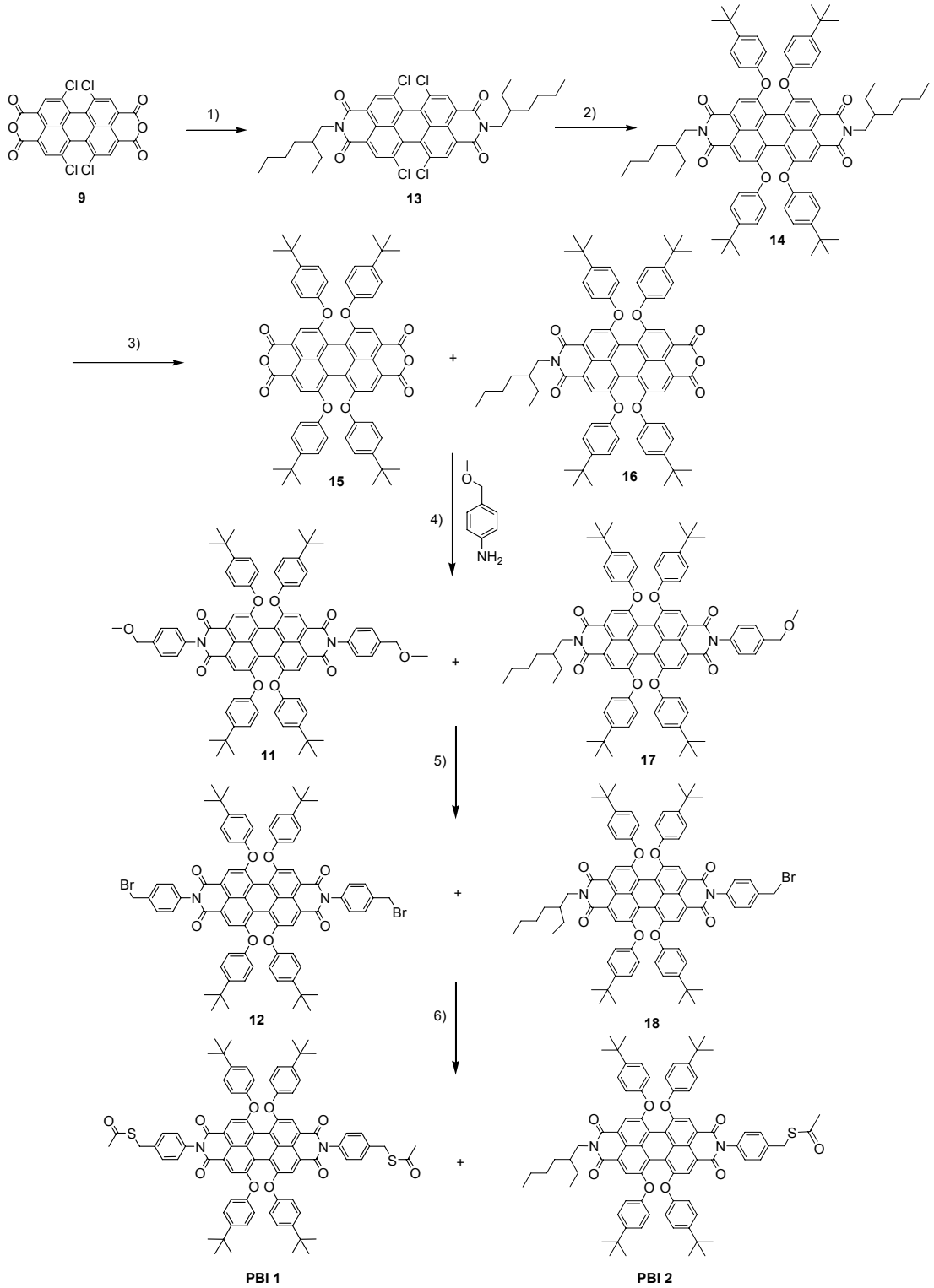

Scheme 2. (1) 2-ethyl-1-hexylamine, propionic acid, argon, 155 °C, 4 h, 88%; (2) 4-*tert*-butylphenol, K_2CO_3, NMP, Argon, 160 °C, 8 h, 51%; (3) KOH, *tert*-butanol, H_2O, Argon, 90 °C, 16 h, 38% for sum of **15** and **16**; (4) $Zn(OAc)_2$, imidazole, argon, 140 °C, 3 h, 83% for sum of **11** and **17**; (5) HBr/HOAc, DCM, argon, rt, 64 h, 78% for sum of **12** and **18**; (6) KSAc, NMP, argon, 60 °C, 3 h, 32% for **PBI 2**, 21% for **PBI 1**.

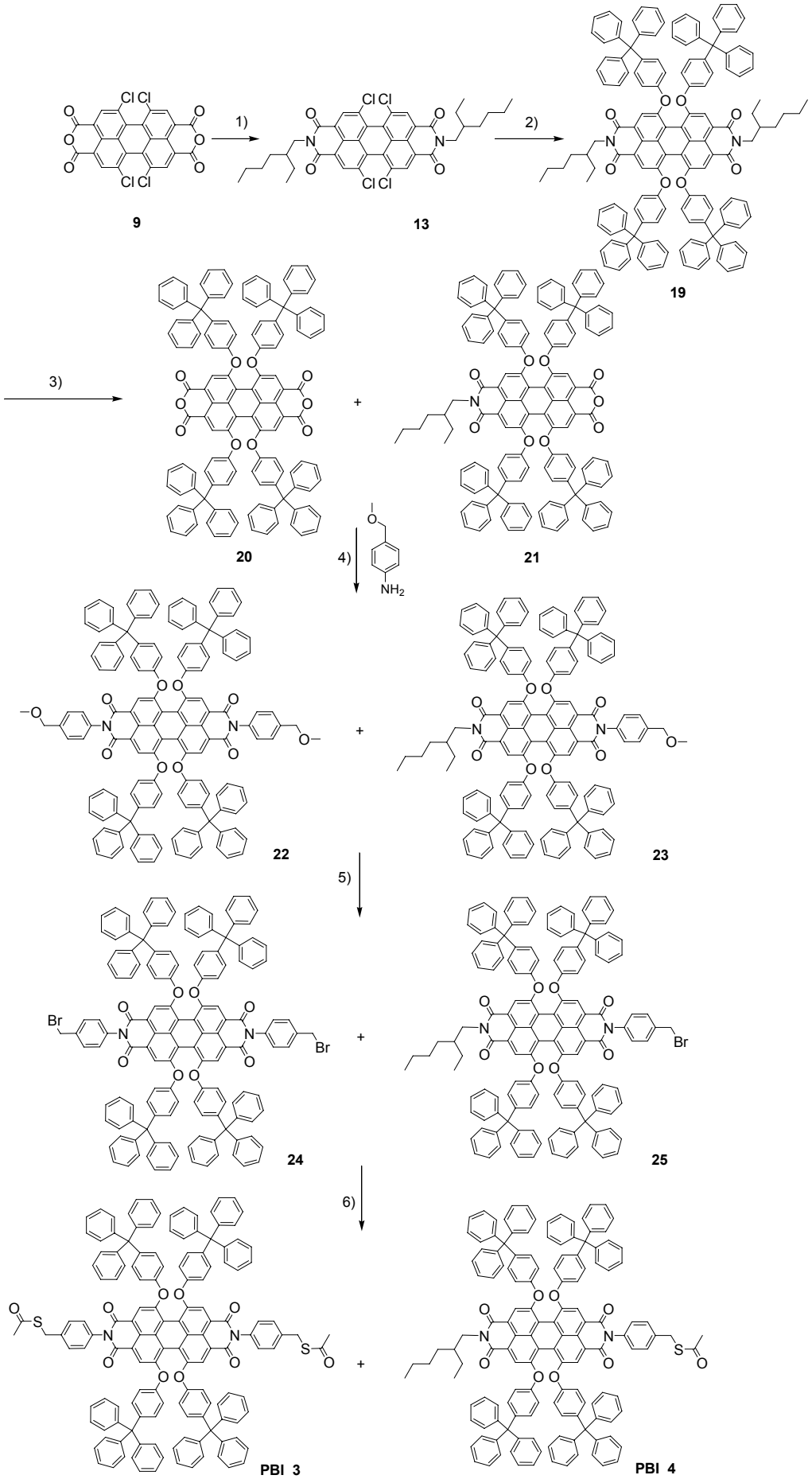
1)
2)
3)
4)
5)
6)
9
13
19
20
21
22
23
24
25
PBI 3
PBI 4

Scheme 3. (1) 2-ethyl-1-hexylamine,propionic acid, argon, 155 °C, 4 h, 88 %; (2) 4-tritylphenol, K_2CO_3, NMP, Argon, 160 °C, 13 h, 20%; (3) KOH, *tert*-butanol, H_2O, Argon, 90 °C, 16 h, 9%; (4) $Zn(OAc)_2$, imidazole, argon, 140 °C, 3 h, 11% for **23**; (5) HBr/HOAc, DCM, argon, rt, 64 h, 88% for **25**; (6) KSAc, NMP, argon, 60 °C, 3 h, 21% for **PBI 3**. **PBI 4** was isolated as a by-product, 18%.

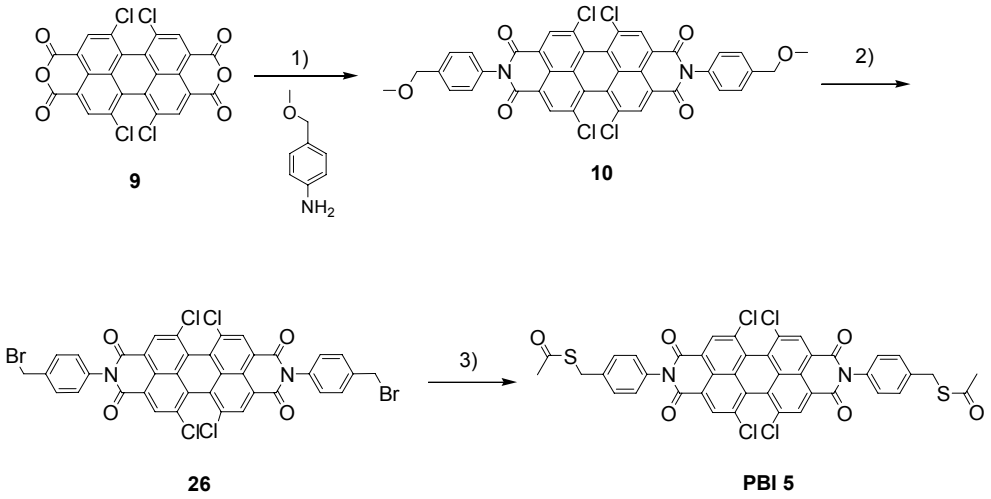

Scheme 4. (1) $Zn(OAc)_2$, imidazole, argon, 140 °C, 6h, 80%; (2) HBr/HOAc, DCM, argon, rt, 64h, 50%; (3) KSAc, NMP, argon, 60 °C, 3h, 7%.

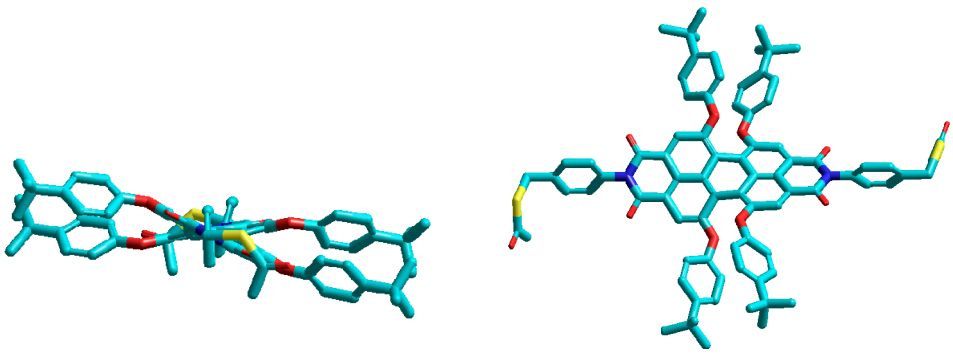

Figure 7. Side view (left) and top view (right) of geometry optimized molecular structure of **PBI 1** (HyperChem, MM+).

6.3.2 Formation of Gold Nanochains

The interaction between PBIs and gold nanorods was investigated by mixing the two components together in solution and then recording time-dependent UV/Vis/NIR spectra. In order to combine the gold nanorods and PBIs in the same solvent system, proper solvents must be found, since gold nanorods are only stable in a water dominated media and PBI can only be dissolved in a few organic solvents. For example, our experiments showed that some organic solvents such as THF can decompose the nanorods gradually. When the volume ratio of THF/water is larger than 1/4, the absorption spectrum of the rods collapses, and the TEM observation indicates a transition of the rod-like structure to spherical particles. However, DMF/water system was found to be a promising medium for the present investigation, since DMF can dissolve PBI molecules well, and it does not alter the rods' absorption and morphology at the volume ratio of 1/4 (DMF/water).

Experimentally, a stock solution of gold nanorods in water was treated under ultrasound for 5 minutes to ensure a sufficient dispersion. The concentration of the rod solution used was determined to be 2.0×10^{-9} mol/L according to Beer-Lambert law.[23] **PBI 1** was dissolved in DMF, and drops of ammonia were added to de-protect the acetyl groups. The overall concentration of **PBI 1** in the solution was 1×10^{-3} M and the ratio of DMF/$NH_3\cdot H_2O$ was calculated as 80/1.

As shown in Figure 8a, upon addition of 20 μl **PBI 1** solution (in DMF, 1×10^{-3} M) into 250μl rods solution (in water, 2.0×10^{-9}), the longitudinal absorption band of the gold nanorods around 700 nm gradually decreases, and a new broad band arises at longer wavelength. In the mean while, the transverse absorption at 517 nm remains unaltered. The red-shift (ca. 200 nm) and the broadening of the longitudinal absorption of gold nanorods is indicative that the nanorods are connected end-to-end to form the gold nanochains.[5a] In the mean while, the absorption of **PBI 1** at the region of 500 nm - 650 nm appears and the intensity increases time-dependently. This indicates the PBI molecules are gradually dissolved in water by bonding to the rod surfaces. Time dependent UV/Vis spectra

revealed the kinetic process of the chain formation by recording the intensity of the emerging band at 1000 nm. As shown in Figure 8b, in 2 hours the reaction reaches the equilibrium and the spectra did not change obviously afterwards. As a reference, when we added the same amount of DMF/$NH_3 \cdot H_2O$ without PBI molecules into 250μl rods solution, the spectra did not change notably, suggesting the organic solvent used in the present investigation does not influence gold nanorods and the spectral changes in Figure 8a are originated from the interaction of PBI molecules and gold nanorods (see inset of Figure 8a).

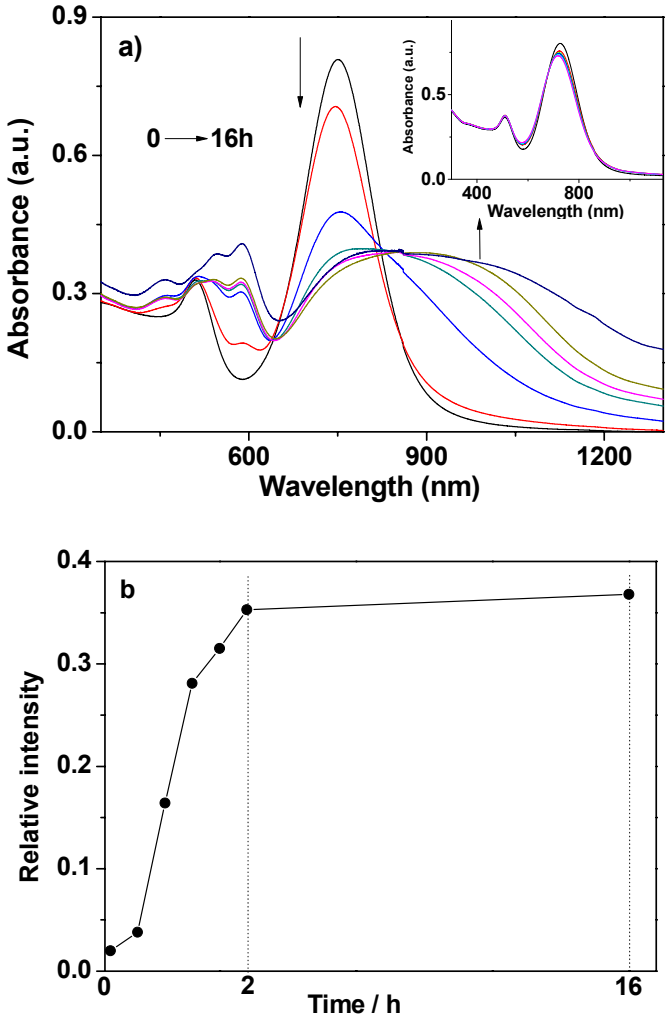

Figure 8. (a) UV/Vis/NIR spectra of 250 μl Au NRs solution (in water) upon addition of 20 μl bi-thiol **PBI 1** solution (in DMF/NH_4OH: 80/1, 1×10^{-3} M) in 16 hours. Inset in (a) is the blank experiment with the addition of 20 μl organic solvent without PBI molecules. (b) Spectra changes of NRs upon addition of **PBI 1** recorded at 1000 nm.

6.3.3 Microscopic Studies of Gold Nanochains

More straightforward evidence for the formation of gold nanochains is obtained from TEM. A drop of prepared PBI-nanorod chain solution (taken from the spectral measurement) was put on a copper grid. The droplet was kept for 2 minutes and the solvent was removed by an absorbent paper tip. The expected "nanochains" could be observed. As shown in Figure 9, the rods were preferentially connected "end to end", but it was also possible that the rods were connected "end to side". The discriminable nanochains are mostly composed of 2-5 individual nanorods.

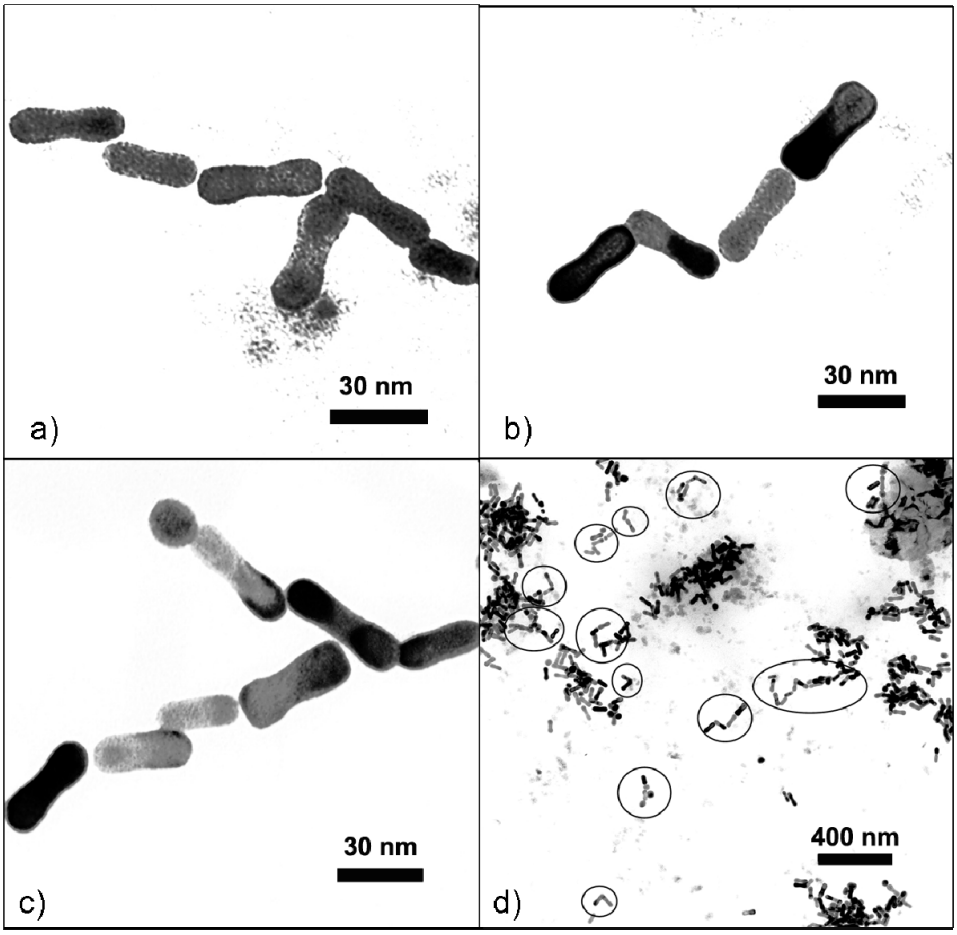

Figure 9. TEM observation of Au Nanochains. (a)-(c): selected images of gold nanochains. (d) Large scale image shows the formation of clusters, and the circles indicate the oligomers with various lengths and shapes

The length of the chains varies from ~50 nm to ~150 nm which is dependent on the number of rod units. The conformation of the chains appears to be flexible, i.e., the connection of the rods is not always straight linear but sometimes adopts a certain angle. It can be explained that the end of the rods are not flat (capped with five triangular facets, see Figure 2), consequently, the attached bi-thiol PBI molecules are not ideally parallel to the long axis of the rods. Note that, although a moderate yield of oligo-chains are formed (see circles in Figure 9d), large scale TEM image shows several "cluster"-like objects, which might be due to the strong inter-chain aggregation in the solution. These clusters can not be re-dispersed in the solution even after under ultrasound treatment for 40 minutes. To control the length of the chains (i.e., dimer, trimer, etc.) and to keep the chains well dispersed in solution are still challenging tasks.

6.4 Conclusions

In this chapter, gold nanorods were synthesized photochemically with a good size distribution. Thioacetate functionalized perylene bisimides (**PBI 1 - PBI 5**) were synthesized and **PBI 1** was used as joint to connect gold nanorods to form gold nanochains. The formation of the chains was certified by UV/Vis/NIR spectra and TEM measurement. Covalent attachment of highly fluorescent PBI chromophores onto gold nanorods might enable photo-induced charge/energy transport processes, which are of importance for new photonic or electronic devices. Further, the oligomeric nanochains which possess gold arms and light-emitting dye nodes might be applicable as optical antenna.

6.5 Experimental Details

Materials and methods: All solvents and reagents were purchased from commercial sources. The solvents for spectroscopic studies were of spectroscopic grade and used as received. $HAuCl_4 \cdot 3H_2O$ was purchased from Merck & Co., Inc. UV/Vis spectra were measured in a Perkin-Elmer Lambda 950 spectrometer. All the solutions were measured in conventional quartz cell with 1 mm path length.

Photochemical Reaction

Gold nanorods were synthesized using a Rayonet Photochemical Reactor RPR-100 equipped with 16 RPR-3000A^o Lamps (Southern New England Ultra Violet Company). Normal operating temperature is approximately 35 ^{o}C with fan in operation. Without the fan the temperature is approximately 60-70 ^{o}C. The reaction vessel is composed of one quartz tube with inner-diameter of 10 mm, and a glass stick with a diameter of 8 mm (see Figure 1).

Transmission electron microscope (TEM)

TEM measurements were performed on a Siemens Elmiskop 101 Electron Microscope, operating at an acceleration voltage of 80-100 kV. For the observation of the gold nanorods, a drop of sample solution was placed on 400-mesh formvar copper grids coated with carbon. About 2 minutes after the deposition, the grid was tapped with filter paper to remove surface water. This step was performed without any staining. The samples are stable on the copper grids and the morphologies can remain at least for 1 week.

Synthesis Details of PBI 1- PBI 5

1-methoxymethyl-4-nitrobenzene 7 [24]

A solution of 4-nitrobenzylalcohol (5.0 g, 33 mmol) and methyl iodide (8.3 ml, 133

mmol) in DMSO (15 ml) was added to a suspension of potassium hydroxide (7.5 g, 133 mmol) in DMSO (65 ml) during 1 hour at room temperature. The reaction mixture was stirred for an additional hour, poured into water (400 ml) and extracted with CH_2Cl_2 (150 ml) for 3 times. The organic layer was washed with 10% sodium bisulfite (150 ml) and water (150 ml) and dried over $MgSO_4$. The solvent was evaporated and the product was purified by column chromatography (eluent: DCM). The product was obtained as yellow solid: 3.94 g, yield: 72%. ^{1}H NMR (400 MHz, $CDCl_3$, 300 K, TMS): δ=8.20 (d, 2 H, *J* = 8.8 Hz), 7.47 (d, 2 H, *J* = 8.8 Hz), 4.55 (s, 2 H), 3.43 (s, 3 H).

4-methoxymethyl-aniline 8 [24]

Iron powder (10 g) and 1 g zeolite was suspended in 5% NaCl (50 ml) and heated under reflux for 30 min. Then 1-methoxymethyl-4-nitrobenzene (2 g, 25.1 mmol) was added and the mixture was refluxed for 3 h. After cooling the reaction mixture was filtered and the filtrate was extracted with diethyl ether. The organic layer was then extracted with 2 N HCl. K_2CO_3 was added until the acidic layer became basic and the basic layer was extracted with diethyl ether. Then the organic layer was dried over Na_2SO_4 and the solvent was evaporated to obtain the product as yellow oil. 520 mg, yield: 32%. ^{1}H NMR (400 MHz, $CDCl_3$, 300 K, TMS): δ=7.13 (d, 2 H, *J* = 8.4 Hz), 6.65 (d, 2 H, *J* = 8.4 Hz), 4.34 (s, 2 H), 3.73 (b, 2 H), 3.35 (s, 3 H).

***N,N*'-bis-(4-methoxymethyl-phenyl)-1,6,7,12-tetrakis-chloro-3,4:9,10-perylene bisimide 10**

Tetra-chloro perylene bisanhydride **9** (200 mg), 4-methoxymethyl-aniline (100 mg) and $Zn(OAc)_2$ (100 mg) were stirred in 3 g imidazole at 140 ^{o}C for 3.5 h under argon. After the reaction mixture was cooled to room temperature 50 ml 2 N HCl was added and the precipitate was collected by filtration. Then the residue was washed with 50 ml water and dried in vacuum to get a crude product (230 mg,

79%). The crude solid was not further purified and used directly for the next step.

***N,N'*-bis-(4-methoxymethyl-phenyl)-1,6,7,12-tetrakis-(4-*tert*-butyl-phenoxy)-3, 4:9,10-perylene bisimide 11**

The crude tetra-chloro-PBI from last step (230 mg) and 4-*tert*-butylphenol (700 mg) were heated in 20 ml *N*-methylpyrrolidone (NMP) at 160 ^{o}C for 7.5 h. After cooling to room temperature the reaction mixture was poured into 2 N HCl and was stirred for another 1 h. Then the product was collected by filtration and washed with water and methanol. The product was further purified by column chromatography (DCM / hexane: 30:1) and the pure compound was obtained as a red solid. 135 mg, yield: 37%. MS (MALDI-TOF, matrix: DCTB): calculated for $C_{80}H_{74}N_2O_{10}$: 1222.534, found 1222.537.^{1}H NMR (400 MHz, $CDCl_3$, 300 K, TMS): δ=8.24 (s, 4 H), 7.45 (d, 4 H J = 8.4 Hz), 7.24 (m, 12 H), 6.85 (d, 8H, J = 8.7 Hz), 4.53 (s, 4 H), 3.40 (s, 6 H), 1.26 (s, 36 H).

***N,N'*-bis-(4-bromomethyl-phenyl)-1,6,7,12-tetrakis-(4-*tert*-butyl-phenoxy)-3,4: 9,10-perylene bisimide 12**

4-Methoxymethyl-phenyl-tetrakis-phenoxy-PBI **11** (49 mg) was dissolved in DCM (8 ml) and 33% hydrobromic acid in acetic acid (12 ml) was added. The mixture was stirred at room temperature for 64 h under argon. After that, water was added and the organic layer was washed with saturated $NaHCO_3$ and dried over Na_2SO_4. The solvent was evaporated and the product was dried under vacuum. The crude product (43 mg, 81%) was not further purified and used for the next step directly.

***N,N'*-bis-(4-thioacetate-methyl-phenyl)-1,6,7,12-tetrakis-(4-*tert*-butyl-phenoxy) -3,4:9,10-perylene bisimide PBI 1**

Crude PBI **12** (43 mg) and KSAc (9 mg) was stirred in 3 ml NMP at 60 ^{o}C for 3 h under argon atmosphere. After the mixture was cooled to room temperature, 100 ml 1 N HCl was added and the precipitate was collected and washed thoroughly with

water. The solid was further purified by column chromatography (Dichloromethane/Methanol: 50/1). The final product was obtained as dark red solid. 24 mg, yield 57 %. Mp: 378 ^{o}C; H^{1}NMR (400 MHz, $CDCl_3$, 300 K, TMS): δ = 8.23 (s, 4H, H_{pery}), 7.40 (d, 4H, J = 8.4 Hz, Ar-H), 7.23 (m, 8H, Ar-H), 7.17 (d, J = 8.4 Hz, 4H, Ar-H), 6.85 (m, 8H, Ar-H), 4.16 (s, 4H, -CH_2-S), 2.35 (s, 6H, CO-CH_3), 1.26 (s, 36H, CH_3). ^{13}C-NMR (100 MHz, $CDCl_3$, 300 K, TMS): 194.9, 163.5, 156.1, 152.8, 147.4, 138.2, 134.1, 133.1, 129.8, 128.7, 126.6, 122.5, 120.7, 120.5, 119.7, 119.3, 34.3, 33.0, 31.4, 30.3; MS (MALDI-TOF, matrix: DCTB): calculated for $C_{82}H_{74}N_2O_{10}S_2$: 1310.478, found 1310.480. UV/Vis (CH_2Cl_2): $\lambda_{max}(\varepsilon)$=453 (40500), 541 (35800), 581 (58600 mol^{-1} L cm^{-1}).

***N,N'*-bis-(2-ethyl-1-hexyl)-1,6,7,12-tetra-chloro-3,4:9,10-perylene bisimide 13**

A suspension of perylene bisanhydride **9** (3.4 g, 6.3 mmol) and 2-ethyl-1-hexylamine (6 ml, 58.5 mmol) in propionic acid (50 ml) was stirred at 155 ^{o}C for 4 h under argon. The reaction mixture was allowed to stand overnight at RT, the residue was collected by filtration and washed thoroughly by water and methanol, to give a crude product (4.26 g, yield 88%). TLC shows the crude product was pure enough for the next step reaction.[25]

***N,N'*-bis-(2-ethyl-1-hexyl)-1,6,7,12-tetrakis-(4-*tert*-butyl-phenoxy)-3,4:9,10-perylene bisimide 14**

Tetra-chloro-PBI **13** (3.84 g, 5 mmol) and 4-*tert*-butylphenol (4.51 g, 30 mmol) were heated in 80 ml *N*-methylpyrrolidone (NMP) at 160 ^{o}C for 7.5 h. After cooling to room temperature the reaction mixture was poured into 2 N HCl and was stirred for another 1 h. Then the product was collected by filtration and washed with water and methanol. The product was further treated with column chromatography (DCM / hexane: 2:1) to give 3.2 g (yield 51%). TLC verified the purity of the solid.[25]

1,6,7,12-tetrakis-(4-*tert*-butyl-phenoxy)-3,4:9,10-perylene bisanhydride 15 and ***N*-(2-ethyl-1-hexyl)-1,6,7,12-tetrakis-(4-*tert*-butyl-phenoxy)-3,4:9,10-perylene monoanhydride 16** [25]

The mixture of compound **14** (2.9 g) and KOH (21 g) in *tert*-butanol (150 ml) and H_2O (10 ml) was stirred at 90 ^oC for 16 h, after cooling to RT, 2 N HCl was added and the precipitate was collected and re-dissolved in a small amount of DCM, then methanol was added and the product was collected by filtration. 900 mg dark red product was obtained which were mixture of compound **15** (ca. 70%) and **16** (ca. 30%). Overall yield: 38%.[25]

***N*-(2-ethyl-1-hexyl)-*N'*-(4-methoxymethyl-phenyl)-1,6,7,12-tetrakis-(4-*tert*-butyl-phenoxy) -3,4:9,10-perylene bisimide 17**

Compound **16** (200 mg, a mixture with compound **15**), 4-methoxymethyl-aniline (68 mg, 0.52 mmol) and $Zn(OAc)_2$ (100 mg) were stirred in 4 g imidazole at 140 ^oC for 3 h under argon. The reaction mixture was cooled to room temperature, 2 N HCl was added and the precipitate was collected by filtration. Then the residue was thoroughly washed with water and dried in vacuum to give a crude product (186 mg, yield: 83%). MS (MALDI-TOF, matrix: DCTB): calculated for $C_{80}H_{82}N_2O_9$: 1214,602, found: 1215.608, $[M+H]^+$.

***N*-(2-ethyl-1-hexyl)-*N'*-(4-bromomethyl-phenyl)-1,6,7,12-tetrakis-4-*tert*-butyl-phenoxy) -3,4:9,10-perylene bisimide 18**

Above obtained PBI **17** (186 mg，crude) was dissolved in DCM (25 ml) and 33% hydrobromic acid in acetic acid (40 ml) was added. The mixture was stirred at room temperature for 64 h under argon. After that, water was added and the organic layer was separated washed with saturated $NaHCO_3$ and dried over Na_2SO_4. The solvent was evaporated and the product was dried under vacuum and was further purified by column chromatography (DCM: Methanol 20:1). The final product was obtained as dark red solid. 145mg, yield: 78%. MS (MALDI-TOF, matrix: DCTB):

calculated for $C_{79}H_{79}BrN_2O_8$: 1262,502, found: 1262.509.

_N_-(2-ethyl-1-hexyl)-_N'_-(4-thioacetate-methyl-phenyl)-1,6,7,12-tetrakis-(4-_tert_-butyl-phenoxy) -3,4:9,10-perylene bisimide PBI 2

PBI **18** (35 mg, crude) and KSAc (40 mg) were stirred in 5 ml NMP at 60 ^oC for 3 h under argon atmosphere. After the mixture was cooled to room temperature, 100 ml water was added and the precipitate was collected. The solid was further purified by column chromatography (DCM: Methanol 50:1). The final product was obtained as dark red solid. 11 mg, yield: 32%. H^1NMR (400 MHz, $CDCl_3$, 300 K, TMS): δ = 8.27 (s, 2H, H_{pery}), δ = 8.21 (s, 2H, H_{pery}), 7.40 (d, 2H, J = 8.4 Hz, Ar-H), 7.26-7.20 (m, 8H, Ar-H), 7.16 (d, J = 8.4 Hz, 2H, Ar-H), 6.84 (m, 8H, Ar-H), 4.15 (s, 2H, -CH_2-S), 4.01 (m, 2H, CH_2), 2.34 (s, 3H, CO-CH_3), 1.87 (m, 1H, CH), 1.40-1.20 (m, 42H, CH_3). 0.92-0.81 (m, 8H, CH_2), MS (MALDI-TOF, matrix: DCTB): calculated for $C_{81}H_{82}N_2O_9S$: 1258.574, found 1258.567.

_N,N'_-bis-(2-ethyl-1-hexyl)-1,6,7,12-tetrakis-(4-tritylphenoxy)-3,4:9,10-perylene bisimide 19

Tetra-chloro-PBI **13** (1.5 g, 2 mmol) and 4-tritylphenol (4.1 g, 12 mmol) were heated in 50 ml *N*-methylpyrrolidone (NMP) at 160 ^oC for 13 h. After cooling to room temperature the reaction mixture was poured into 2 N HCl and was stirred for another 1 h. Then the product was collected by filtration and washed with water and methanol. The product was further purified by column chromatography (DCM / hexane: 2:1), to give product 780 mg, yield 20%. MS (MALDI-TOF, matrix: DCTB): calculated for $C_{140}H_{114}N_2O_8$: 1950.858, found 1950.870. H^1NMR (400 MHz, $CDCl_3$, 300 K, TMS): δ = 8.28 (s, 4H, H_{pery}), 7.22-7.12 (m, 76H, H_{trityl}), 7.10 (d, J = 8.9 Hz, 8H, Ar-$H_{phenoxy}$), 6.71 (d, J = 8.9 Hz, 8H, Ar-H), 4.16-4.00 (m, 4H, CH_2), 1.89 (m, 2H, CH), 1.44-1.20 (m, 28H, H_{alkyl}).

1,6,7,12-tetrakis-(4-tritylphenoxy)-3,4:9,10-perylene bisanhydride 20 and ***N*-(2-ethyl-1-hexyl)-1,6,7,12-tetrakis-(4-tritylphenoxy)-3,4:9,10-perylene monoanhydride 21**

The mixture of PBI **19** (1.46 g) and KOH (16 g) in *i*-propanol (105 ml) and H_2O (11 ml) in a round flask were put into ultrasonic for 5 minutes, and then allowed to stir at 105 ^oC for 19 h. After cooling to RT, 200 ml 2 N HCl was added and the precipitate was collected and re-dissolved in a small amount of DCM, then methanol was added and the product was collected by filtration to give a red product which are mixture of compound **20** and **21** (ca. 2:1). The overall yield of this step is 120 mg (9%). MS (MALDI-TOF, matrix: DCTB): bisanhydride **20**, calculated for $C_{124}H_{80}O_{10}$: 1729.578, found 1729.576; monoanhydride **21**: calculated for $C_{132}H_{97}NO_9$: 1840.719, found 1840.716.

***N,N*'-bis-(4-methoxymethyl-phenyl)-1,6,7,12-tetrakis-(4-tritylphenoxy)-3,4:9,10-perylene bisimide 22**

Above mixture of **20** and **21** (173 mg, 0.1 mmol), 4-methoxymethyl-aniline (30 mg, 0.21 mmol) and $Zn(OAc)_2$ (40 mg) were stirred in 3 g imidazole at 140 ^oC for 3 h under argon. The reaction mixture was cooled to room temperature and 2 N HCl was added and the precipitate was collected by filtration. Then the residue was thoroughly washed with water and dried in vacuum. The solid was further purified by column chromatography (DCM: Methanol 30:1), to get product 22 mg, Yield: 11%. MS (MALDI-TOF, matrix: DCTB): calculated for $C_{140}H_{98}N_2O_{10}$: 1966.722, found: 1966.714. H^1NMR (400 MHz, $CDCl_3$, 300 K, TMS): δ = 8.31 (s, 4H, H_{pery}), 7.50-7.48 (d, 4H, Ar-H), 7.20-7.18(d, 4H, Ar-H), 7.15 (m, 68H, Ar-H), 6.75-6.72(d, 8H, Ar-H), 4.56 (s, 4H, -CH_2-O), 3.44 (s, 6H, -CH3).

In this step, PBI **23** was obtained as a by-product which was not purified and used directly for the next step.

_N,N'_-bis-(4-bromomethyl-phenyl)-1,6,7,12-tetrakis-(4-tritylphenoxy)-3,4:9,10-perylene bisimide 24

PBI **22** (38 mg) was dissolved in DCM (20 ml) and 33% hydrobromic acid in acetic acid (30 ml) was added. The mixture was stirred at room temperature for 72 h under argon. After that, water was added and the organic layer was separated washed with saturated $NaHCO_3$ and dried over Na_2SO_4. The solvent was evaporated and the product was dried under vacuum. The crude product (35 mg, 88%) was not further purified and used for the next step directly. MS (MALDI-TOF, matrix: DCTB): calculated for $C_{138}H_{92}Br_2N_2O_8$: 2065.523, found: 2065.520.

_N,N'_-bis-(4-thioacetate-methyl-phenyl)-1,6,7,12-tetrakis-(4-tritylphenoxy)-3,4: 9,10-perylene bisimide PBI 3

Above crude PBI **23** (35 mg) and KSAc (9 mg) was stirred in 5 ml NMP at 60 ^oC for 3 h under argon atmosphere. The mixture was cooled to room temperature and 100 ml water was added and the precipitate was collected. The solid was further purified by column chromatography (DCM: Methanol 50:1). The final product was obtained as a dark red powder. Get 7 mg, yield: 21%. MS (MALDI-TOF, matrix: DCTB): calculated for $C_{142}H_{98}N_2O_{10}S_2$: 2054,666, found $[M+H]^+$: 2055.573. ^{13}C-NMR (100 MHz, $CDCl_3$, 300 K, TMS):146.6, 132.7, 131.0, 127.6, 126.0, 122.9, 118.2, 64.5; H^1NMR (400 MHz, $CDCl_3$, 300 K, TMS): δ = 8.31 (s, 4H, H_{pery}), 7.45-7.43 (d, 4H, Ar-H), 7.15 (m, 72H, Ar-H), 6.74-6.72(d, 8H, Ar-H), 4.19 (s, 4H, -CH_2-S), 2.38 (s, 6H, -CH3).

_N_-(2-ethyl-1-hexyl)-_N'_-(4-thioacetate-methyl-phenyl)-1,6,7,12-tetrakis-(4-trityl phenoxy)-3,4:9,10-perylene bisimide PBI 4

During the synthesis of **PBI 3**, **PBI 4** was obtained as a by-product to get 5 mg, 18%. MS (MALDI-TOF, matrix: DCTB): calculated for $C_{141}H_{106}N_2O_9S$: 2003.765, found: 2003.767. ^{13}C-NMR (100 MHz, $CDCl_3$, 300 K, TMS):153.5, 146.6, 144.6, 143.1, 132.7, 131.1, 127.6, 126.1, 122.7, 121.1, 118.3, 64.6, 23.1, 14.1, 11.4, 10.7; H^1NMR (400 MHz, $CDCl_3$, 300 K, TMS): δ = 8.31 (s, 2H, H_{pery}), 8.27 (s, 2H,

H_{pery}), 7.45-7.42 (d, 2H, Ar-H), 7.25-7.05 (m, 72H, Ar-H), 6.76-6.68(d, 8H, Ar-H), 4.19 (s, 2H, -CH_2-S), 4.18-4.00 (m, 2H, N-CH_2), 2.38 (s, 3H, CO-CH3), 1.90 (m, 1H, CH), 1.39-1.09 (m, 8H, CH_2), 1.00-0.80 (m, 6H, CH_3)

***N,N'*-bis-(4-thioacetate-methyl-phenyl)-1,6,7,12-tetrakis-chloro-3,4:9,10-perylene bisimide PBI 5**

PBI **10** (90mg) was dissolved in DCM (20 ml) and 33% hydrobromic acid in acetic acid (30 ml) was added. The mixture was stirred at room temperature for 72 h under argon. After that, water was added and the organic layer was separated washed with saturated $NaHCO_3$ and dried over Na_2SO_4. The solvent was evaporated and the product was dried under vacuum. The crude product (PBI **26**, 50 mg, yield: 50%) was not further purified due to the very bad solubility in common organic solvents and used for the next step directly. Above crude PBI **26** (50 mg) and KSAc (35 mg) was stirred in 10 ml NMP at 60 ^oC for 3 h under argon atmosphere. The mixture was cooled to room temperature and 100 ml water was added and the precipitate was collected. The solid was further purified by column chromatography (DCM: Methanol 50:1). Get PBI 5 as a light red powder, 3 mg, yield: 7%. MS (MALDI-TOF, matrix: DCTB): calculated for $C_{42}H_{22}Cl_4N_2O_6S_2$: 855.964, found 855.972. H^1NMR (400 MHz, $CDCl_3$, 300 K, TMS): δ = 8.73 (s, 4H, H_{pery}), 7.71 (m, 4H, Ar-H), 7.52 (m, 4H, Ar-H), 4.15 (s, 4H, -CH_2-S), 2.30 (m, 6H, -CH3).

6.7 References and Notes

1 (a) K. Watanabe, D. Menzel, N. Nilius, H.-J. Freund, *Chem. Rev.* **2006**, *106*, 4301-4320; (b) R. W. Murray, *Chem. Rev.* **2008**, *108*, 2688-2720.

2 (a) M. A. El-Sayed, *Acc. Chem. Res.* **2001**, *34*, 257-264; (b) C. J. Murphy, T. K. Sau, A. M. Gole, C. J. Orendorff, J. Gao, L. G, S. E. Hunyadi, T. Li, *J. Phys. Chem. B* **2005**, *109*, 13857-13870.

3 C. Burda, X. Chen, R. Narayanan, M. A. El-Sayed, *Chem. Rev.* **2005**, *105*, 1025-1102.

4 (a) K. K. Caswell, J. N. Wilson, U. H. F. Bunz, C. J. Murphy, *J. Am. Chem. Soc.* **2003**, *125*, 13914-13915; (b) S. T. S. Joseph, B. I. Ipe, P. Pramod, K. G. Thomas, *J. Phys. Chem. B* **2006**, *110*, 150-157; (c) P. Pramod, S. T. S. Joseph, K. G. Thomas, *J. Am. Chem. Soc.* **2007**, *129*, 6712-6713.

5 (a) K. G. Thomas, P. V. Kamat, *Acc. Chem. Res.* **2003**, *36*, 888-898; (b) Z. Shen, M. Yamada, M. Miyake, *J. Am. Chem. Soc.* **2007**, *129,* 14271-14280; (c) M. Jebb, P. K. Sudeep, P. Pramod, K. G. Thomas, P. V. Kamat, *J. Phys. Chem. B* **2007**, *111*, 6839-6844.

6 F. Würthner, *Chem. Commun.* **2004**, 1564-1579.

7 P. Ranke, I. Bleyl, J. Simmer, D. Harrer, A. Bacher, H. W. Schmidt, *Appl. Phys. Lett.* **1997**, *71*, 1332-1334.

8 C. D. Dimitrakopoulos, P. R. L. Malenfant, *Adv. Mat.* **2002**, *14*, 99-117.

9 M. Thelakkat, P. Pösch, H. W. Schmidt, *Macromolecules* **2001**, *34*, 7441-7447.

10 (a) P. Muhlschlegel, H. J. Eisler, O. J. F. Martin, B. Hecht, D. W. Pohl, *Science* **2005**, *308,*1607-1609; (b) S. A. Kalele, N. R. Tiwari, S. W. Gosavi, S. K. Kulkarni, *Journal of Nanophotonics* **2007**, *1,* 012501-012520; (c) D. P. Fromm, A. Sundaramurthy, P. J. Schuck, G. S. Kino, W. E. Moerner, *Nano Lett.* **2004**, *4*, 957-961.

11 (a) C. A. Foss, G. L. Hornyak, J. A. Stockert, C. R. Martin, *J. Phys.Chem.* **1992**, *96*, 7497-7499; (b) B. M. I. van der Zande, M. R. Böhmer, L. G. J.

Fokkink, C. Schönenberger, *J. Phys. Chem. B* **1997**, *101*, 852-854.

12 Y. Y. Yu, S. S. Chang, C. L. Lee, C. R. C. Wang, *J. Phys. Chem. B* **1997**, *101*, 6661-6664; (b) S. S. Chang, C. W. Shi, C. D. Chen, W. C. Lai, C. R. C. Wang, *Langmuir* **1999**, *15*, 701-709.

13 (a) N. R. Jana, L. Gearheart, C. J. Murphy, *J. Phys. Chem. B* **2001**, *105*, 4065-4067; (b) C. J. Murphy, N. R. Jana, *Ad*v. *Mater.* **2002**, *14*, 80-82; (c) N. R. Jana, L. A. Gearheart, S. O. Obare, C. J. Johnson, K. J. Edler, S. Mann, C. J. Murphy, *J. Mater. Chem.* **2002**, *12*, 2909-2912; (d) L. Gou, C. J. Murphy, *Chem. Mater*. **2005**, *17*, 3668-3672.

14 (a) F. Kim, J. H. Song, P. Yang, *J. Am. Chem. Soc.* **2002**, *124*, 14316-14317; (b) Y. Niidome, K. Nishioka, H. Kawasaki, S. Yamada, *Chem. Commun.***2003**, 2376-2377; (c) K. G. Thomas, S. Barazzouk, B. I. Ipe, S. T. S. Joseph, P. V. Kamat, *J. Phys. Chem. B* **2004**, *108*, 13066-13068.

15 (a) B. Nikoobakht, M. A. El-Sayed, *Chem. Mater.* **2003**, *15*, 1957-1962; (b) T. K. Sau, C. J. Murphy, *J. Am. Chem. Soc.* **2004**, *126*, 8648-8649.

16 M. Grzelczak, J. Pérez-Juste, P. Mulvaney, L. M. Liz-Marzán, *Chem. Soc. Rev.* **2008**, *37*, 1783-1791.

17 N. R. Jana, L. Gearheart, C. J. Murphy, *Adv. Mater.* **2001**, *13*, 1389-1393.

18 P. Pramod, K. G. Thomas, *Adv. Mater.* **2008**, *20*, 4300-4305.

19 (a) Z. Nie, D. Fava, E. Kumacheva, S. Zou, G. C. Walker, M. Rubinstein, *Nature Mater.* **2007**, *6*, 609-614; (b) Z. Nie, D. Fava, M. Rubinstein, E. Kumacheva, *J. Am. Chem. Soc.* **2008**, *130*, 3683-3689; (c) D. Fava, Z. Nie, M. A. Winnik, E. Kumacheva, *Adv. Mater.* **2008**, *20*, 4318-4322.

20 (a) K. Imura, T. Nagahara, H. Okamoto, *J. Am. Chem. Soc.* **2004**, *126*, 12730-12731; (b) P. Hanarp, M. Kall, D. S. Sutherland, *J. Phys. Chem. B* **2003**, *107*, 5768-5772; (c) M. Gluodenis, C. A. Foss, Jr. *J. Phys. Chem. B* **2002**, *106*, 9484-9489; (d) J. R. Lakowicz, C. D. Geddes, I. Gryzczynski, J. Malicka, Z. Gryzczynski, K. Aslan, J. Lukomski, E. Matveera, J. Zhang, R. Badugn, J. Huang, *J. Fluorescence* **2004**, *14*, 425-441.

21 (a) S. A. Maier, M. L. Brongersma, P, G. Kik, S. Meltzer, A. A. G. Requichia, H. Atwater, *Ad*v. *Mater*. **2001**, *13*, 1501-1505; (b) S. A. Maier, P. G. Kik, H. A. Atwater, S. Meltzer, E. Harel, B. E. Koel, A. A. Requichia, *Nature Mater.* **2003**, *2*, 229-232.

22 J. M. Tour, L. Jones II, D. L. Pearson, J. J. S. Lamba, T. P. Burgin, G. M. Whitesides, D. L. Allara, A. N. Parikh, S. Atre, *J. Am. Chem. Soc*. **1995**, *117*, 9529-9534.

23 C. J. Orendorff, C. J. Murphy, *J. Phys. Chem. B* **2006**, *110*, 3990-3994.

24 J. Baggerman, D. C. Jagesar, R. A. L. Vallee, J. Hofkens, F. C. De Schryver, F. Schelhase, F. Vögtle, A. M. Brouwer, *Chem. Eur. J.* **2007**, *13*, 1291-1299.

25 (a) C.- C. You, F. Würthner, *J. Am. Chem. Soc.* **2003**, *125*, 9716-9725. (b) F. Würthner, C. Thalacker, S. Diele, C. Tschierske, *Chem. Eur. J.* **2001**, *7,* 2245-2253. (c) D. Dotcheva, M. Klapper, K. Müllen, *Macromol. Chem. Phys.* **1994**, *195*, 1905-1911;

Chapter 7

Summary

Perylene bisimide (PBI) dyes are a widely used class of industrial pigments, and currently have gained significant importance for organic-based electronic and optical devices. Structural modification at the PBI core results in changes of the optical and electronic properties, which enable tailored functions. Moreover, the aggregation behavior of PBIs is alterable and controllable to achieve new materials, among which organogels are of particular interest because of their potential for applications as supramolecular soft materials. In this work, new PBI-based organic gelators were designed, synthesized, and characterized, and the aggregation behaviors under different conditions were intensively studied by various spectroscopic and microscopic methods.

In chapter 2, a brief overview is given on the structural and functional features of organogel systems. The definition, formation and reversibility of organogels are introduced. Some examples on dye based organogel are selected, among which PBI-based organogelators reported so far are especially emphasized. Some basic knowledges of supramolecular chirality are also overviewed such as characterization, amplification, and symmetry breaking of the chiral aggregates.

According to our former experiences, PBIs tend to form aggregates because the planer aromatic cores interact with one another by π–π interaction. In chapter 3, a new PBI molecule is introduced which possesses amide groups between the conjugated core and periphery alkyl chains (Figure 1, top). It is found that well oriented aggregates are formed by hydrogen bonding and the π–π interaction of the cores. These interactions enable the aggregates to grow in one-dimension forming very long fibers, and these fibers further intercross to 3D network structures, e.g.,

organogels. In comparison to the very few PBI-based gelators reported before, one advantage of this gelator is that, it is more versatile and can gelate a wide range of organic solvents. Moreover, the well-organized fibers that are composed of extended π-stacks provide efficient pathways for *n*-type charge carriers. At room temperature, the sum of the isotropic electron and hole mobility is $\Sigma\mu_{TRMC} = 0.052$ $cm^2V^{-1}s^{-1}$. This value is higher than the values for related PBIs without hydrogen-bonding motif determined by the same method.

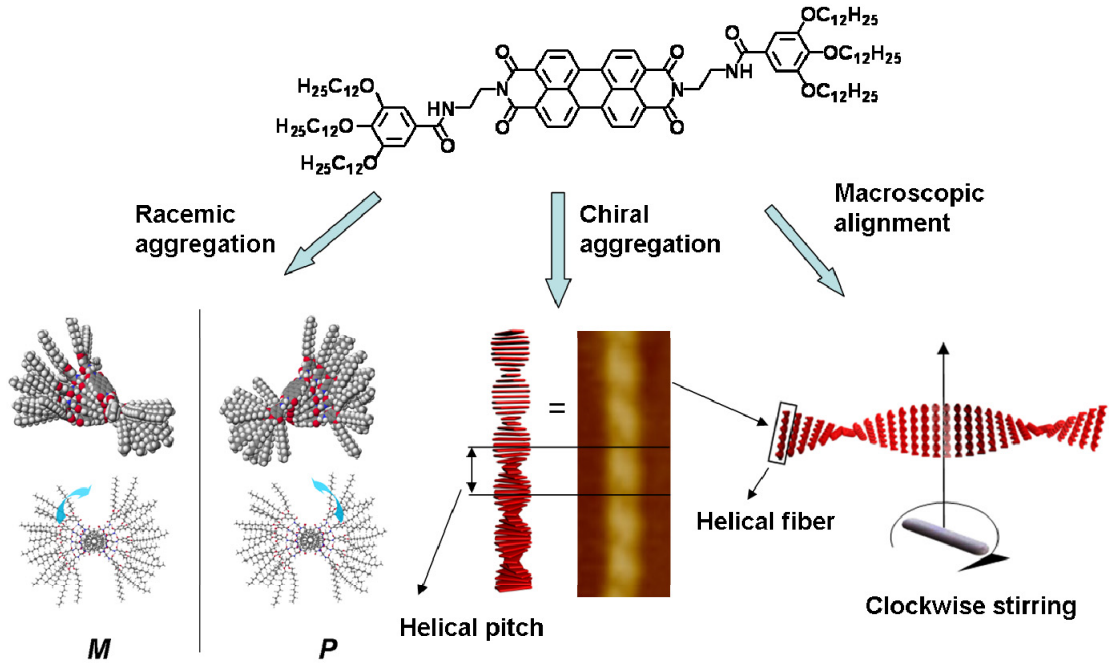

Figure 1. Schematic representation of the self-assembly behavior of the core-unsubstituted PBI: (Left) in achiral solvent such as toluene it forms racemic helical aggregates; (middle) chiral solvent induced enantiomer enrichment; (right) macroscopic alignment of the nanofibers in vortex flow.

Interestingly, AFM studies reveal that the PBI molecules form well-defined helical fibers in toluene. Both left-handed (*M*) and right-handed (*P*) helicities can be observed without any preference for one handedness because the building block is intrinsically achiral (Figure 1, left). In chapter 4, we tried to influence the *M*/*P*

enantiomeric ratio by applying external forces. For example, we utilized chiral solvents to generate chiral aggregates with a preferential handedness. AFM analysis of the helices showed that a enantiomeric ratio of about 60: 40 can be achieved by aggregation in chiral solvents *R*- or *S*-limonene (Figure 1, middle). Moreover, the long aggregated fibres can align at macroscopic level in vortex flows upon rotary stirring (Figure 1, right).

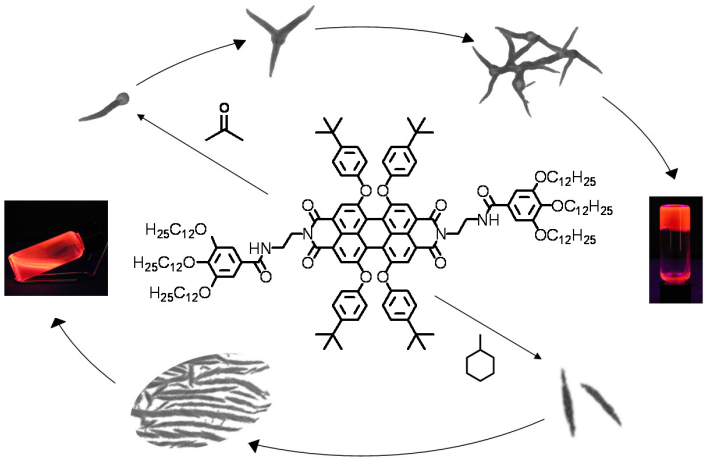

Figure 2. Schematic presentation for the of formation of organogels in acetone and lyotropic mesophase in MCH based on aggregation of core-twisted PBI

In chapter 5, bulky tetra-phenoxy groups are introduced in the bay area of the PBI gelator (Figure 2). The conjugated core of the new molecule is now distorted because of the steric hindrance. UV/Vis studies reveal a J-type aggregation in apolar solvents like MCH due to intermolecular π-π-stacking and hydrogen-bonding interactions. Microscopic studies reveal formation of columnar aggregates in apolar solvent MCH, thus this molecule lacks the ability to form gels in this solvent, but form highly fluorescent lyotropic mesophases at higher concentration. On the other hand, in polar solvents like acetone and dioxane, participation of the solvent molecules in hydrogen bonding significantly reduced the aggregation propensity but enforced the gel formation. The outstanding

fluorescence properties of the dye in both J-aggregated viscous lyotropic mesophases and bulk gel phases suggest very promising applications in photonics, photovoltaics, security printing, or as fluorescent sensors.

In chapter 6, we did some studies on combining PBI molecules with inorganic gold nanorods. Gold nanorods were synthesized photochemically. By virtue of the thioacetate functionalized PBIs, the rods were connected end to end to form gold nanochains, which were characterized by absorption spectra and TEM measurement. Such chromophore-nanorod hybrids might be applied to guide electromagnetic radiation based on optical antenna technology.

Zusammenfassung

Perylenbisimide (PBI) sind eine weitverbreitete Pigmentklasse und haben gegenwärtig große Bedeutung für die organische Elektronik sowie für optische Bauteile gewonnen. Strukturelle Modifikationen am PBI-Kern führen zur Änderung der optischen und elektronischen Eigenschaften, welche maßgeschneiderte Funktionen ermöglichen. Außerdem ist das Aggregationsverhalten der PBIs wandel- und kontrollierbar um neue Materialien zu erhalten. Dabei sind Organogele, aufgrund ihres Potentials zur Anwendung supramolekularer Materialien, von Interesse. In der vorliegenden Arbeit wurde neue Organogelatoren auf PBI-Basis konzipiert, synthetisiert und charakterisiert. Das Aggregationsverhalten unter verschiedenen Bedingungen wurde mittels verschiedener spektroskopischer und mikroskopischer Methoden untersucht.

In Kapitel 2 wird eine kurze Übersicht über die strukturellen und funktionellen Merkmale der Organogelsysteme gegeben. Hierbei wir sowohl eine Begriffsdefinition gegeben als auch die Bildung und Reversibilität von Organogelen beschrieben. Es werden einige Beispiele zu farbstoffbasierten Organogelen vorgestellt, wobei der Schwerpunkt auf PBIs gelegt wird. Außerdem werden grundlegende Erkenntnisse über supramolekulare Chiralität zusammengefasst, beispielsweise die Charakterisierung, Verstärkung sowie der Symmetriebruch chiraler Aggregate.

Entsprechend unseren vorangehenden Erfahrungen, neigen PBIs dazu Aggregate zu bilden, was auf die π-π-Stapelwechselwirkung der planaren aromatischen Kerne zurückzuführen ist. In Kapitel 3 wird ein neues PBI-Derivat vorgestellt, das Amidgruppen zwischen konjugiertem Kern und den peripheren Alkylgruppen besitzt (Abbildung 1, oben). Hierbei wird beobachtet, dass orientierte Aggregate durch Wasserstoffbrücken sowie π-π-Wechselwirkung der Kerne gebildet werden. Diese Wechselwirkungen ermöglichen das eindimensionale Wachstum der

Aggregate. Dies führt zur Bildung von Fasern, welche weiterhin 3D-Strukturen, wie z.B. Organogele, bilden. Im Vergleich zu den sehr wenigen bereits bekannten Organogelen, welche auf PBIs beruhen, hat dieser vielseitige Gelator den Vorteil in einer Vielzahl an organischen Lösungsmitteln zu gelieren. Außerdem besitzen diese gut organisierten Fasern, welche aus ausgedehnten π-Stapeln bestehen, eine effiziente Elektronenleitfähigkeit. Bei Raumtemperatur beträgt die Summe aus isotroper Elektron- und Lochmoblität $\Sigma\mu_{TRMC} = 0.052\ cm^2V^{-1}s^{-1}$. Dieser Wert ist höher als es für andere PBI-Derivate ohne Wasserstoffbrücken der Fall ist.

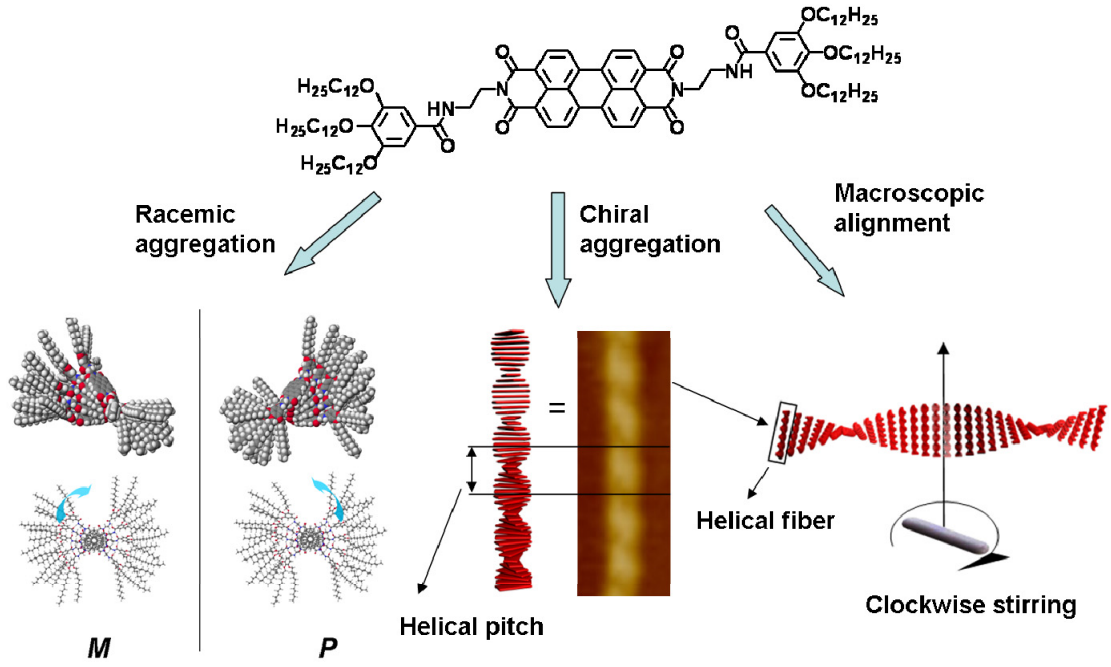

Abbildung 1. Schematische Darstellung der Selbstorganisation des kernunsubstituierten PBIs: (links) in achiralen Lösungsmitteln wie Toluol werden racemische helicale Aggregate gebildet; (Mitte) chirale Lösungsmittel induzieren das Anreichern eines Enantiomers; (rechts) makroskopische Ausrichtung der Nanofasern in einem durch Rühren erzeugten Wirbel.

Interessanterweise zeigen AFM-Studien, dass PBI-Moleküle wohldefinierte helicale Fasern in Toluol bilden. Hierbei werden sowohl links- (*M*) als auch rechtshändige (*P*)- Helices beobachtet, wobei jedoch aufgrund der intrinsischen

Achiralität keine Präferenz zu beobachten ist (Abbildung 1, links). In Kapitel 4 haben wir versucht das *M/P*-Enantiomerenverhältnis durch äußere Einwirkung zu beeinflussen. So haben wir beispielsweise chirale Lösungsmittel verwendet, um chirale Aggregate mit einer bevorzugten Händigkeit zu generieren. Durch AFM-Analyse der Helices konnte gezeigt werden, dass in *R*- oder *S*-Limonen durch Aggregation ein Verhältnis von ca. 60:40 erzielt werden kann (Abbildung 1, Mitte). Außerdem können sich die Fasern in einem durch Rühren erzeugten Wirbel auf makroskopischer Ebene ausrichten (Abbildung 1, rechts).

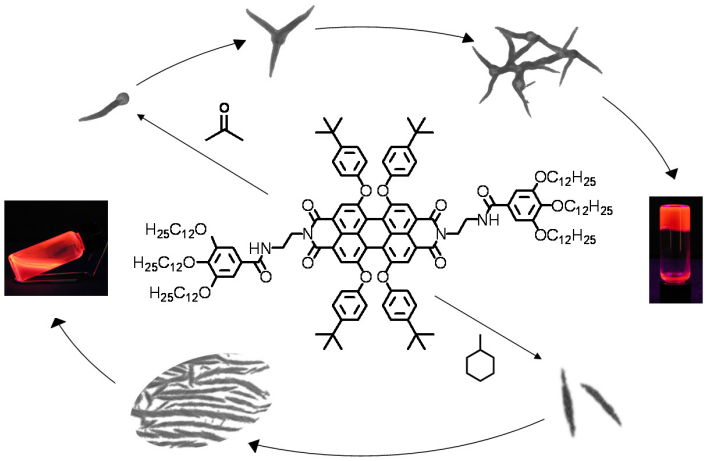

Abbildung 2. Schematische Darstellung der Bildung von Organogelen in Aceton sowie einer lyotropen Mesophase in MCH aufgrund von Aggregation des kernverdrillten PBIs.

In Kapitel 5 wurden sperrige Tetraphenoxy-Gruppen in der Bay-Region des PBI-Gelators eingeführt (Abbildung 2). Der konjugierte Kern des Moleküls ist nun aufgrund des sterischen Anspruchs verdreht. UV/Vis-Studien zeigen J-Aggregation in apolaren Lösungsmitteln wie beispielsweise MCH aufgrund intermolekularer π-π-Stapelwechselwirkung und Wasserstoffbrücken. Mikroskopische Studien lassen die Bildung columnarer Aggregate im apolaren Solvens MCH erkennen, so dass dieses Molekül in diesem Lösungsmittel nicht zu gelieren vermag. Allerdings bildet es stark fluoreszierende lyotrope Mesophasen bei höheren Konzentrationen. Andererseits wird das Aggregationsverhalten in polaren Lösungsmitteln wie Aceton

oder Dioxan aufgrund deren Beteiligung an den Wasserstoffbrücken eingeschränkt, die Gelbildung jedoch verstärkt. Die herausragenden Fluoreszenzeigenschaften des Farbstoffs in J-aggregierten viskosen lyotropen Mesophasen sowie im Gel legen vielversprechende Anwendung in den Bereichen Photonik, Photovoltaik, Sicherheitsdruck oder als Fluoreszenzsensor nahe.

In Kapitel 6 haben wir PBI-Moleküle mit anorganischen Goldnanopartikeln kombiniert und untersucht. Die Goldnanostäbchen wurde photochemisch synthetisiert. Aufgrund der Thioacetatfunktionalisierung des PBIs, wurden die Stäbchen durchgehend zu Goldnanoketten verbunden, welche durch Absorptionsspektroskopie und TEM charakterisiert wurden. Solche Chromophor-Nanostäbchen-Hybride könnten dazu verwendet werden, elektromagnetische Strahlung aufgrund optischer Antennentechnologie zu leiten.

Publications

- *Highly Fluorescent Lyotropic Mesophases and Organogels Based on J-Aggregates of Core-Twisted Perylene Bisimide Dyes*
  X.-Q. Li, X. Zhang, S. Ghosh, F. Würthner, *Chem. Eur. J.* **2008**, *14*, 8074-8078.

- *Control of H- and J-Type π Stacking by Peripheral Alkyl Chains and Self-Sorting Phenomena in Perylene Bisimide Homo- and Heteroaggregates*
  S. Gosh, X.-Q. Li, V. Stepanenko, F. Würthner, *Chem. Eur. J.* **2008**, *14*, 11343-11357.

- *Electrochemical gate-controlled electron transport of redox-active single perylene bisimide molecular junctions*
  C. Li, A. Mishchenko, Z. Li, I. Pobelov, Th. Wandlowski, X.-Q. Li, F. Würthner, A. Bagrets, F. Evers, *J. Phys.: Condens. Matter* 20 (**2008**) 374122 (11pp).

- *Functional Organogels From Highly Efficient Organogelator Based on Perylene Bisimide Semiconductor*
  X.-Q. Li, V. Stepanenko, Z. Chen, P. Prins, L. D. A. Siebbeles, F. Würthner, *Chem. Commun.* **2006**, 3871-3873.

- *The Importance of Nanoscopic Ordering on the Kinetics of Photoinduced Charge Transfer in Aggregated π-Conjugated Hydrogen-Bonded Donor−Acceptor Systems*
  E. H. A. Beckers, Z. Chen, S. C. J. Meskers, P. Jonkheijm, A. P. H. J. Schenning, X.-Q. Li, P. Osswald, Frank Würthner, R. A. J. Janssen, *J. Phys. Chem. B*, **2006**, *110*, 16967-16978.

Workshop and Conferences:

- *Poster presentation*
  International CECAM-Workshop *'Quantum transport at the molecular scale'*
  September 14th-18th, 2009, Bremen, Germany

- *Poster presentation*
  Chem-Systm (Chemie-Symposium der Studierenden Mainfrankens)
  December, 2nd, 2008, Würzburg, Germany

- *Poster presentation*
  Electronic Processes in π-Conjugated Materials
  October 7th-10th, 2008, Würzburg, Germany

- *Poster presentation*
  Fπ8, The 8th International Symposium on Functional π-Electron Systems
  July 21st – 25th, 2008, Graz, Austria

- *Poster presentation*
  Referee-Panel-Meeting of SPP 1243 *'Quantum transport at the molecular scale'*
  March 6th-7th, 2008, Bad Honnef, Germany

- *Oral presentation*
  Conjugated Oligomers And Polymers from Synthesis to Electronic Function
  September 24th – 27th, 2007, Blaubeuren (Ulm), Germany

- *Poster presentation*
  Midterm Meeting SPP 1243 *'Quantum transport at the molecular scale'*
  June 24th – 27th, 2007, at the IUB (International University Bremen), Germany

Acknowledgement

First of all, I would like to express my sincere gratitude to Prof. Dr. Frank Würthner for giving me the chance to do fascinating research in his group. I am very thankful for his valuable guidance and suggestions on my projects. Furthermore, I think I have learned how to do proper science from him, and I appreciate him on this point very much.

I want to thank Prof. Dr. Th. Wandlowski (University of Bern), Prof. Dr. B. Hecht (University of Würzburg), Prof. Dr. L. D. A. Siebbeles and Dr. P. Prins (Technical University of Delft), for their nice discussion and kind help on my projects.

I am grateful to Dr. C. Saha-Möller for his careful correction on my manuscripts and posters. I thank Ms. C. Toussaint for her kind help on a lot of paperwork.

Dr. V. Stepanenko helped me to get very nice AFM results. Dr. M. Grüne and Dr. M. Büchner helped me a lot on the NMR and MS measurements. I am very grateful to them.

I thank all our group members, they are: Hao, Zhijian, Xin, Volker, Theo, Stefanie, Sabin, Cornelia, Catharina, Valerie, Peter, Changzhun, Johann, Andreas, Sanchita, Jun, Zengqi, Linlin, Shinobu, Suhrit, Martin, Felix, Marcel, Marina, Ralf, Joachim, Manuela, Ana-Maria, Hannah, Gustavo, etc., I enjoy the happy time with all of them very much.

Finally I would like to thank my families for their concern and selfless support.